DAMPING STRATEGIES IN ADDITIVE MANUFACTURING: HYBRID MATERIALS, METAMATERIALS, AND PARTICLE DAMPING

MURAT CAN ÖZDEN

ÖZYEĞİN UNIVERSITY

MAY, 2025

DAMPING STRATEGIES IN ADDITIVE MANUFACTURING: HYBRID MATERIALS, METAMATERIALS, AND PARTICLE DAMPING

by

MURAT CAN ÖZDEN

Dissertation
Submitted in Partial Fulfillment of the
Requirements for the Degree of

Doctor of Philosophy

in
Department of Mechanical Engineering

Advisor: Assoc. Prof. Polat Şendur

Graduate School of Science and Engineering
Özyeğin University
İstanbul

May, 2025

DAMPING STRATEGIES IN ADDITIVE MANUFACTURING: HYBRID MATERIALS, METAMATERIALS, AND PARTICLE DAMPING

Approved by:

Assoc. Prof. Polat Şendur, Advisor
Department of Mechanical Engineering
Özyeğin University

Assoc. Prof. Güllü Kızıltaş Şendur
Department of Mechatronics Engineering
Sabancı University

Prof. G. Güven Yapıcı
Department of Mechanical Engineering
Özyeğin University

Assoc. Prof. Bekir Bediz
Department of Mechatronics Engineering
Sabancı University

Asst. Prof. Ramazan Ünal
Department of Mechanical Engineering
Özyeğin University

Approval Date: May 13, 2025

To my family

DECLARATION OF ORIGINALITY

I hereby declare that I am the sole author of this thesis and that this is the true copy of my thesis, including the final revisions, approved by my thesis committee. All data and information have been obtained, produced, and presented in accordance with the rules of research ethics and principles of academic honesty. As required by these rules, to the best of my knowledge I have acknowledged ideas, thoughts, and any copyrighted material in accordance with the standard referencing rules. I certify that any part of this thesis has not been submitted for a degree or diploma in another educational institution.

Murat Can Özden

ABSTRACT

This thesis explores innovative strategies to enhance damping in structural systems for vibration control applications. Three distinct approaches are investigated: (1) the hybridization of additively manufactured Triply Periodic Minimal Surface (TPMS) metal parts with silicone polymers, (2) the integration of metamaterials with constrained layer damping (CLD) techniques using TPMS structures and viscoelastic polymers, and (3) the optimization of particle dampers through a hybrid computational framework. Each method employs finite element modeling (FEM) and experimental modal testing to validate significant improvements in damping performance.

In the first study, Cobalt-Chrome TPMS structures are combined with silicone polymers, resulting in up to a sixfold increase in time-domain damping and a thirty-fold improvement in frequency-domain analysis. The second study integrates aluminum TPMS structures with silicone polymer layers for CLD applications, achieving a fivefold enhancement in damping performance and reduced cumulative vibration response. The third study focuses on optimizing particle dampers by employing a hybrid computational framework that combines finite element analysis, artificial neural networks (ANN), and genetic algorithms (GA), leading to substantial reductions in vibratory response.

Collectively, these findings demonstrate the transformative potential of advanced manufacturing techniques, hybrid material systems, and computational optimization in developing next-generation structural damping solutions for engineering applications.

Keywords: Structural Damping, TPMS Structures, Constrained Layer Damping (CLD), Particle Dampers Optimization, Computational Intelligence

ÖZET

Bu tez, titreşim kontrol uygulamaları için yapısal sistemlerde sönümleme performansını artırmaya yönelik yenilikçi stratejileri araştırmaktadır. Çalışma üç farklı yaklaşımı incelemiştir: Katmanlı imalat yöntemiyle üretilmiş üç yönlü periyodik minimal yüzeyler (TPMS) metal parçalarının silikon polimerlerle hibritleştirilmesi,TPMS yapıları ve viskoelastik polimerler kullanılarak metamaterial yapıların sınırlı tabakalı sönümleme (CLD) teknikleriyle entegrasyonu ve parçacık sönümleyicilerin hibrit bir hesaplama çerçevesi kullanılarak optimize edilmesi. Her bir yöntem, sonlu elemanlar modellemesi (FEM) ve deneysel modal testler aracılığıyla değerlendirilmiş ve sönümleme performansında önemli iyileşmeler elde edildiği doğrulanmıştır.

İlk çalışmada, Cobalt-Chrome TPMS yapıları silikon polimerlerle birleştirilmiş ve zaman domeninde sönüm oranında altı kata kadar, frekans domeni analizinde ise otuz kata kadar iyileşme sağlanmıştır. İkinci çalışmada, alüminyum TPMS yapıları silikon polimer tabakaları ile CLD uygulamaları için entegre edilmiş ve sönümleme performansında beş kat artış ile birlikte birikimli titreşim yanıtında önemli bir azalma elde edilmiştir. Üçüncü çalışmada ise, parçacık sönümleyici tasarımı, sonlu elemanlar analizi, yapay sinir ağları (ANN) ve genetik algoritmaların (GA) bir arada kullanıldığı hibrit bir hesaplama çerçevesiyle optimize edilmiş ve titreşim yanıtında kayda değer bir azalma sağlanmıştır.

Bu bulgular bir araya geldiğinde, ileri üretim teknikleri, hibrit malzeme sistemleri ve hesaplamalı optimizasyon yöntemlerinin, mühendislik uygulamaları için gelecek nesil yapısal sönümleme çözümlerinin geliştirilmesinde dönüştürücü bir potansiyele sahip olduğunu ortaya koymaktadır.

Anahtar Kelimeler: Yapısal Sönümleme, TPMS Yapıları, Sınırlı Tabakalı Sönümleme (CLD), Parçacık Sönümleyici Optimizasyonu, Hesaplamalı Zeka

ACKNOWLEDGEMENTS

I would like to extend my heartfelt thanks to Dr. Polat Şendur, my PhD supervisor, for being an incredible mentor throughout this journey. His steady support, insightful advice, and encouraging attitude made a significant difference during my thesis work. Beyond his role as an academic advisor, his brotherly guidance and belief in me helped me stay focused and motivated at every step.

I am also deeply grateful to Dr. Güllü Kızıltaş Şendur Dr. Güney Güven Yapıcı, Dr. Ramazan Ünal and Dr. Bekir Bediz for serving on my thesis committee. Their thoughtful feedback and critical perspective allowed me to approach my research with greater clarity and depth, ultimately strengthening the quality of this study.

I would also like to sincerely thank my friends Dr. Uğur Şimşek, Mirhan Özdemir, and Cemal Efe Gayır for their continuous support and contributions throughout this work. I am truly grateful for the time and effort they shared with me, and for always being there whenever I needed help or encouragement.

Last but certainly not least, I would like to express my deepest gratitude to my beloved family and friends, who have supported me unconditionally since the very first day of my doctoral journey. Their constant encouragement and presence have been a source of strength and comfort throughout this process.

TABLE OF CONTENTS

DECLARATION OF ORIGINALITY iv

ABSTRACT v

ÖZET vi

ACKNOWLEDGEMENTS vii

LIST OF TABLES xi

LIST OF FIGURES xii

LIST OF ACRONYMS AND ABBREVIATIONS xiv

1 INTRODUCTION 1

1.1 Literature Review 1

1.1.1 Damping Enhancement through TPMS Metal–Silicone Polymer Synergy 1

1.1.2 Hybrid Vibration Control of TPMS Structures via CLD Silicone–Viscoelastic Layers 6

1.1.3 AI-Driven Particle Damper Optimization: FEM, ANN, and Genetic Algorithm Integration 12

1.2 Research Gaps 23

1.3 Objectives of the Thesis 25

2 DAMPING ENHANCEMENT THROUGH TPMS METAL–SILICONE POLYMER SYNERGY 28

2.1 Design of TPMS Structures 28

2.2 Finite Element Method Modeling 29

2.3 Polymer Material Selection 31

2.4 Damping Characterisation Methods 35

2.5 Fabrication and Experimental Validation 40

2.5.1 FEM Analysis 40

2.5.2 Manufacturing Process of Test Specimen 42

2.5.3 Modal Test & Validation 44

2.6 Summary 49

3 HYBRID VIBRATION CONTROL OF TPMS STRUCTURES VIA CLD SILICONE–VISCOELASTIC LAYERS 52

3.1 Design of CLD TPMS Structure 52

3.2 FEM Modeling 56

3.3 Damping Characterization Methods 58

3.3.1 The Logarithmic Decrement Method 59

3.3.2 Integral of Frequency Response Method 60

3.4 Manufacturing Process of Test Specimen 61

3.5 Results 63

3.5.1 FEM analysis 63

3.5.2 Modal test and validation 64

3.5.3 Time domain damping results 67

3.5.4 IFR results 69

3.6 Summary 70

4 AI-DRIVEN PARTICLE DAMPER OPTIMIZATION: FEM, ANN, AND GENETIC ALGORITHM INTEGRATION 75

4.1 Concept of Design of Experiments (DoEs) 75

4.2 Manufacturing Process of Test Specimen 78

4.3 Damping Characterization Method 78

4.4 FEM Modeling Approach 82

4.5 Optimization Algorithm 87

4.5.1 Design Parameters and Feature Set 89

4.5.2 Network Architecture 91

4.5.3 Training Procedure 92

4.5.4 Genetic Algorithm for Design Optimization 93

4.6 Results & Summary 98

5 CONCLUSIONS 102

6 FUTURE WORK 105

REFERENCES 106
VITA 116

LIST OF TABLES

Table 2.1: Material card parameters [99] 31

Table 2.2: Modal Test Results. 47

Table 2.3: Damping Ratio (ξ) and Settling Time. 49

Table 2.4: Comparison of FEM and experimental results. 51

Table 3.1: Material parameters used in FEM model. 58

Table 3.2: Comparison of FEM and experimental results. 68

Table 3.3: Damping ratio (δ) and settling time. 69

Table 3.4: IFR Results ($\frac{\mathrm{ms}^{-2}}{\mathrm{N\,Hz}}$). 70

Table 4.1: Experimental Groups and Parameter Definitions 76

Table 4.2: Specimen design parameters 77

Table 4.3: Comparison of Test and FEM Frequency Results 85

Table 4.4: Optimization Problem Formulation 88

LIST OF FIGURES

Figure 2.1: Primitive lattice's (a) iso-surface (b) unit cell with relative density $\rho^* = 0.2$ and (c) fabricated structure. 30

Figure 2.2: FEM model of hybrid structure. 32

Figure 2.3: Density - Mechanical loss coefficient graph [100]. 34

Figure 2.4: Density – Acoustic velocity graph [100]. 35

Figure 2.5: HPBW method for damping [102]. 36

Figure 2.6: Nyquist Diagrams Parameters [101]. 38

Figure 2.7: Logarithmic decrement technique parameters [105]. 39

Figure 2.8: Acceleration FRFs of FEM Analysis. 41

Figure 2.9: Mode Shapes from FEM Analysis. 41

Figure 2.10: Additively fabricating lattice illustration. 43

Figure 2.11: Fabricated metal-silicone hybrid structure. 44

Figure 2.12: Modal test setup. 46

Figure 2.13: Comparison of the test results in terms of accelerance: hybrid vs. metal parts. 46

Figure 2.14: Acceleration vs time history. 48

Figure 3.1: The design methodology for the creation of the metal part of the CLD TPMS 55

Figure 3.2: Design of CLD TPMS Structures 56

Figure 3.3: FEM model of hybrid structure 57

Figure 3.4: The logarithmic decrement 60

Figure 3.5: The manufacturing process of the test specimen 62

Figure 3.6: Fabricated metal and hybrid CLD structures 63

Figure 3.7: Modes and mode shapes of the metal and hybrid CLD structure from FEM analysis 64

Figure 3.8: Modal Test Setup 66

Figure 3.9: Comparison of the test results in terms of accelerance: metal structure vs. hybrid CLD structure 67

Figure 3.10: Acceleration vs time history 69

Figure 4.1: Side view of the test specimens 77

Figure 4.2: Visualization of the particle damping effect in modal test transfer functions..... 79

Figure 4.3: HPBW method for damping..... 80

Figure 4.4: Modal test setup..... 82

Figure 4.5: FEM Model 83

Figure 4.6: FEM Elements a) CDAMP4 element, and b) CONM2 and RBE3 element 84

Figure 4.7: Mode shapes from (a) modal test, and (b) FEM 84

Figure 4.8: Displacement FRF response between input (point 1) and output (point 2) 86

Figure 4.9: Relative error between FEM and modal test 87

Figure 4.10: Overall Workflow: GA + ANN Surrogate for Beam Cavity Optimization 89

Figure 4.11: ANN Diagram 92

Figure 4.12: Convergence History Performace of the Optimization Code a) without ANN integration, b) with ANN Integration 97

Figure 4.13: Optimized Beam Design Plot & 3D Model 99

LIST OF ACRONYMS AND ABBREVIATIONS

ANN	Artificial Neural Network
CDAMP4	Discrete Damper Element 4
CLD	Constrained Layer Damping
CONM2	Concentrated Mass Element 2
DEM	Discrete Element Method
DoE	Design of Experiments
FEM	Finite Element Method
FRF	Frequency Response Function
GA	Genetic Algorithm
HPBW	Half-Power Bandwidth
IFR	Integral of Frequency Response
IPC	Interpenetrating Phase Composite
LPBF	Laser Powder Bed Fusion
MISO	Multiple Input Single Output
RBE3	Rigid Body Element 3
RSS	Root Sum of Squares
SLM	Selective Laser Melting

TPMS	Triply Periodic Minimal Surface
WEDM	Wire Electrical Discharge Machining

1. INTRODUCTION

1.1 Literature Review

In this chapter, the literature on relevant topics is presented. More specifically, it covers the literature on damping characteristics through hybridization studies of TPMS structures (Section 1.1.1), hybrid approaches combining TPMS perspectives with CLD hybrid structure studies (Section 1.1.2), and the optimization of particle dampers for vibration control studies (Section 1.1.3) in detail.

1.1.1 Damping Enhancement through TPMS Metal–Silicone Polymer Synergy

Additive manufacturing of TPMS structures has drawn considerable interest in recent years because of their special geometry and mechanical performance. These structures can reduce surface area while preserving a continuous repeating pattern in three dimensions, which leads to a high strength-to-weight ratio and favorable stiffness properties [1, 2]. As a result, TPMS structures have become strong candidates for various mechanical applications, including lightweight parts in industries such as aerospace and automotive. Another advantage of producing TPMS structures via additive manufacturing is the ability to adjust pore sizes and overall dimensions without major cost increases [3, 4]. This design freedom allows for improved efficiency and better customization, making TPMS structures useful in areas like filtration, biomedical implants, and energy absorption systems. Ongoing research also focuses on refining printing processes and choosing suitable materials to maximize the mechanical performance and reliability of these TPMS-based components.

Obtaining optimal damping behavior is a crucial aspect in engineering applications; however, it can also be a challenging task because of the trade-offs between the

stiffness and damping properties of systems, fatigue, durability, and cost considerations. Although there are many optimization studies on the improvement of TPMS structures' stiffness properties, literature on damping characterization of these structures are limited. Characterization and optimization of damping in TMPS structures and metamaterials are actively ongoing, as in many current engineering topics.

Monkova et al. [5] explored the mechanical vibration damping and compression properties of lattice structures, highlighting how variations in lattice configurations influence damping performance. Similarly, Rajpal et al. [6] focused on parametric studies regarding the bending stiffness and damping ratio of sandwich structures, providing insights into the interaction between structural and material properties. Abusabir et al. [7] extended this research by examining the viscoelastic behavior of architected 3D-printed cubic lattice structures, demonstrating their potential in enhancing damping characteristics.

The impact of volumetric density on damping behavior has been extensively studied. Xu et al. [8] investigated two-phase lightweight carbon fiber-reinforced polymer microlattices, demonstrating how optimized densities contribute to superior stiffness and damping properties. Elmadih et al. [9] focused on vibration bandgaps within surface-based lattices, emphasizing their effectiveness in isolating vibrations. Zhang et al. [10] proposed a porous lattice structure with independently adjustable pore sizes and porosities, showing significant advancements in the field of damping optimization for biomedical applications.

Another promising area of research involves the use of multi-material layer structures. Prajapati et al. [11] demonstrated the advantages of combining lightweight closed-cell foam-filled lattice structures in multi-material additive manufacturing for improved mechanical and damping properties. Ehlers et al. [12] proposed particle dampers specifically designed for additive manufacturing applications, highlighting the role of embedded

damping elements in lattice structures. Furthermore, Guo et al. [13] carried out numerical and experimental studies on additively manufactured particle dampers at low frequencies, validating their effectiveness in dissipating vibrational energy.

These findings collectively underscore the importance of lattice type, volumetric density, and material combinations in achieving optimal damping behavior in TPMS structures. The integration of advanced manufacturing techniques, such as additive manufacturing, continues to drive innovation in the field, enabling the development of highly customized and effective damping solutions.

Polymers are preferred materials in many engineering applications requiring damping performance due to their unique mechanical properties and ability to absorb mechanical energy owing to their atomic structures. With their distinctive capabilities, such as low elastic modulus values and high damping capacities, polymers can impart desired capabilities to engineering systems, such as reduction of vibration amplitude and energy absorption under dynamic loads for stable performance in engineering systems. Silicone, which is a member of this material family, stands out from other members of the material family with its high-temperature resistance, oxidation resistance, chemical resistance, and high elasticity properties. Its high damping capacity makes it a good damping system element for many engineering systems. These aspects have been extensively studied, and we will detail these studies in the subsequent sections.

Chakraborty and Ratna [14] comprehensively reviewed the use of polymers in vibration damping applications, emphasizing their effectiveness in dissipating mechanical energy under various loading conditions. Badkar and Benal [15] used the half-power bandwidth method to estimate the damping ratio of silicone rubber, providing valuable insights into its energy dissipation properties. Yu et al. [16] investigated the dynamic characteristics of silicone rubber isolators, highlighting their suitability for vibration isolation in engineering systems. Similarly, Zhang et al. [17] studied the mechanical and thermal

properties of silicone rubber/EPDM damping materials, demonstrating their enhanced performance under thermal and mechanical stresses. Recently, Lin et al. [18] analyzed the viscoelastic behavior of silicone composites reinforced with graphene nanoplatelets, showcasing enhanced damping properties and mechanical stability. Furthermore, Chen et al. [19] investigated the role of microstructural modifications in improving the damping efficiency of silicone-based materials under cyclic loading. Lastly, Ahmed et al. [20] demonstrated the effectiveness of 3D-printed silicone structures in energy absorption and vibration control, highlighting the advantages of advanced manufacturing techniques in tailoring material properties.

These studies collectively demonstrate the critical role of silicone-based materials in engineering applications requiring high damping performance. Their unique combination of mechanical, thermal, and chemical properties makes them indispensable for a wide range of applications, from vibration isolation to dynamic load management.

The unique damping properties of polymer materials are utilized in various hybrid structures by combining them with the desired engineering properties of other materials to achieve superior performance. Interpenetrating Phase Composite (IPC) materials, which have been the subject of much research in recent years, are examples of such hybrid structures. In this composite approach, materials consisting of two or more interpenetrating phases occupy the same volume. In these materials, the phases are continuous and interconnected, and they can be made up of different materials with different properties. These aspects have been extensively studied, and we will detail these studies in the subsequent sections.

Liu et al. [21] analyzed constrained layer damping tool holders with IPC designs, demonstrating their effectiveness in enhancing stability during turning processes by leveraging the unique damping properties of polymers. Fang et al. [22] further explored the potential of IPC materials in topology optimization, focusing on maximizing the modal

loss factor of plates with constrained layer damping treatments, which is critical in vibration suppression applications. Dalaq et al. [23] investigated the elastic properties of IPC materials with architecture 3D sheet reinforcements, using finite element methods to predict their effective properties. These studies reveal the versatility of IPCs in improving mechanical and dynamic performance.

From the perspective of rigidity, Hussain et al. [24] examined the integration of IPCs into tendon-driven modular grippers, highlighting their ability to maintain structural stiffness while allowing for soft-rigid hybrid designs. Singh et al. [25] and Guo et al. [26] investigated the energy absorption capacity of IPCs, focusing on network-based stochastic designs and TPMS lattice structures, respectively. Their findings underscore the adaptability of IPCs in applications demanding high energy dissipation. Furthermore, Betters et al. [27] examined the elastic properties of IPCs, emphasizing how internal features in additive manufacturing processes can dynamically modify stiffness to meet specific application requirements.

These studies collectively showcase the significant potential of IPC materials in hybrid structures, combining polymer damping properties with complementary material attributes to meet diverse engineering demands. Their contributions to rigidity, energy absorption, and elastic properties underline the critical role of IPCs in advancing material engineering solutions.

After this detailed literature review, the literature gap our study addresses is elaborated under the relevant section of the thesis.The methods, validations, and numerical and experimental results are presented in Chapter 2.

1.1.2 Hybrid Vibration Control of TPMS Structures via CLD Silicone– Viscoelastic Layers

Contemporary engineering practice emphasizes the pivotal role of structural design and vibration mitigation. Lightweight, resilient structures adept at effectively managing vibrations are indispensable across various industrial domains. An important aspect of this study is the selection of the TPMS architecture for vibrational damping applications. TPMS structures, with their continuous smooth surfaces and high surface area, provide uniform stress distribution, supporting efficient energy dissipation and enhancing structural damping. Their complex and periodic geometries allow vibrational energy to be evenly distributed throughout the structure, reducing localized resonances and improving overall vibration damping performance. They exhibit the potential to increase surface area while preserving a recurrent three-dimensional pattern, resulting in a superior strength-to-weight ratio, stiffness, and other advantageous mechanical properties [28]. In contrast, alternative lattice structures like truss or octet lattices may exhibit localized stress concentrations and anisotropic properties, leading to inconsistent damping performance and challenges in integrating damping materials. Therefore, TPMS architecture offers distinct advantages over traditional lattice structures for developing hybrid structures with superior damping characteristics. These inherent properties of TPMS architecture render them one of the optimal selections for engineering applications that necessitate stringent vibration damping specifications.

Attaining optimal damping behavior stands as a paramount concern in engineering applications; however, due to the trade-offs among system stiffness, damping, durability, and cost, it remains a challenging endeavor. Despite numerous optimization studies aimed at enhancing the stiffness characteristics of TPMS structures, the literature pertaining to the damping characterization of these structures is limited. Many previous metamaterial studies have primarily focused on static properties such as strength and stiffness, often

neglecting dynamic properties like damping and vibration attenuation, which are crucial for real-world engineering applications. This imbalance highlights a significant gap in the research landscape, prompting the need for a comprehensive investigation into the dynamic performance of these advanced materials.

Ren et al. [29] and Feng et al. [30] analyzed the stiffness optimization of TPMS lattice structures, revealing how transition boundaries and lattice configurations affect their mechanical performance. While these studies provide valuable insights into enhancing stiffness, they do not delve deeply into the dynamic properties such as damping and vibration attenuation. Krishnan et al. [31] and Fu et al. [32] extended this understanding by examining the effects of relative density on the stiffness and dynamic behaviors of TPMS structures. Fu et al. experimentally investigated the nonlinear dynamic behaviors of TPMS structures, bridging the gap between theoretical models and practical applications. These findings underline the intricate relationship between material density and damping performance, laying the groundwork for further exploration.

Recent advancements have also seen the exploration of multi-layered and multi-cell lattice structures for enhanced damping performance. Zhang et al. [33] demonstrated the vibration characteristics of additive manufactured IWP-type TPMS lattice structures, showcasing their potential for high-frequency damping applications. Similarly, Jin et al. [34] introduced multicell interlacing Gyroid lattice structures, fabricated using laser powder bed fusion, and emphasized their ultra-high hyperelastic response and suitability for dynamic load-bearing applications. Gharehbaghi and Farrokhabadi [35] investigated bi-material lattice structures based on quadrilateral bipyramid unit cells, revealing significant energy absorption capacities that make them suitable for impact mitigation scenarios.

Zhang et al. [36] expanded on these concepts by introducing multi-dimensional hybridized TPMS structures with high energy absorption capabilities, emphasizing the role of hybrid philosophies in achieving superior damping behavior. Lastly, Kim et al.

[37] explored the application of TPMS-based auxetic structures for high-performance airless tires, demonstrating their variable stiffness properties under deformation and their inherent hysteretic damping capabilities.

These studies collectively reveal the untapped potential of TPMS structures in dynamic applications, especially for damping and vibration control. By systematically tailoring parameters such as lattice configuration, relative density, and material composition, researchers can optimize these structures to meet the demanding requirements of modern engineering applications. The integration of multi-layer and hybrid philosophies further enriches the functional capabilities of TPMS structures, paving the way for innovative solutions in fields ranging from automotive to aerospace engineering.

However, their intrinsic damping characteristics often fall short under dynamic loading conditions, making them inadequate for high-performance damping applications without further optimization or hybridization strategies. While this limitation identifies them as potential candidates for alternative passive damping solutions, their insufficiency for dynamic operational conditions in most engineering applications necessitates the exploration of hybrid approaches. These strategies aim to combine materials with complementary properties to enhance overall damping performance and address the deficiencies of standalone materials.

There is a growing interest in utilizing structures with hybrid damping capabilities to overcome these limitations. Studies in this area have demonstrated that hybrid approaches can provide a viable alternative by integrating materials with distinct yet synergistic properties. For instance, Ozden et al. [38] investigated the enhancement of damping characteristics through the hybridization of TPMS additive metals and silicone polymers. Their research highlighted the synergistic effects of combining the high stiffness and durability of TPMS structures with the superior damping and energy dissipation properties of silicone polymers, resulting in significantly improved dynamic performance.

The findings by Ozden et al. [38] emphasize the importance of hybridization in developing advanced damping solutions. By leveraging the unique attributes of each material, hybrid designs not only enhance damping performance but also expand the applicability of these materials to a broader range of engineering challenges. These hybrid structures pave the way for innovations in passive damping systems, ensuring reliable performance under dynamic loading conditions.

CLD stands as a well-established passive vibration attenuation technique, renowned for its efficacy in diverse engineering domains. The operational concept of CLD involves the absorption and dissipation of vibrations by the upper layer, leveraging the underlying viscoelastic damping material. This mechanism effectively reduces the propagation and dispersion of vibrations, thereby mitigating undesirable noise and vibration levels. By integrating these principles, CLD has become a cornerstone in the design of systems where vibration control is critical [39].

Baz [39] provides a comprehensive exploration of both active and passive vibration damping techniques, with a particular emphasis on the fundamental principles and applications of CLD. The study underscores the critical role of viscoelastic materials in energy dissipation, highlighting their ability to convert mechanical energy into heat, thus minimizing vibration amplitude. This conversion not only enhances the performance of engineering systems but also extends their operational lifespan by reducing structural fatigue.

Building on these foundational concepts, Jackstadt et al. [40] present an analytical modeling approach for investigating CLD in hybrid laminates. Their work employs a unified plate formulation to predict the damping performance of hybrid structures, offering valuable insights into the optimization of material layers for specific engineering applications. By examining various configurations, the study demonstrates how tailored CLD designs can significantly improve vibration attenuation while maintaining structural

integrity.

CLD is an application that is continually evolving both industrially and academically, with numerous active studies focusing on this subject in literature. Foremost among these studies are optimization efforts in CLD applications. Such studies have conducted optimization using various design and material parameters, including those in the polymer layers. These optimization efforts have been aligned with performance criteria such as acoustics [41] and vibrations [42]. For example, Ling et al. [41] explored topology optimization of constrained layer damping plates coupled with an acoustical cavity, demonstrating the impact of structural configurations on sound insulation. Similarly, Madeira et al. [42] applied multiobjective optimization for vibration reduction in composite plate structures, emphasizing the balance between structural efficiency and damping performance.

Active and passive isolation strategies are another contemporary area of research in CLD applications. Researchers have explored active CLD applications through control algorithms and signal optimization [43, 44], examined thermal effects under dynamic conditions [45], and analyzed design criteria [46] with a focus on performance metrics like acoustics [47] and vibration [48]. For instance, Li et al. [43] studied the influence of control signal phase on the vibration reduction effect in active CLD systems, while Chi et al. [44] applied algorithms to enhance vibration control of piezoelectric beams. These studies underscore the role of advanced control strategies in achieving effective active damping. Fang et al. [45] further examined the thermal effects on active constrained layer damping treatments, providing insights into material behavior under varying temperature fields.

In passive CLD applications, ongoing studies are actively investigating impact [49], acoustics [50], and vibration [51, 52, 53] performances. Jackstadt et al. [49] analyzed the influence of low-velocity impact damage on hybrid elastomer-metal laminates,

revealing significant effects on constrained-layer damping performance. Wang and Min [50] studied the damping contribution of viscoelastic cores on airborne sound insulation in finite constrained layer damping panels, particularly at low and middle frequencies. Gröhlich et al. [51] introduced a novel approach for shape optimization of CLD treatments across varying ambient temperatures, expanding the possibilities for customized passive damping solutions.

Further research continues to develop FEM models [54] of CLD applications. Zhang et al. [54] provided finite element dynamic modeling and vibration reduction analysis of bolted thin plates with partially attached constrained layer damping, bridging the gap between theoretical and experimental insights. Comparative performance studies [55] between active and passive applications also represent a significant area of current research. Gupta et al. [55] compared the damping capabilities of viscoelastic composites for active and passive constrained layer damping, highlighting the relative merits of each approach in different operational scenarios.

CLD and various approaches are widely implemented across a variety of commercial sectors, including aerospace [56] and automotive [57]. In aerospace, Trzepieciński et al. [56] explored the application of incremental sheet forming of metal-based composites, while Xiao et al. [57] reviewed the mechanical properties of hybrid fiber metal laminates in the automotive industry. The performance improvements of CLD applications in automotive contexts have been particularly evident in enhancing interior quietness, a critical factor for in-vehicle comfort [58]. Gur et al. [58] demonstrated the effectiveness of radiating panel NVH performance evaluations in vehicle design, emphasizing CLD's reliability as a vibration performance solution.

These studies collectively illustrate the multifaceted potential of CLD applications across various industries. By leveraging both active and passive strategies, researchers and practitioners continue to optimize CLD systems to meet the dynamic demands of modern

engineering challenges.

Following this detailed literature review, the literature gap addressed by our study is elaborated under the relevant section of the thesis. The methods, validations, and numerical and experimental results are presented in Chapter 3.

1.1.3 AI-Driven Particle Damper Optimization: FEM, ANN, and Genetic Algorithm Integration

Damping characteristics have long been a critical design criterion in engineering applications, serving as a primary focus in both academic research and industrial practices [59, 60]. The control of vibrations is paramount in fields such as aerospace, automotive, and civil engineering, where excessive vibrations can lead to structural fatigue, diminished performance, and even catastrophic failures. For instance, in aerospace engineering, vibrations can compromise the integrity of aircraft components, while in civil engineering, they can cause discomfort or damage in buildings and bridges. Traditional damping methods, including viscoelastic materials and tuned mass dampers, have been extensively employed to mitigate these issues [38, 61]. However, these conventional approaches often come with significant drawbacks. Viscoelastic materials, for example, can add substantial weight to the structure, which is particularly undesirable in weight-sensitive applications like aircraft or spacecraft. Additionally, these materials may degrade over time due to environmental factors, reducing their effectiveness. Tuned mass dampers, while effective for specific frequency ranges, require precise tuning and can introduce additional complexity and cost to the system. Their performance is also limited to narrow frequency bands, making them less versatile for applications with varying vibrational characteristics. These limitations have prompted the search for alternative damping solutions that can provide effective vibration attenuation without compromising structural integrity or adding excessive weight.

In recent years, particle damping has emerged as a promising alternative that addresses many of the shortcomings of traditional methods [62]. Particle damping involves the use of granular materials, such as metal or polymer particles, confined within cavities integrated into the structure. As the structure vibrates, the particles move and collide with each other and the cavity walls, dissipating vibrational energy through inelastic collisions and friction. This mechanism allows for effective damping across a broad range of frequencies, making particle dampers versatile and adaptable to various applications. Unlike tuned mass dampers, particle dampers do not require precise tuning and can be effective over a wider frequency spectrum. Furthermore, particle dampers can be designed to be passive, requiring no external power source, which enhances their reliability and reduces maintenance needs. Another advantage is that the particles can be made from materials that are compatible with the host structure, minimizing issues related to thermal expansion or chemical interactions.

The performance of particle damping systems is highly dependent on several factors, including particle size, shape, material properties, fill ratio, and the geometry of the cavities [63, 64, 65]. For example, particle size plays a crucial role in determining the frequency range over which the damper is effective; smaller particles generally provide better damping at higher frequencies due to their increased surface area and interaction rates, while larger particles are more suitable for lower frequencies. The shape of the particles can also influence damping efficiency; studies have shown that irregular shapes, such as angular or elongated particles, can enhance energy dissipation through increased friction and interlocking between particles compared to spherical particles. Material properties, such as density, coefficient of restitution, and surface roughness, affect the energy dissipation characteristics during collisions and frictional interactions. For instance, particles with a lower coefficient of restitution will dissipate more energy per collision, leading to higher damping. The fill ratio, or the volume fraction of the cavity occupied by particles,

is another critical parameter; there is often an optimal fill ratio that maximizes damping for a given system, beyond which further increases in particle volume can reduce damping effectiveness due to restricted particle movement. Additionally, the design of the cavities, including their size, shape, and location within the structure, plays a crucial role in determining the overall effectiveness of the damping system. Cavities placed near areas of high vibrational amplitude can be more effective, while the shape of the cavity can influence particle motion and interaction patterns.

The advent of additive manufacturing, also known as 3D printing, has significantly advanced the feasibility of implementing particle damping solutions in engineering systems [66]. Additive manufacturing allows for the creation of complex geometries that would be difficult or impossible to achieve with traditional manufacturing methods, such as subtractive processes or casting. This capability is particularly beneficial for particle damping, as it enables the precise integration of cavities of various shapes and sizes directly into the structure during the manufacturing process. For example, techniques like selective laser sintering (SLS) or fused deposition modeling (FDM) can be used to create intricate cavity networks within a component, tailored to optimize damping performance. Moreover, additive manufacturing supports a wide range of materials, including metals, polymers, and composites, allowing for the selection of materials that best suit the specific requirements of the damping system. This flexibility also extends to the particles themselves, which can be custom-designed in terms of size, shape, and material to achieve desired damping characteristics. By leveraging these capabilities, engineers can optimize parameters such as particle geometry, fill ratio, and distribution to achieve superior damping performance while maintaining the primary structural functions.

However, the implementation of particle damping systems is not without challenges. Design trade-offs must be carefully considered to ensure that the benefits of damping do not come at the expense of other critical performance metrics. For instance,

the addition of particle dampers can increase the overall mass of the structure, which may be undesirable in applications where weight is a critical factor, such as in aerospace or automotive industries. Additionally, the presence of particles and cavities can alter the natural frequencies of the structure, potentially affecting its dynamic response in unintended ways. For example, the added mass or the stiffness changes due to cavity integration might shift resonance frequencies, necessitating a redesign of the structure to avoid new resonance issues. The manufacturing process itself can also be complex, requiring precise control over the placement and containment of particles within the cavities, especially in additively manufactured parts where post-processing might be limited. Furthermore, accurately modeling the behavior of particle damping systems can be challenging due to the non-linear and stochastic nature of particle interactions, which complicates the prediction of damping performance. These challenges underscore the importance of a holistic design and optimization approach that takes into account all aspects of the system's performance, manufacturability, and operational requirements [67, 68, 69].

The literature is replete with studies investigating the operating principles of particle damping systems, providing valuable insights into the factors that influence their performance. These studies have focused on understanding how various particle parameters, such as size, shape, material, and fill ratio, affect the overall vibration damping mechanism. For example, research has shown that particle size plays a significant role in determining the frequency range over which the damper is effective; smaller particles generally provide better damping at higher frequencies due to their increased surface area and interaction rates [70]. Conversely, larger particles are more effective at lower frequencies, as they can store and dissipate more kinetic energy per collision. Particle shape has also been a subject of investigation, with studies comparing spherical particles to non-spherical ones. Findings suggest that irregular shapes can enhance energy dissipation through increased friction and interlocking between particles [71]. For instance, particles

with rough surfaces or angular geometries tend to lock together, creating more opportunities for frictional energy loss. Material properties, such as the coefficient of restitution and surface roughness, have been examined for their impact on the inelastic collisions and frictional interactions that underlie energy dissipation. Particles with lower coefficients of restitution dissipate more energy per collision, while higher surface roughness increases frictional forces. Furthermore, extensive research on fill ratio has revealed that there is often an optimal fill ratio for a given system, beyond which further increases in particle volume can actually decrease damping effectiveness due to reduced particle mobility [70, 71]. At very high fill ratios, particles become densely packed, limiting their ability to move and collide, thereby reducing the damping effect. These studies have provided engineers with critical guidance on which design factors most significantly influence damping efficiency and structural dynamic response.

Beyond parametric studies, numerous works have delved into the modal and vibrational behaviors of integrated structures equipped with particle dampers. These investigations typically involve detailed analyses of how the inclusion of particle dampers affects the natural frequencies, mode shapes, and damping ratios of the system [72, 73, 74, 75, 76, 77]. For instance, some studies have employed finite element modeling to simulate the behavior of particle dampers and validate their findings with experimental modal testing. FE models can capture the complex interactions between the structure and the particles, although they often require simplifications or approximations due to computational constraints. Other researchers have developed analytical models for simplified cases, such as single-degree-of-freedom systems with particle dampers, deriving closed-form solutions that offer insights into the fundamental mechanics of particle damping. These analytical approaches are useful for understanding basic principles but may not fully capture the complexities of real-world structures. Often, these studies incorporate

parametric analyses to explore the design space and identify trends, followed by optimization processes to determine the most effective configurations for specific applications [78, 79, 80, 81, 82]. Optimization objectives may include maximizing the damping ratio for a particular mode, minimizing the vibration amplitude at a critical frequency, or achieving a desired frequency response across a range of operating conditions. Through these efforts, a deeper understanding of how the incorporation of particle dampers influences both local responses (e.g., stress concentrations around cavities) and global responses (e.g., overall vibration levels and structural integrity) has been achieved, thereby facilitating more informed design decisions.

The optimization of particle damping systems presents a significant challenge due to the high-dimensional nature of the design space. This design space encompasses a multitude of parameters, including the location, number, size, and shape of cavities within the structure, the type and properties of the particles, the fill ratio, and the distribution of particles within the cavities. Each of these parameters can interact in complex ways, making it difficult to predict how changes in one parameter will affect the overall damping performance. For example, the optimal location of cavities may depend on the specific vibration modes that need to be damped, with cavities placed near antinodes being more effective for certain modes. Similarly, the fill ratio can influence the frequency range over which the damper is effective, with lower fill ratios favoring higher frequencies and vice versa. In optimization studies focused on vibration control and energy absorption, researchers have employed various techniques to navigate this complex design space. Some have used gradient-based optimization methods, such as the method of steepest descent, to fine-tune parameters for maximum damping efficiency [83].

However, these methods can be limited by their tendency to converge to local optima and their requirement for differentiable objective functions. To overcome these limitations, other studies have applied evolutionary algorithms, such as GAs, which are

better suited for exploring a broader range of configurations and identifying global optima [84, 85]. GAs, inspired by natural selection, iteratively evolve a population of candidate solutions through processes like selection, crossover, and mutation, allowing them to escape local optima and explore diverse regions of the design space. These optimization efforts aim to achieve the best possible performance in terms of reducing vibration amplitudes, enhancing energy dissipation, or meeting specific design constraints, such as weight or cost limitations. Additionally, recent advancements in machine learning and deep learning have opened new avenues for modeling and optimizing particle damping systems. Techniques such as ANNs have been used to create surrogate models that predict damping performance based on input parameters, significantly reducing the computational cost compared to traditional simulation methods [86]. By training ANNs on a dataset of simulation or experimental results, researchers can quickly evaluate the performance of new design configurations without running time-consuming simulations. Deep learning approaches, such as convolutional neural network, have been applied to analyze experimental data or simulation results, extracting patterns and relationships that may not be apparent through conventional analysis [87]. For instance, convolutional neural networks can be used to process images or sensor data to identify optimal particle distributions or detect defects in additively manufactured parts. These machine learning based methods have not only facilitated more efficient optimization but also provided deeper insights into the behavior of particle damping systems, inspiring the development of the hybrid structure presented in our study.

Traditional optimization methods, such as trial-and-error approaches and parametric studies, have been widely used in the past for designing and tuning particle damping systems. However, these methods often prove inadequate for several reasons. Trial-and-error is inherently time-consuming and may not lead to the optimal solution, especially in high-dimensional design spaces where many parameters interact in non-intuitive ways.

Parametric studies, which involve systematically varying one or more parameters while keeping others fixed, can provide valuable insights but are limited by the curse of dimensionality. As the number of parameters increases, the number of required simulations or experiments grows exponentially, making the computational or experimental cost prohibitive. Moreover, these methods typically explore only a small portion of the design space, risking the omission of better configurations that lie outside the investigated range. In recent years, advances in machine learning and metaheuristic algorithms have offered promising alternatives for efficiently exploring complex design spaces. Machine learning techniques, such as ANNs, can be trained on existing data to create predictive models that approximate the relationship between design parameters and performance metrics. These models, often referred to as surrogate models, can then be used to quickly evaluate a large number of potential configurations, significantly reducing the computational burden.

Metaheuristic algorithms, such as GAs and simulated annealing, are designed to search for global optima in complex, multimodal landscapes. For instance, GAs use principles of evolution, such as selection, crossover, and mutation, to iteratively improve a population of candidate solutions. These algorithms are particularly well-suited for problems where the objective function is non-linear, discontinuous, or difficult to model analytically, as is often the case in particle damping systems. In the context of particle damping optimization, ANNs can be employed to predict damping performance based on input parameters, while GAs can be used to search for the parameter combinations that maximize this performance [88]. The combination of these advanced methods allows for a more comprehensive exploration of the design space and increases the likelihood of finding optimal or near-optimal configurations while keeping computational costs manageable.

GAs have emerged as an effective tool for optimizing parameters in additive manufacturing processes and enhancing the quality of produced parts. Additive manufacturing

techniques, such as selective laser melting (SLM), involve numerous parameters—such as laser power, scanning speed, layer thickness, and hatch spacing—that significantly influence the mechanical properties, surface finish, and dimensional accuracy of the final product. Optimizing these parameters is critical but challenging due to their complex interactions and trade-offs. For example, increasing laser power may improve part density but can also lead to excessive heat input, resulting in thermal distortion or residual stresses. GAs are particularly well-suited for this task because of their ability to handle multi-objective optimization, where conflicting criteria, such as maximizing strength while minimizing porosity, must be balanced. In studies focusing on critical manufacturing parameters, researchers have developed hybrid GA approaches that combine GAs with other techniques, such as response surface methodology, for the multi-objective optimization of key parameters in the SLM process [89]. Response surface methodology can be used to create approximate models of the objective functions, which are then optimized using GAs to find Pareto-optimal solutions. These hybrid methods leverage the global search capabilities of GAs to efficiently explore the parameter space and identify solutions that represent the best trade-offs among the objectives. Similarly, GA-based optimization methods aimed at reducing defects commonly encountered in additive manufacturing, such as porosity, residual stresses, and surface roughness, have significantly contributed to achieving performance levels close to the global optimum [90]. By iteratively evolving a population of parameter sets, GAs can navigate the complex, non-linear relationships between process parameters and part quality, avoiding local optima that might trap gradient-based methods. Furthermore, GAs have found applications beyond process parameter optimization in additive manufacturing. They are currently employed as a powerful optimization tool in the design of TPMS lattices, which are gaining popularity in additive manufacturing for their unique mechanical properties and lightweight

structures. TPMS lattices are characterized by their periodic, smooth surfaces that minimize surface area, making them ideal for applications requiring high strength-to-weight ratios, such as in aerospace or biomedical implants. The design of TPMS lattices involves adjusting parameters such as unit cell size, wall thickness, and orientation to achieve desired performance metrics like stiffness, strength, or energy absorption. GAs facilitate this optimization by efficiently searching the vast design space to identify configurations that meet the specified criteria [91]. For example, a GA can be used to optimize the unit cell parameters of a TPMS lattice to maximize its energy absorption capacity under impact loading, while ensuring that the structure remains within manufacturing constraints. These examples illustrate the versatility and effectiveness of GAs in addressing a wide range of optimization challenges in additive manufacturing, from process control to structural design.

Similarly, ANNs play a crucial role in modeling the complex and non-linear relationships between 3D printing parameters and the resulting mechanical properties in additive manufacturing processes. ANNs, with their ability to learn from data and approximate arbitrary functions, have proven to be invaluable tools for tackling this challenge. They consist of interconnected nodes or neurons organized in layers, which can be trained on experimental or simulation data to capture the intricate mappings between inputs (process parameters) and outputs (mechanical properties). For instance, ANNs have been developed to predict properties such as tensile strength, fatigue life, and surface roughness based on parameters like laser power, scanning speed, and powder characteristics in 3D printing processes [92]. The training process involves adjusting the weights of the connections between neurons to minimize the error between predicted and actual outputs, typically using algorithms like backpropagation. Once trained, these models can provide rapid and accurate predictions, enabling engineers to optimize process parameters without

the need for extensive physical testing. This capability is particularly beneficial in scenarios where quick adjustments can be made during production to ensure part quality, such as in real-time process control systems. Beyond property prediction, ANNs have been applied to other critical aspects of additive manufacturing. For example, an ANN-based approach has been integrated into additive manufacturing systems to detect potential errors and defects, such as layer misalignment, porosity, or lack of fusion, at an early stage [93]. By analyzing in-situ monitoring data, such as thermal images, acoustic emissions, or laser scanning data, the ANN can identify anomalies in real-time, allowing for immediate corrective actions or termination of the process to prevent waste. This proactive defect detection can significantly reduce material waste and improve overall production efficiency. Additionally, studies have investigated the effects of design parameters on the performance of additively manufactured parts and used ANNs to model these relationships. For instance, in the design of lattice structures, ANNs can predict how variations in strut thickness, cell size, or topology affect mechanical properties like stiffness, strength, or energy absorption [94]. By providing a fast and accurate mapping from design parameters to performance metrics, ANNs enable the use of optimization algorithms to find designs that meet specific requirements. These studies demonstrate that ANNs serve as efficient tools in optimization studies by providing fast and reliable surrogate models that can be used in conjunction with optimization algorithms, such as GAs. The capacity of ANNs to model non-linear relationships and generalize from limited data offers critical advantages in the control and optimization of additive manufacturing processes, where experiments can be costly and time-consuming.

Following this detailed literature review, the research gap addressed by our study has been elaborated under the relevant section of the thesis.The methods, validations, and numerical and experimental results are presented in Chapter 4.

1.2 Research Gaps

This section outlines the key research gaps addressed in the three main components of this thesis. Although the literature presents substantial progress in the fields of hybrid materials, metamaterial damping systems, and particle dampers, several critical gaps remain unaddressed, particularly at the intersection of novel structural topologies, material integration, and computational optimization. By identifying and responding to these gaps, this thesis aims to contribute meaningful advancements to the field of structural damping.

While numerous studies have explored the damping behavior of polymers in hybrid configurations, there is a noticeable gap in the literature regarding the integration of additively manufactured TPMS metal structures with silicone polymers. Most existing works focus either on conventional metal-polymer interfaces or on the static mechanical benefits of TPMS geometries, without addressing their potential in dynamic vibration environments. Furthermore, limited attention has been given to how the intrinsic geometric advantages of TPMS, such as high surface area-to-volume ratio and tunable mechanical response, can be harnessed to enhance damping when combined with viscoelastic materials. The current body of research also lacks a detailed exploration of how these hybrid structures perform under both time-domain and frequency-domain excitations. Additionally, a systematic methodology that combines experimental validation with FEM-based modeling for these advanced material systems is yet to be fully developed. This study addresses these shortcomings by developing and characterizing hybrid materials composed of Cobalt-Chrome and aluminum TPMS structures filled with silicone polymers. These hybrid structures are experimentally and numerically evaluated for their enhanced damping characteristics, contributing to the broader understanding of multifunctional materials in structural vibration control. Although constrained layer damping is a well-established vibration mitigation technique in engineering, its integration into architected materials

such as TPMS structures remains underexplored. The current literature lacks studies that systematically combine the periodic design flexibility of metamaterials with the energy dissipation mechanisms offered by CLD. While isolated efforts exist to characterize the acoustic and mechanical benefits of either metamaterials or viscoelastic layer independently, there is limited understanding of their combined effect in a unified hybrid system. Most studies also fail to assess how the frequency response behavior of such systems evolves across a wide operational bandwidth, which is critical in real-world applications. Moreover, there is a methodological gap in using high-resolution voxel-based FEM models to simulate and predict the behavior of these hybrid damping materials. This study fills this gap by incorporating viscoelastic silicone polymer layers onto aluminum TPMS structures, leveraging both the structural tunability of metamaterials and the damping benefits of CLD. A voxel-based finite element modeling framework, validated through experimental testing, is used to capture and analyze the dynamic response of these novel hybrid systems, offering a new direction for advanced CLD applications in structural design.

Despite advancements in the field, comprehensive studies that integrate experimental, numerical, and optimization approaches in the design of particle damping systems remain scarce. While individual methods have been thoroughly investigated, their combined application offers synergistic benefits that have yet to be fully realized. In particular, the use of experimental modal testing, FE modeling, and hybrid optimization techniques involving ANNs and GAs has not been sufficiently explored in the context of particle damping systems. Experimental modal testing provides essential empirical data on the dynamic behavior of the structure, including natural frequencies, mode shapes, and damping ratios, which serve as benchmarks for validating numerical models. Techniques such as impact hammer testing or shaker excitation can be used to measure the frequency response functions of the structure, from which modal parameters can be extracted using methods like curve fitting or operational modal analysis. FE modeling, on the other hand,

allows for detailed simulations of structural response under various conditions without the need for physical prototypes, enabling the exploration of design alternatives. This is where optimization techniques, particularly ANNs and GAs, come into play. ANNs can be trained on a subset of FE simulation results or experimental data to create fast surrogate models that predict the performance of different design configurations. These surrogate models can then be used within a GA framework to efficiently search for optimal parameter sets that maximize damping performance while satisfying design constraints, such as weight limits or manufacturing feasibility. By combining these methods, an integrated framework can be established that leverages the strengths of each approach: the accuracy of experimental data, the flexibility of numerical modeling, and the efficiency of advanced optimization algorithms. This study aims to fill this gap by presenting such an integrated framework for the design and optimization of particle damping systems. Through this holistic approach, we seek to achieve superior vibration control performance, paving the way for more effective and efficient damping solutions in a wide range of engineering applications.

1.3 Objectives of the Thesis

The primary objective of this thesis is to advance the field of structural damping by exploring and optimizing innovative strategies for vibration control in engineering systems. Vibration suppression remains a critical challenge across industries such as aerospace, automotive, and civil engineering, where uncontrolled oscillations can compromise performance, safety, and structural integrity. Traditional damping solutions often fall short in addressing the demands of modern, complex systems, necessitating the development of novel materials and design methodologies. This thesis responds to this need by investigating three distinct yet complementary approaches: (1) the hybridization of additively manufactured TPMS metal structures with silicone polymers, (2) the integration

of metamaterials with CLD techniques using TPMS structures and viscoelastic polymers, and (3) the optimization of particle dampers through a hybrid computational framework. Each approach is rigorously evaluated using FEM, experimental modal testing, and advanced computational techniques to ensure both theoretical depth and practical relevance.

The first objective is to develop and characterize hybrid materials that combine additively manufactured TPMS structures specifically, Cobalt-Chrome (CoCr) and aluminum alloys with silicone polymers. TPMS structures, known for their lightweight architecture and high stiffness, are leveraged for their potential in vibration applications when enhanced with viscoelastic materials. This study aims to quantify the damping improvements achieved through this hybridization, with a focus on identifying the most effective damping mechanisms. Finite element modeling and experimental modal testing are employed to validate the enhancements in both time-domain and frequency-domain damping performance.

The second objective investigates the integration of metamaterials with CLD techniques by utilizing aluminum TPMS structures coated with viscoelastic silicone polymer layers. This approach aims to exploit the unique dynamic properties of metamaterials to achieve superior vibration suppression over a broad frequency range. The study uses voxel-based FEM models to analyze the damping behavior, with experimental testing conducted to validate the computational results. The goal is to establish measurable improvements in damping performance, contributing to the development of next-generation CLD applications.

The third objective focuses on optimizing the design and placement of particle dampers within structural systems using a hybrid computational framework that combines FEM, ANN, and GA. Although particle dampers are highly effective in dissipating vibrational energy, their nonlinear behavior makes them challenging to model and optimize. This research addresses these challenges by developing an ANN-based surrogate

model to predict damping performance efficiently, enabling the use of GA for rapid optimization. The objective is to achieve significant reductions in vibratory response while maintaining the mechanical feasibility of the damper configurations.

Together, these objectives aim to push the boundaries of current damping technologies by integrating advanced manufacturing, hybrid material systems, and computational intelligence. The thesis provides a comprehensive understanding of how these innovative strategies can be applied to real-world engineering problems, offering new avenues for the design of more resilient and efficient structural systems. Ultimately, this research contributes to the broader goal of enhancing vibration control in critical applications, thereby improving the performance, safety, and longevity of engineering structures.

2. DAMPING ENHANCEMENT THROUGH TPMS METAL–SILICONE POLYMER SYNERGY

Under this heading, the materials used in the study, as well as the numerical and experimental methods and the results, are detailed. Section 2 focuses on enhancing damping through the synergy between TPMS metal structures and silicone polymers. It begins with the design of TPMS structures (2.1), followed by FEM modeling (2.2) to simulate their behavior. The selection of suitable polymer materials (2.3) is then discussed, along with the methods used to characterize damping (2.4). The fabrication and experimental validation (2.5) section includes subsections on FEM analysis (2.5.1), the manufacturing process of test specimens (2.5.2), and modal testing and validation (2.5.3). The chapter concludes with a summary (2.6) of the findings.

2.1 Design of TPMS Structures

In this study, the primitive structure, a unique member of surface-based TPMS family, is used as a base material for fabricating a novel composite structure with enhanced damping properties. TPMS structures are unique geometric structures that exhibit a high degree of symmetry and are defined by a mathematical relationship between two interpenetrating periodic lattices. There are numerous variations of TPMS with different symmetries, shapes, and sizes, each with unique properties and potential applications. In this study, we utilize primitive structures as the fundamental building block for our composite material due to their simplicity and ease of fabrication. However, the methodology presented can also be applied to other TPMS structures.

The mathematical expressions of TPMS structures are complex and variable. However, in general, TPMS structures are created by assembling two-dimensional layers sequentially, and their mathematical expressions are usually represented as Fourier series

[95]. The coefficients expressing these series can be used to control TPMS topologies and their mechanical properties as well. The surface function equations that represent the explicit mathematical expressions of surface-based primitive lattice structure are given in Eq. (2.1):

$$u_p(x, y, z, t) = (\cos(k_x x) + \cos(k_y y) + \cos(k_z z))^2 - t^2 \tag{2.1}$$

where t is level-set parameter to control the offset value from the iso surface $U = 0$. $k_i\,(i = x, y, z)$ terms represent the periodicity of the TPMS structures in x, y, and z directions as given in Eq. (2.2):

$$k_i = 2\pi \frac{n_i}{l_i} \tag{2.2}$$

where n_i and l_i are the number of lattices and absolute size of the structure in x, y, and z directions.

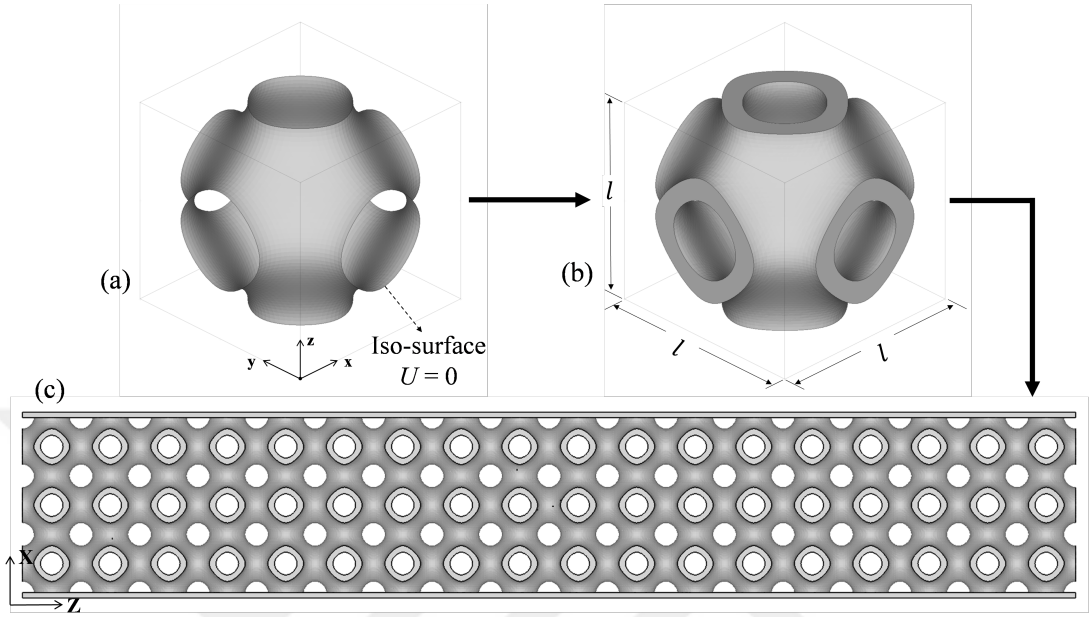
In this study, a primitive structure with a relative density, ρ^*, of 0.2 was used. The iso-surface, unit cell with relative density $\rho^* = 0.2$, and fabricated structure are presented in Figure 1 a to c, respectively.

To demonstrate and quantify the enhancement in the damping performance of the proposed composite structure, a test specimen geometry was proposed (see Figure 2.1 c). The 36×36×216 mm test specimen, consisting of primitive unit-cells with a 12 mm unit-cell size, was sandwiched between metallic plates with a 1 mm thickness. The void volume in the metallic core was then filled with a polymeric material.

2.2 Finite Element Method Modeling

FEM was used as the numerical analysis method in this study. To characterize the dynamic performance of the proposed test specimen, a comprehensive set of finite element analyses was performed. The dimensions and FEM model details of the test specimen are

Figure 2.1: *Primitive lattice's (a) iso-surface (b) unit cell with relative density* $\rho^* = 0.2$ *and (c) fabricated structure.*



illustrated in Figure 2.2. To construct the model, the lattice core was initially modelled using voxel elements generated through a MATLAB script. This approach was selected based on the computational advantages of voxel modelling for lattice structures, which have been extensively discussed in the literature [96]. Comparative studies have shown that voxel-based modelling not only simplifies the representation of complex geometries but also improves computational efficiency, particularly for large-scale simulations.

A mesh convergence study was conducted to determine the optimal number of elements through the thickness, ensuring the accuracy of the FEM results. This step followed the recommendations of prior studies that emphasize the importance of mesh refinement for capturing the dynamic response of complex structures [97]. For consistency, the polymeric volume was also modelled with voxel elements, aligning its mesh characteristics with those of the lattice core. The plates, on the other hand, were represented using shell

elements, with appropriate section properties assigned to reflect their thickness and mechanical behavior accurately.

The finite element models of the metal-only and hybrid configurations comprised 750K and 3.6M elements, respectively. In modelling the hybrid structure, the interaction nodes between the metal and polymer components were merged under the assumption of equivalent behavior. This assumption was justified by the need to balance computational accuracy with efficiency. Introducing contact formulations for these interfaces would have significantly increased the computational cost due to the high number of elements and nodes. By merging the nodes, the study effectively minimized computational time while maintaining the fidelity of the results. The decision to merge nodes aligns with established practices in FEM studies, where simplifying assumptions are often employed to address the trade-offs between model complexity and computational resources [98].

FEM modeling was conducted under free-free conditions without any preload or boundary conditions in two distinct approaches. Given that the examination of the hybrid structure's impact on damping capacity relative to the metal structure falls within the scope of this study, the nonlinear influences of preload and boundary conditions were excluded from the analyses. The relevant material properties used in the FEM model are presented in presented in Table 2.1 [99].

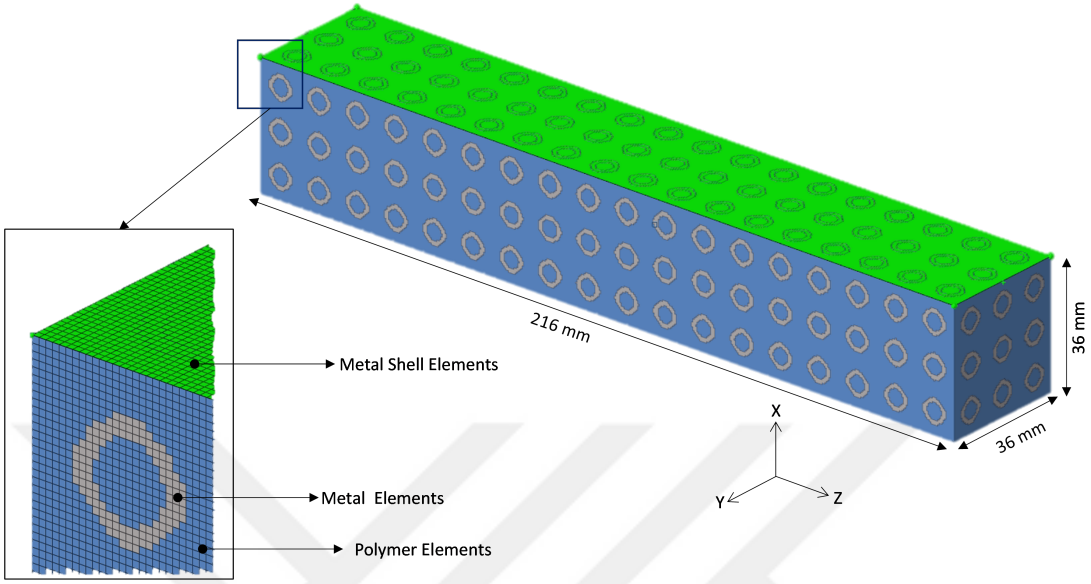
Table 2.1: *Material card parameters [99]*

Material	**Elastic Modulus (GPa)**	**Poisson's Ratio**	**Density (g/cm^3)**
CoCr	236	0.33	8.3
Silicone	0.03	0.47	1.1

2.3 Polymer Material Selection

Material assessment was predicated on a triad of selection criteria. The primary criterion is the material's density, with emphasis on its minimization to ensure the weight

Figure 2.2: *FEM model of hybrid structure.*



efficacy of the emergent structure remains unencumbered. Subsequently, the mechanical loss coefficient served as the second determinant, elucidating the material's intrinsic vibration attenuation attributes. The mechanical loss coefficient or damping coefficient, η, is the measurement of the absorption of vibrational energy of a material. Assuming a material is elastically loaded, the elastic energy (U) per unit volume under the force $\sigma_{\max}$ can be expressed as in Eq. (2.3):

$$U = \int_0^{\sigma_{\max}} \sigma \, d\varepsilon \approx \frac{\sigma_{\max}^2}{2E} \tag{2.3}$$

The energy dissipated or dampened, when the load is applied and removed, is given in Eq. (2.4):

$$\Delta U = \oint \sigma \, d\varepsilon \tag{2.4}$$

The loss coefficient is shown in Eq. (2.5):

$$\eta = \frac{\Delta U}{2\pi U} \tag{2.5}$$

The damping coefficient in the above formulation is dependent on time and cycling frequency. In the pursuit of constructing a hybrid structure via the integration of a polymer layer, the optimal criterion would be the selection of a polymer exhibiting an elevated tan delta value. Mechanical loss coefficient, also known as the tan δ, refers to the measure of a material's mechanical damping properties. It quantifies the energy dissipation of a material resulting from its non-elastic behavior. This metric serves as an indicator of the material's damping capacity, thereby enhancing its ability to absorb vibration energy effectively [100].

The final criterion is the acoustic velocity, denoting the propagation speed of an acoustic wave within a given medium. The sound transmission is invariably modulated by the medium's impedance, leading to energy dissipation. This metric elucidates the anticipated acoustic isolation proficiency of the prospective polymer selection. Notably, a correlation may exist between a material's acoustic isolation and its vibration-damping capacities. The inclusion of acoustic velocity as a selection metric also augments the foresight into the hybrid structure's applicability in prospective acoustic investigations.

Selection of the material was rigorously predicated upon the aforementioned attributes. For this endeavour, we consulted the comprehensive material repository in Ansys® GRANTA Research Selector. Polymers, encompassing categories such as composites, elastomers, foams, and plastics, were evaluated as potential candidates for the augmentation of the hybrid structure. A plot delineating the mechanical loss factor against density for these materials is illustrated in Figure 2.3 [100]. The material would exhibit a juxtaposition of minimal density and augmented mechanical loss coefficient. Tan δ serves as an indicator of a material's ability to respond to a vibration wave [64]. The graphical representation reveals the supremacy of low-modulus silicone material in this

realm. Complementarily, a criterion visualized through the acoustic velocity-density plot is elucidated in the subsequent Figure 2.4 [100]. The silicon-based materials assume a desired locus in this density-acoustic velocity matrix, epitomizing low-density and attenuated acoustic velocity attributes. Synthesizing these selection frameworks, notably the high tan δ and diminished acoustic velocity attributes, the silicon-based compounds were identified as preeminent, driven by their intrinsic compatibility characteristics.

Figure 2.3: *Density - Mechanical loss coefficient graph [100].*

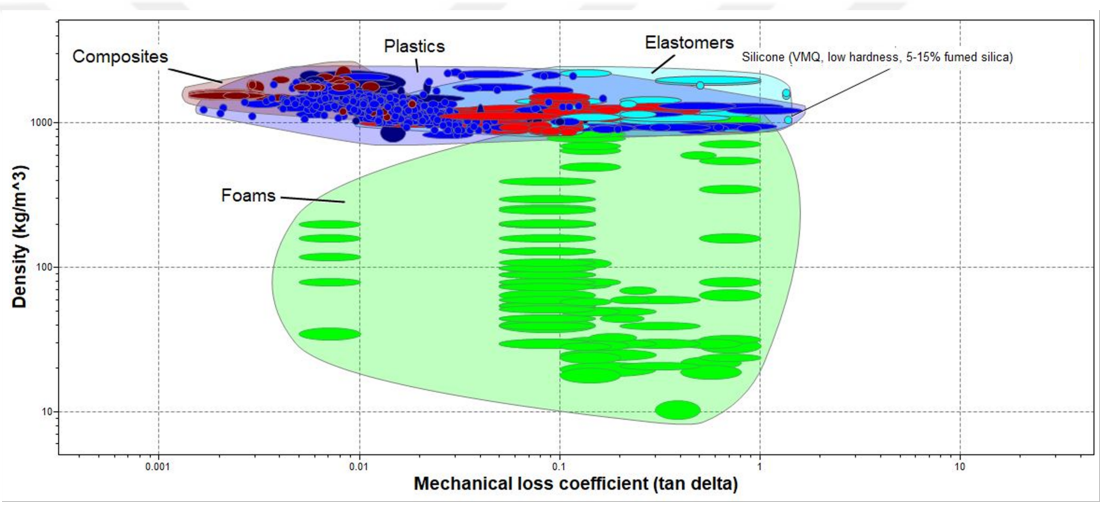
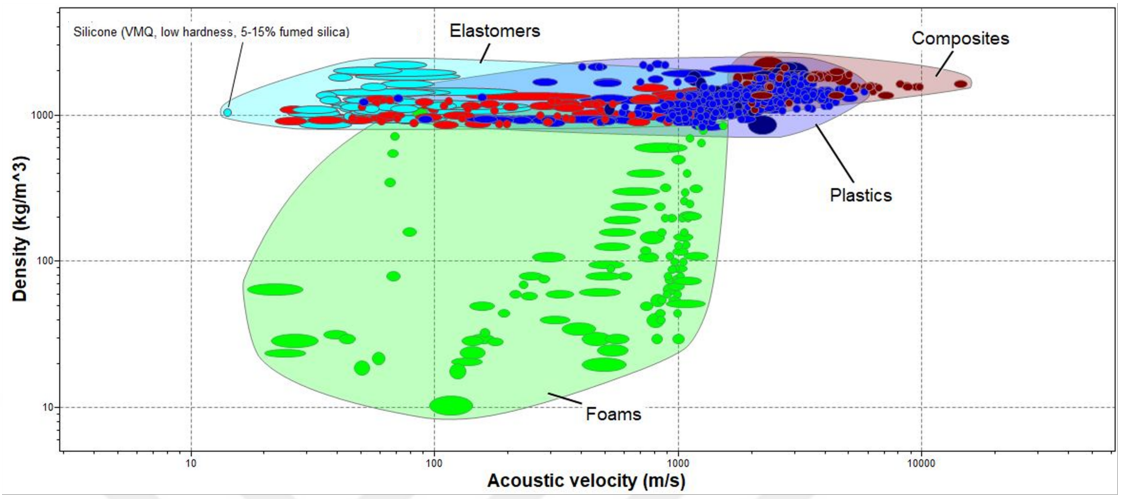


Figure 2.4: *Density – Acoustic velocity graph [100].*

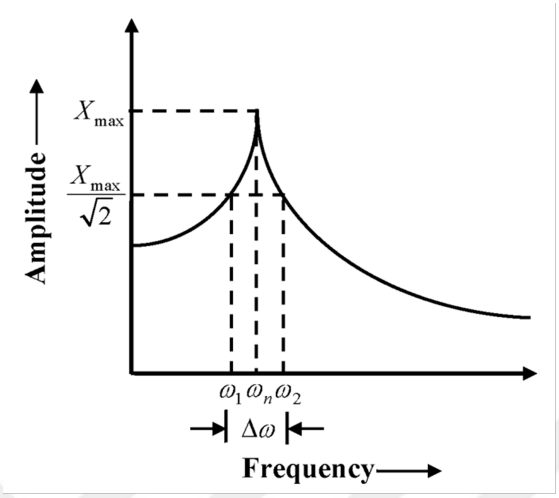


2.4 Damping Characterisation Methods

Determining the damping properties is an important step in understanding the vibration characteristics of structural systems. The half-power bandwidth method is a simple method for quick and accurate calculation of modal damping ratios. It can also determine the differences in damping ratios between different modes in a structure [101].

The HPBW was used to determine the half-power points in the frequency spectrum around a natural frequency. The half-power bandwidth is calculated by comparing the frequency range between the two points where the power is reduced to half in comparison to the amplitude at the natural frequency of this mode. The half-power points correspond to lower and upper frequencies where the maximum amplitude of the mode is 70.7% of its peak value (see Figure 2.5) [102]. The HPBW of a mode is the frequency difference between its half-power points.

Figure 2.5: *HPBW method for damping [102].*



Once HPBW is calculated, the modal damping ratio can be determined as the ratio between the HPBW and mid-frequency (or natural frequency) as given in Eq. (2.6). Subsequently, the damping ratio is determined by applying the formula for the half-power bandwidth as provided in the literature [102]. X_{max} represents maximum dynamic amplitude at resonance and resonant frequency (ω_n).

$$\zeta = \frac{\omega_2 - \omega_1}{\omega_n} \tag{2.6}$$

In characterizing the damping behaviour of dynamic systems, two pivotal parameters—the half, power bandwidth ($\Delta\omega$) and the quality factor (Q-factor), stand out as quintessential descriptors for resonance and energy dissipation attributes of the system. The Q-factor offers insight into the sharpness of resonance and is formulated as the inverse of the ratio of the half-power bandwidth to the resonant frequency.

Intrinsically, there exists a reciprocal relationship between these parameters: a pronounced, high Q-factor typifies a system with a sharply delineated resonance peak,

suggestive of low damping, while a diminished Q-factor corresponds to a broader resonance spectrum, indicative of augmented damping [103]. Concurrently, the damping ratio (ζ) is derived as:

$$\zeta = \frac{1}{2Q} \tag{2.7}$$

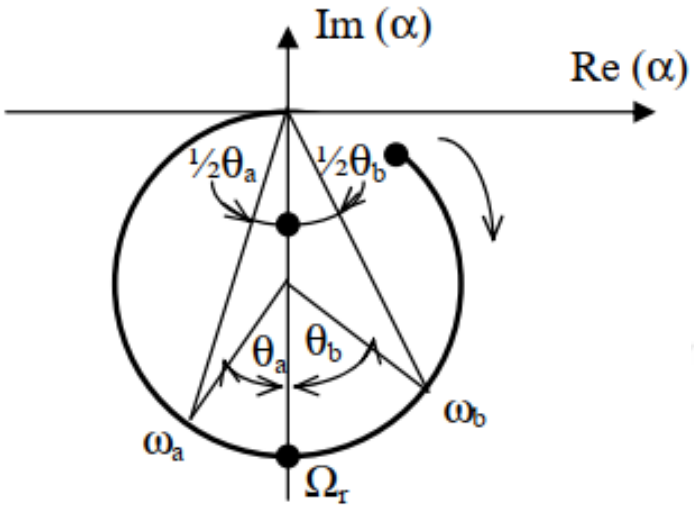
This serves as an auxiliary gauge to discern the system's transient oscillation decay and response dynamics.

In certain instances, Q-factor analysis may prove inefficient, particularly when applied to closely spaced resonant peaks, resulting in unreliable outcomes. The inefficiency arises from the proximity of the half-power points selected as the calculation parameter [104].

In light of the inefficiency observed with the Q factor at resonance peaks in close proximity, we opted to analyze the test data using the Nyquist diagram under such conditions. The Nyquist diagram leverages phase information alongside the amplitude parameter to ascertain modal damping. This characteristic renders the method effective in characterizing damping even when dealing with resonance peaks in close proximity. The distinct phase behavior associated with each modal resonance facilitates the determination of modal behavior and damping, enhancing the method's efficiency [104].

The Nyquist diagram determines damping by employing the angles derived from the circle fit method applied to the resonance and the two frequencies closest to this resonance frequency. The parameters of a sample Nyquist diagram are shown in Figure 2.6. The damping ratio, ζ_{ND}, is given in Eq. (2.8).

Figure 2.6: *Nyquist Diagrams Parameters [101].*



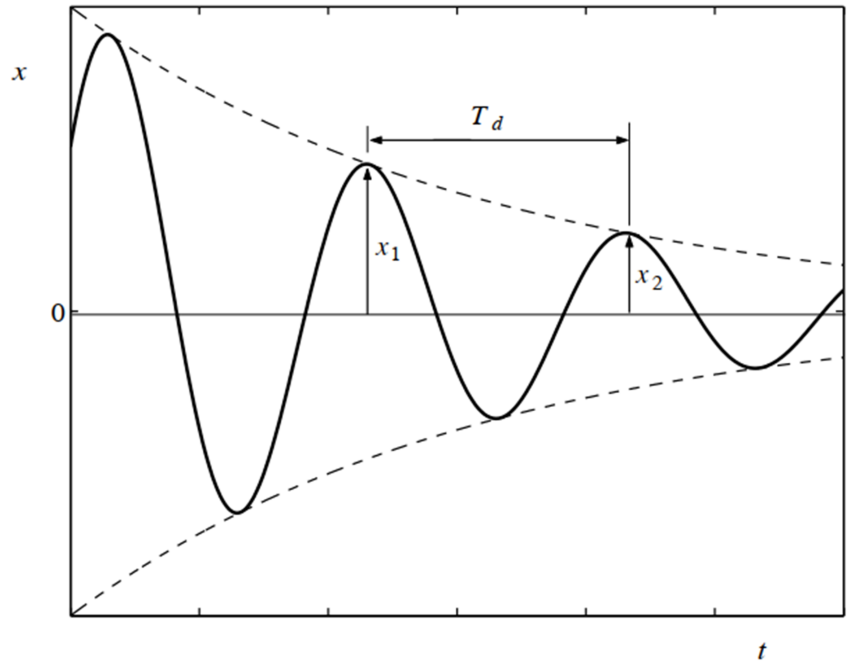
$$\zeta_{ND} = 2 \cdot \frac{\omega_a - \omega_b}{\Omega_r \cdot (\tan(\theta_a/2) + \tan(\theta_b/2))} \tag{2.8}$$

Where ζ_{ND} denotes the damping ratio, Ω_r denotes the resonance peak, and ω_a and ω_b represent the two frequency values proximate to this peak.

In the frequency-based analysis, the root sum of squares (RSS) of the overall accelerance function was used to compare the vibration behavior of the metal and hybrid parts with a single value.

In addition to frequency domain analysis, damping characteristics were also analysed with time domain data. Analyses with time domain data were obtained using the logarithmic decrement technique. Logarithmic decrement, ζ, is the natural logarithm of the amplitude ratios between two consecutive peaks (x_1, x_2) (see Figure 2.7) [105].

Figure 2.7: *Logarithmic decrement technique parameters [105].*



where x_1 represents the first amplitude peak and x_2 is the second amplitude peak. The damping ratio, ξ, is then calculated by the following formula:

$$\xi = \frac{1}{\sqrt{1 + \left(\frac{2\pi}{\bar{\zeta}}\right)^2}} \tag{2.9}$$

In the present research, three distinct damping coefficients, the Q-factor, Nyquist diagram damping ratio, and the logarithmic decrement damping ratio, were considered. The synergistic interpretation of these damping facilitates an exhaustive exploration of damping behaviour across both frequency and temporal domains. Additionally, collecting these metrics from diverse experimental methodologies bolsters the study's robustness and repeatability, thereby enhancing the veracity and comprehensiveness of the resultant findings.

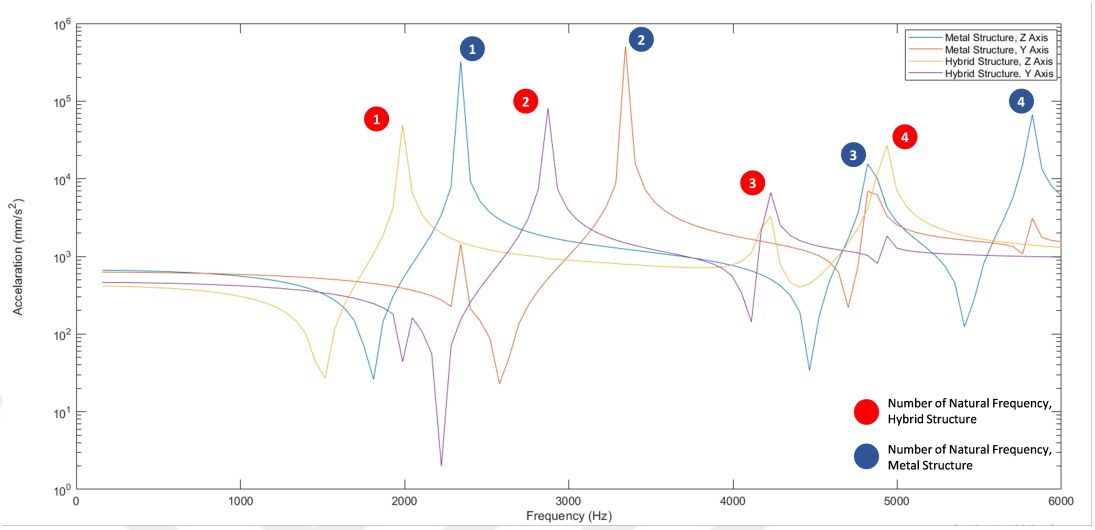
2.5 Fabrication and Experimental Validation

In this section, comprehensive FEM analyses are presented along with the finalized design particulars resulting from these analyses, the production methodologies employed for fabricating the test specimens, and culminating verification studies with corresponding modal test outcomes.

2.5.1 FEM Analysis

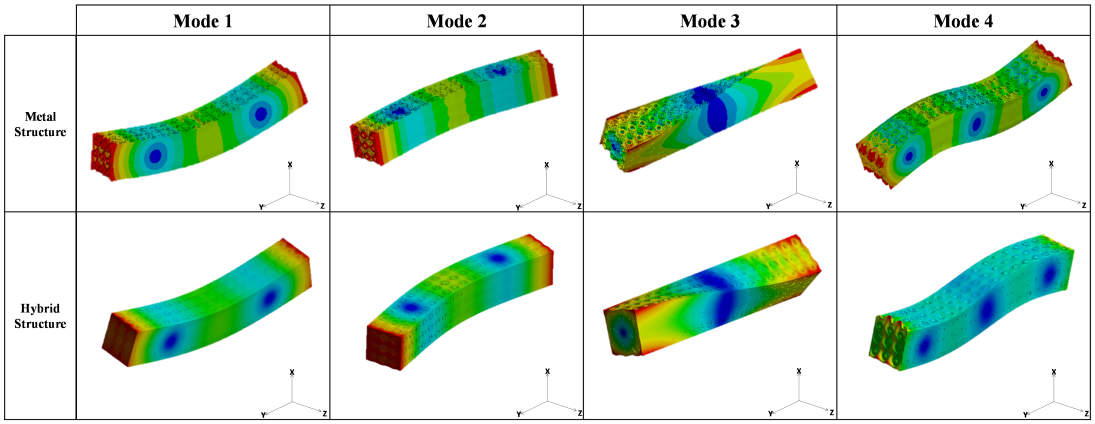
In the FEM analysis conducted for this study, the mesh strategy used ensured an accurate representation of both the metallic and polymer regions of the TPMS structure. After the natural frequency analysis, Frequency Response Function (FRF) data were obtained for the metal and hybrid structures as a result of the harmonic analysis. The related FRF data were generated separately for each response axis and are presented on a single graph. The obtained analysis results were consistent with the observed experimental modal test findings and further strengthened the accuracy and robustness of the finite element model. Observations from FRF graphs in Figure 2.8, distinctly indicate a transition of modal frequencies towards lower values. The analysis simulations also provided valuable insights into potential design modifications that could further exploit the combined potential of the TPMS additive metal and silicone polymer to achieve even higher damping performance.

Figure 2.8: *Acceleration FRFs of FEM Analysis.*



The mode shapes obtained after the modal analysis shared in Figure 2.9 shows parallelism for hybrid and metal structures.

Figure 2.9: *Mode Shapes from FEM Analysis.*



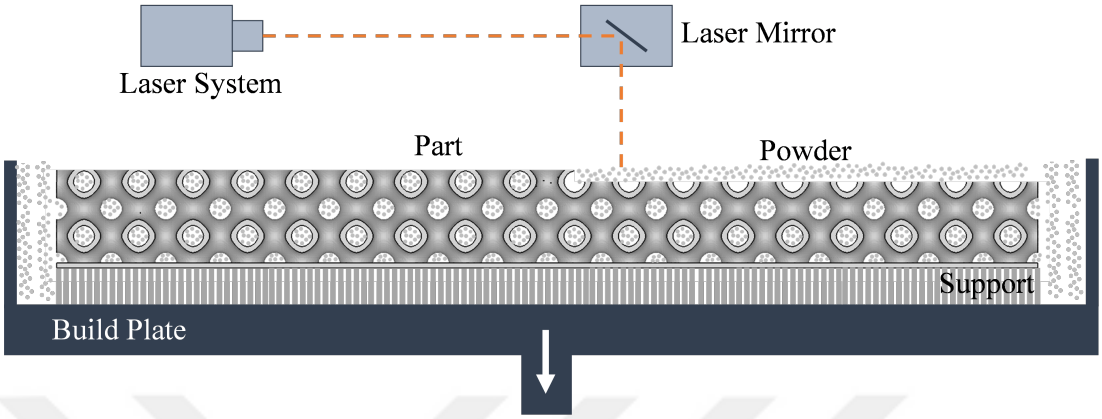
2.5.2 Manufacturing Process of Test Specimen

In the conducted research, a CoCr test specimen infilled with primitive lattices were printed using LPBF technology. Breakaway supports were used between the lattice part and build plate to minimize distortions, which may occur due to high thermal gradients and cause build failure. The contact surface area between support structures and the lattice part were optimized to enable their simple removal without sacrificing its main functionality [91].

For the fabrication phase (see Figure 10), the build data, encoded in a machine-interpretable format, was inputted into a Concept Laser™ M2 Cusing system. The powder chamber was loaded with a spherical CoCr powder, characterized by a particle size distribution ranging from 10 to 45 μm. The LPBF process parameters were carefully calibrated, setting the layer thickness at 50 μm, and utilizing a laser power setting of 180 W, a scanning speed of 1500 mm/s, and a hatch spacing of 60 μm, all under a controlled Argon atmosphere.

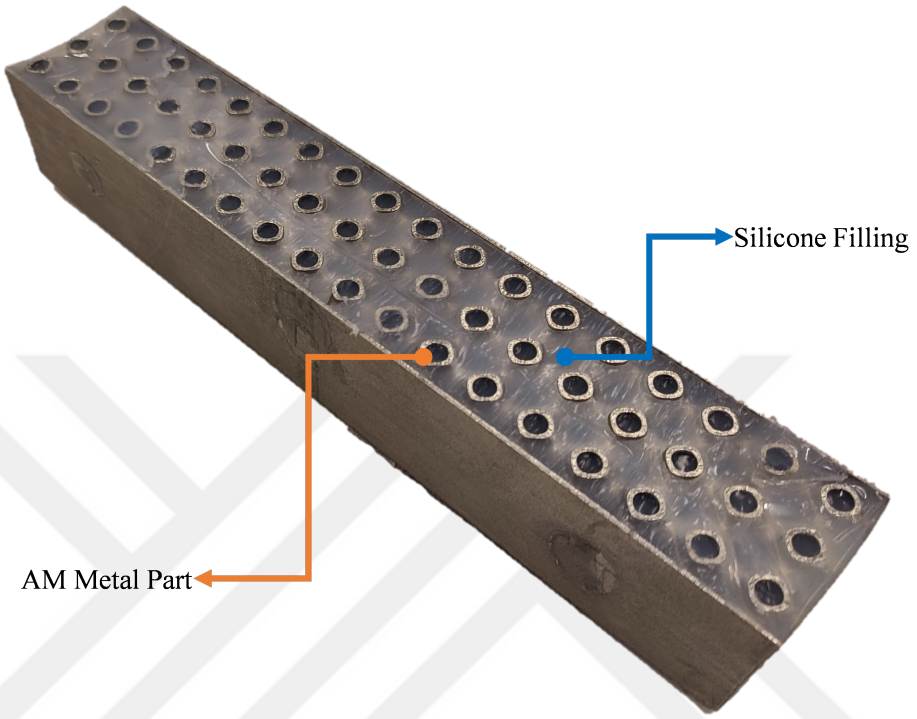
The production was carried out by build plate and 100 °C pre-heating processes in carbon steel. Subsequent to the LPBF process, the removal of residual powder particles adhering to the specimens was achieved via the SFM-AT800 system. The delineation of the specimens from the build plate was conducted using Wire Electrical Discharge Machining (WEDM). This was followed by the manual detachment of the breakaway support structures [91].

Figure 2.10: *Additively fabricating lattice illustration.*



The voids in the metal structure were filled using liquid silicone mixed with a curing activator. More specifically, a 5-shore translucent silicone with a commercial name of RTV 3005 was mixed with a commercial type of catalyst called RTV-3000 at a ratio of 2%. The mixture was then slowly applied in liquid form to the voids of the TPMS metal structure. After a 24-hour curing time at room temperature, the desired hybrid structure was obtained. Ensuring the exhaustive occupancy of the voids was meticulously gauged via a combination of the polymer's known density and stringent control over the cavity volume. Employing this methodology, the aggregate weight of the hybrid structure post-void-filling was compared to a theoretical weight, derived from the established density of the silicone polymer and the designated fill volume. Photographs of the metal and hybrid structure are shown in Figure 2.11.

Figure 2.11: *Fabricated metal-silicone hybrid structure.*



2.5.3 Modal Test & Validation

Modal testing is an experimental method that is used to determine the natural frequencies and associated mode shapes of structural systems. Generally, this method encompasses three primary steps: excitation, measurement, and post-processing of the results. In this process, structures are typically excited with devices such as impact hammers or shakers. Following this, the vibration response of the structural system is measured using accelerometers. Ultimately, the data collected is post-processed to ascertain the natural frequencies and mode shapes of the structural system. In this study, a modal analysis was conducted utilizing an impact hammer and an accelerometer, aiming to determine the natural frequencies and mode shapes of metallic and hybrid structural systems.

Particularly, the transfer function between the excitation force and acceleration response data of the test piece was analyzed. The transfer function between measured acceleration and force is known as the accelerance of the frequency response.

To simulate a free-free structure with no initial conditions such as boundary conditions or preloads, for the test piece in modal testing, the test specimen is placed on PU foam. DEWESoft hardware and software were used for data acquisition and processing of the modal test results in modal tests. The analogue signals are converted to digital signals using DEWESoft Sirius hardware. For the test equipment, an MMF brand accelerometer with a sensitivity of 102mV/g and a DJB brand impact hammer with a sensitivity of 2.5mV/N were used. The modal test setup is shown in Figure 2.12.

A modal test was conducted using the Multiple Input Single Output (MISO) method. The acceleration data is collected from a single point from the accelerometer while the impact hammer excites the structure from 5 different locations. These locations are marked on the test specimen as shown in Figure 2.12.

The accelerance frequency response results from modal testing are shown for metal and hybrid structures in Figure 2.13. The accelerance amplitude is given in dB. The peak points in the transfer function graphs represent the natural frequency points of this structure.

The modal analysis revealed marked distinctions between the dynamic behaviour of the metal and hybrid structures. Two methods that conducted for modal test results HPBW and Nyquist diagrams, were generated from the modal test results of both metal and hybrid structures to determine the damping values of each resonance peak. The resulting damping values and Q-factors are shown in Table 2.2. Upon examination of the damping ratios, it is evident that while damping ratios of 0.001 were observed in the first four modal behaviors of the metal structure, these ratios increased to 0.068 for the first two modes and 0.042 for the third and fourth mode in the hybrid structure.

Figure 2.12: *Modal test setup.*

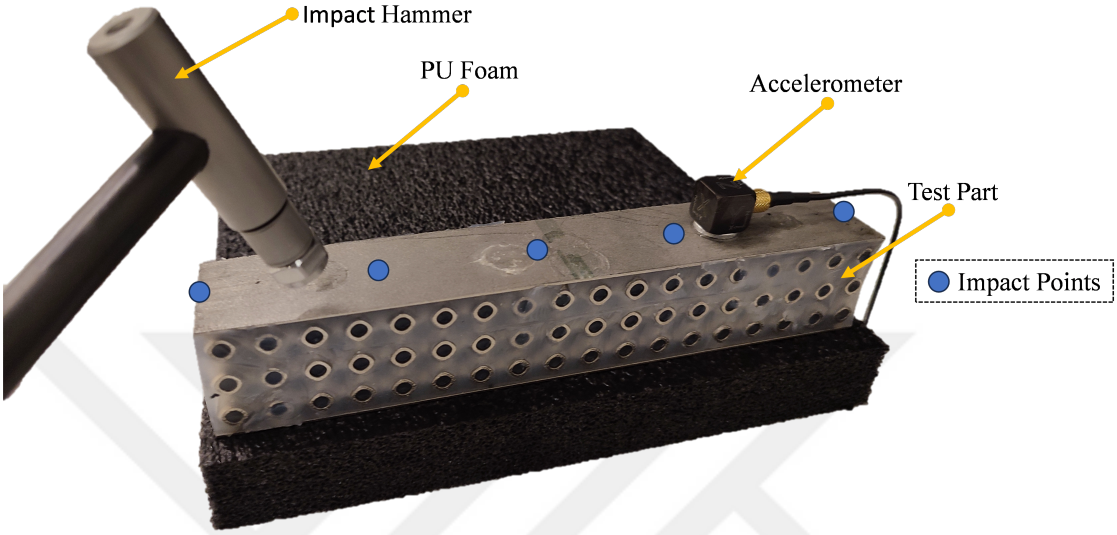


Figure 2.13: *Comparison of the test results in terms of accelerance: hybrid vs. metal parts.*

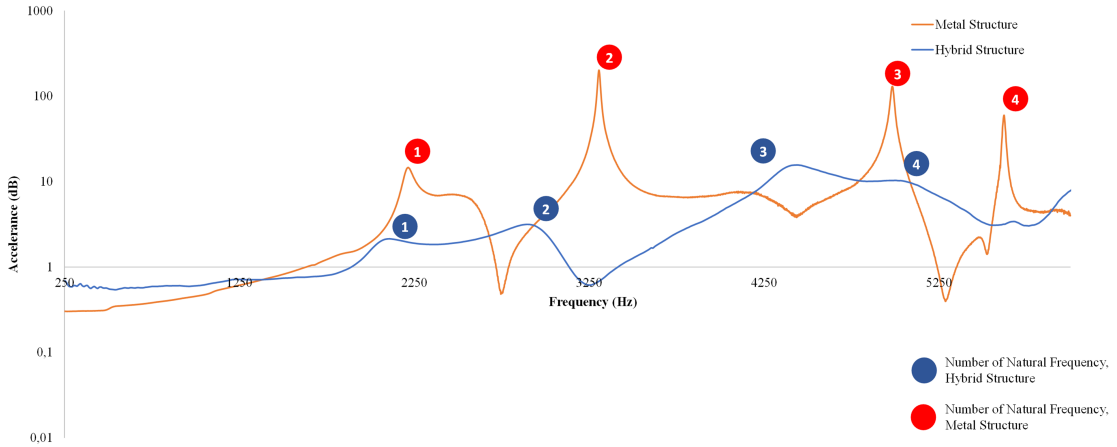


Table 2.2: *Modal Test Results.*

Test Part	**Frequency (Hz)**	**HPBW Q-factor**	**Nyquist Diagram Damping Ratio (ζ_{ND})**
Metal	2212	78.5	0.001
	3304	220.6	0.002
	4981	237.4	0.001
	5623	294.8	0.001
Hybrid	2041	2.3	0.068
	2958	7.6	0.063
	4443	10.8	0.042
	4961	4.5	0.041

In the RSS analysis, which is the other analysis performed on the modal test results, it was found that the vibration response of the metal structure to the overall acceleration was reduced by 90% when the RSS data derived from acceleration was compared with the accelerometer data.

The incorporation of the hybrid materials seems to have bolstered the energy dissipation capabilities, altering the intrinsic vibrational characteristics. This highlights the pivotal role of material hybridization in tailoring and potentially enhancing the vibrational response of structures.

The damping characteristic tests in the time domain of our research focused on the damping over time of a pulse of similar amplitude generated in the test pieces. The impacts were obtained with a modal hammer and the impact amplitudes were kept within the same limits and the test pieces were tested under the same test conditions. When analyzing the damping characteristics, we extracted two main aspects: the logarithmic decrease of the vibration due to the impact and the subsequent damping rates, and the energy

damping time, in Figure. 2.14 data. Using the damping ratio data obtained from logarithmic damping as a benchmark, we further characterized the overall damping behaviour. The hybrid structure exhibited a fast-damping capacity, neutralizing the vibrations in just 0.005 seconds, which is the reference data of the damping coefficients obtained by logarithmic damping. In parallel, we also took into account the time required to absorb the impact energy, providing a holistic view of how quickly the effects of the impact dissipate. The data obtained are presented in Table 2.3.

The in-depth time domain analysis highlighted the superior damping capabilities of the hybrid structure. By employing both the logarithmic damping ratio and the duration for energy dissipation as key indicators, the hybrid material's prowess in swiftly mitigating the vibrations from a consistent external impact became evident. The rapidity with which it neutralizes vibrations, in merely 0.005 seconds, offers compelling evidence of its robust damping potential. Moreover, the concurrent consideration of the energy absorption time frame enriches our understanding of the hybrid's ability to minimize the after-effects of sudden impact.

Figure 2.14: *Acceleration vs time history.*

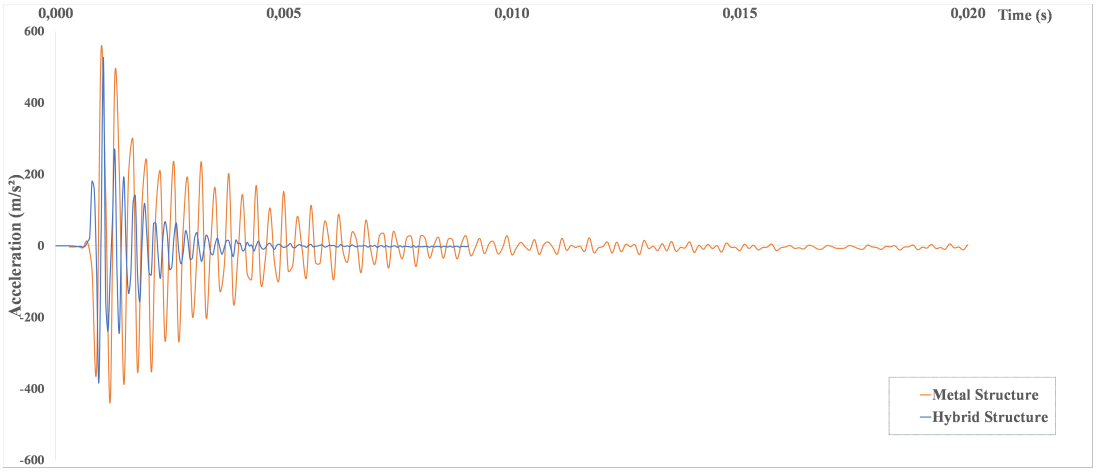


Table 2.3: *Damping Ratio (ξ) and Settling Time.*

Test Part	Damping Ratio (ξ)	Settling Time (s)
Metal	0.12	0.04
Hybrid	0.80	0.005

2.6 Summary

In conclusion, this study has showcased the promising potential of TPMS additive metal parts combined with silicone polymer in revolutionizing damping properties for various engineering applications. Insights from FEM modeling, complemented by experimental modal testing, have established a robust synergy between metal and polymer components, resulting in significant advancements in damping characteristics.

One of the key findings of this study pertains to frequency-based damping analyses. From a resonance peak damping perspective, the hybrid structure exhibits an approximately 25% higher damping capacity compared to the metal TPMS structure using the HPBW method, and at least 30 times higher damping ratios using the Nyquist diagram method. This observation signifies an enhancement in the hybrid structure's ability to remain stable during resonance occurrences.

Moreover, the damping values acquired through the log-decay method, which were employed to assess the damping characteristics of abrupt responses, indicate a sixfold increase in effectiveness compared to the metal structure. Furthermore, the overall accelerance values obtained from frequency-based analyses represent another significant outcome, showcasing a tenfold reduction in RSS data. This reduction serves as an additional indicator of the hybrid structure's ability to enhance the system's damping capacity under dynamic loads.

Additionally, the precision achieved in modeling, with a maximum error of only 6% in both testing and FEM analyses, reinforces the reliability and accuracy of the established models. By analysing the results in both frequency and time domains, it was

evident that enhanced damping performance was achieved, especially noticeable in the reduction of vibration amplitude.

Upon examination of the FEA results, which closely align with experimental data exhibiting minimal discrepancies, shown in Table 2.4, the enhanced damping potential of the hybrid structure having been augmented by the polymer component, becomes evident. This is manifestly reflected in the diminished frequency shifts and attenuation in amplitude discerned within the FRF plots. Furthermore, a comparative assessment of the mode shapes for both the metal and hybrid configurations reveals a noteworthy observation: the presence of the polymer does not perturb the mode shapes, ensuring consistent mode shapes across both entities.

From a time-domain analysis perspective and considering the RSS data, it is evident that the hybrid structure demonstrates superior damping characteristics compared to the metallic structure. However, the analyses of the experimental results were carried out by more than one method within the framework of the competences of the methods, HPBW and Nyquist diagrams. As the Q factor values obtained from the HPBW method proved inefficient in cases where two resonances closely coexisted, the analyses were extended using Nyquist diagrams. According to the Q factor values, an increase in damping ranging from 20% to 27% was observed for the first three modes, with the fourth mode exhibiting a ratio of approximately 50%. This augmentation is attributed to the inefficiency of the method caused by the proximity of the third and fourth modes. Conversely, examination of damping values derived from the Nyquist diagram method reveals that while damping ratios of 0.001 were recorded in the initial four modal behaviors of the metal structure, these ratios escalated to 0.068 for the first two modes and 0.042 for the third and fourth modes in the hybrid structure.

Efficiency of the metal-polymer contacts utilized in the FEM modeling of the hybrid structure is observed to be effective within the first four natural frequency bands;

however, their efficacy in higher frequency bands warrants extra analysis. Furthermore, investigating the efficiency of this hybrid structure across different TPMS models and diverse metal-polymer combinations is critically important for expanding the impact of the findings of this study.

Cumulatively, these insights corroborate the hypothesis that the FEM framework accurately captures the augmented damping efficacy inherent to the hybrid construct, thereby reaffirming the model's predictive fidelity.

The findings from this study suggest that the hybrid structure can be pivotal in applications related to vibration damping and acoustics. The vibration-damping proficiency exhibited by the hybrid architecture from this research undeniably positions it as a paradigm for subsequent scientific inquiries aiming to harness its inherent potentialities, especially acoustic isolation systems. As such, it offers a foundational reference for diversified studies aiming to utilize these hybrid structures in these domains. As the field of materials science continues to evolve, the insights from this study pave the way for future endeavours, aiming to harness the optimal benefits of hybrid structures in addressing critical damping and acoustic challenges across various engineering spectrums.

Table 2.4: *Comparison of FEM and experimental results.*

Structure	**Test Results (Hz)**	**CAE Results (Hz)**	**% Rel. Error**
Metal Structure	1. Mode 2212	2340	6%
	2. Mode: 3304	3358	2%
	3. Mode: 4981	4841	3%
	4. Mode: 5623	5810	3%
Hybrid Structure	1. Mode: 2041	1994	2%
	2. Mode: 2958	2867	3%
	3. Mode: 4443	4208	5%
	4. Mode: 4961	4918	1%

3. HYBRID VIBRATION CONTROL OF TPMS STRUCTURES VIA CLD SILICONE–VISCOELASTIC LAYERS

Under this heading, the materials and methods used in the study, the production techniques, and the results of the validation studies are detailed. Section 3 explores hybrid vibration control of TPMS structures using CLD with silicone-viscoelastic layers. It starts with the design of CLD TPMS structures (3.1) and proceeds to finite element modeling (3.2). The damping characterization methods (3.3) are detailed, including the logarithmic decrement method (3.3.1) and the integral of frequency response method (3.3.2). The manufacturing process of the test specimen (3.4) is then described. The results section (3.5) covers FEM analysis (3.5.1), modal test and validation (3.5.2), time domain damping results (3.5.3), and IFR results (3.5.4). Finally, a summary (3.6) concludes the chapter.

3.1 Design of CLD TPMS Structure

There are multiple types of lattice structures within TPMS; in the present investigation, Schwarz-P structures, which represent a distinctive category within the surface-based TPMS group, have been employed as the fundamental components in constructing the CLD TPMS framework for the case study. TPMS frameworks are distinguished by their intricate geometric forms, which are mathematically described as the interrelation between two nested periodic lattices demonstrating extensive symmetry. There exists a wide array of TPMS variants, each characterized by unique symmetries, shapes, and scales, endowed with distinctive features and prospective applications [106]. For this research, due to their straightforward nature and manufacturability, Schwarz-P structures were chosen as the principal elements for our CLD TPMS configuration, although the proposed methodology is applicable to other TPMS types.

TPMS lattices can be expressed using implicit mathematical expressions, often

depicted as Fourier series [107]. The coefficients of these series define the topology and hence the mechanical properties of the TPMS structures.

In this research, an innovative geometric design based on two iso-surfaces has been developed for the creation of the viscoelastic layer within the CLD structure. The formation of this geometry involves extracting the viscoelastic layer from the geometry subsequent to the construction of the primary metal structure. In alignment with this design philosophy, the final design in this study was generated by extracting a viscoelastic iso-surface layer with a relative density (ρ) of 0.1 from a metallic structure created with an iso-surface of 0.4 relative density. The selection of these specific relative density values for the hybrid CLD structure was strategically determined to facilitate manufacturability. The design methodology for the creation of the CLD TPMS structure is depicted in Figure 3.1.

CLD applications fundamentally consist of three layers. The base and constraining layers are typically made from metal-based materials, while the critical damping layer, situated between these metal layers, comprises viscoelastic materials. These viscoelastic materials possess both viscous and elastic properties, consuming energy during deformation.

The vibration behavior of the metal TPMS structure can be represented by the classical free vibration equation, considering only the stiffness (k), mass (m), and a minimal inherent damping coefficient (c). By introducing the CLD structure through the addition of a polymer layer, the system's damping properties are significantly altered due to the viscoelastic characteristics of the polymer. This modification leads to a more complex vibration response, which can be modeled using an updated vibration equation that accounts for the enhanced damping effect as given in Eq. (3.1):

$$m\ddot{x} + c_{\text{eff}}\dot{x} + k_{\text{eff}}x = F_0 \cos(\omega t) \tag{3.1}$$

where c_{eff} and k_{eff} represent the effective damping and stiffness coefficients, respectively, influenced by the addition of the polymer layer.

The polymer layer alters the dynamic properties of the system, introducing additional energy dissipation mechanisms. Consequently, the system's damping ratio increases, and the overall vibration amplitude is reduced. This behavior can be further analyzed using the complex modulus approach, where the loss factor (η) is defined according to Eq. (3.2):

$$\eta = \frac{E''}{E'} \tag{3.2}$$

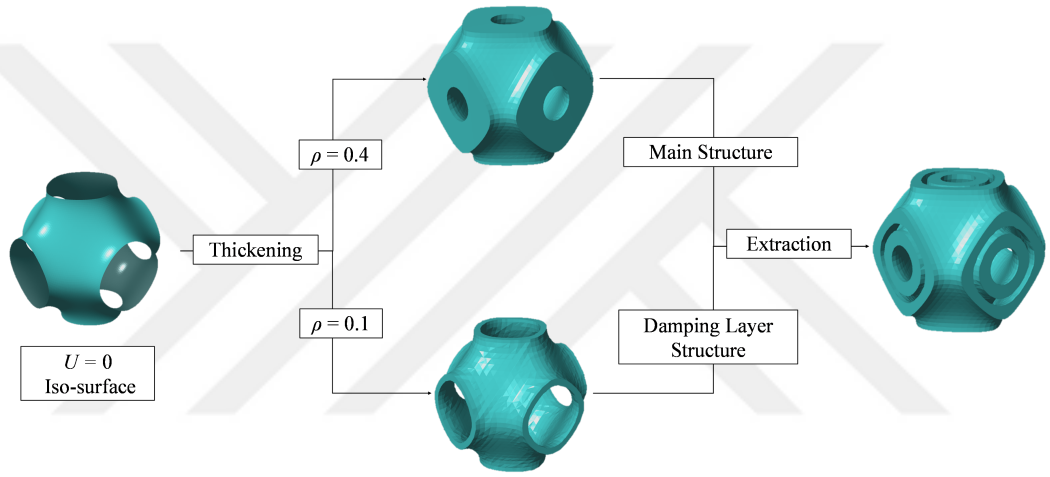
where, E' is the storage modulus (representing stiffness), and E'' is the loss modulus (representing energy dissipation), reflecting the enhanced damping capability of the CLD structure compared to the original metal-only configuration.

In the metallic TPMS structure, vibration attenuation is primarily governed by hysteretic (structural) damping, which results from internal friction within the metal, offering limited energy dissipation. However, in this work, a viscoelastic damping mechanism is introduced by adding a polymer layer, forming a CLD structure. Viscoelastic material provides significant energy dissipation through shear deformation, which converts mechanical energy into heat. This results in a more efficient damping process compared to the purely metallic structure. The vibration attenuation in the CLD structure is characterized by the complex modulus of the viscoelastic material, where the loss modulus (E'') determines the extent of energy dissipation. Additionally, the interaction between the metal and polymer layers generates interfacial shear forces, further contributing to the overall damping effect [108].

Ensuring the integration of these layers is crucial for maintaining structural integrity. The primary challenge in applying CLD to TPMS structures lies in this geometric

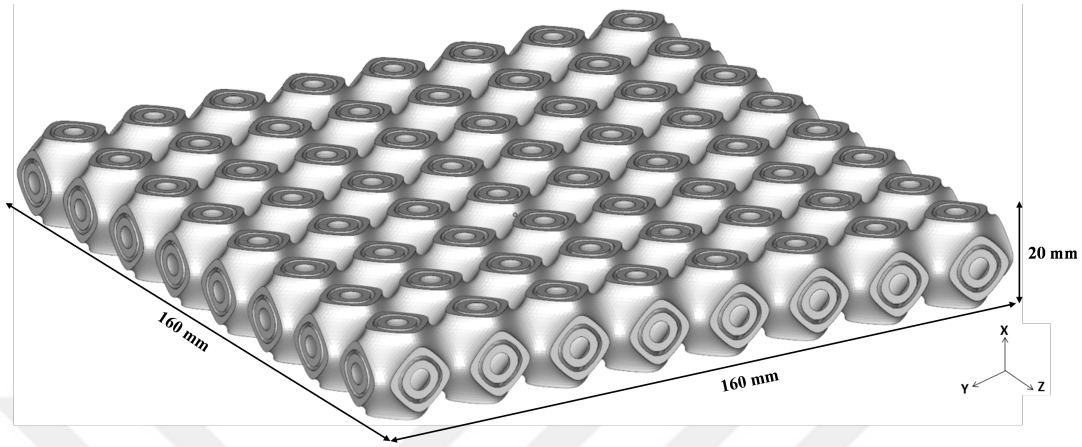
integration. The complex and continuously curved surfaces of TPMS structures complicate the application of CLD layers. Additionally, achieving a homogeneous distribution of viscoelastic material across the TPMS structure and ensuring its adhesion to the surfaces pose significant challenges. Given these difficulties, the hybridization of CLD with a TPMS lattice structure underscores the importance and impact of the study's outcomes.

Figure 3.1: *The design methodology for the creation of the metal part of the CLD TPMS*



In the study, a test piece with dimensions of 160×160×20 mm with a unit cell size of 20 mm was used with reference to the plate model as shown in Figure 3.2.

Figure 3.2: *Design of CLD TPMS Structures*



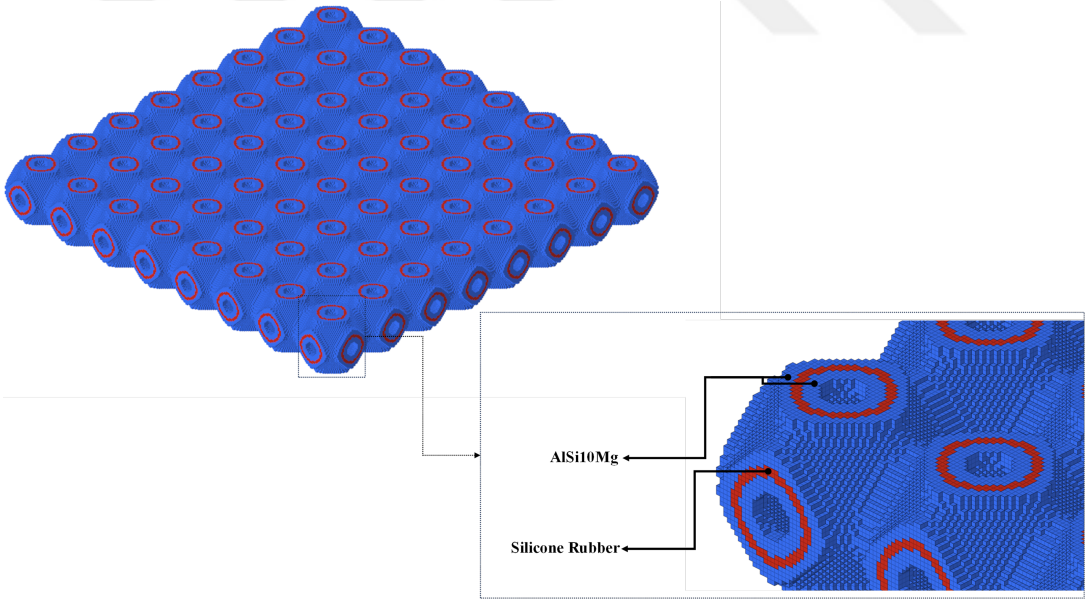
3.2 FEM Modeling

In this study, the modal analysis of a sample part was conducted using the FEM models. A novel hybrid structure was developed by integrating the CLD application with the dimensions of the test model determined based on a plate model. The FEM model of the hybrid CLD structure is shown in Figure 3.3. The model was initially designed as a lattice structure incorporating voxel elements, utilizing a script written in MATLAB software. Voxel modeling is particularly advantageous for complex lattice structures due to its ease of implementation and high computational efficiency. A mesh convergence study was performed by varying the number of elements across the structure's thickness from 5 to 20 elements. The natural frequencies obtained from the FRF results were monitored to assess convergence. It was observed that beyond 10 elements, the changes in natural frequencies were less than 1%, indicating convergence. Therefore, a mesh with 10 voxel elements representing the thickness of both metal and polymer layers was selected for the final simulations, balancing accuracy and computational efficiency. The CLD structure was designed by merging interaction nodes of metal and polymer components, assuming

the equivalent behavior of elements and nodes. The CLD structure was modeled by directly merging the nodes at the interfaces between the metal and polymer components, effectively creating node-to-node connections. This approach assumes perfect bonding between the layers, with no relative motion or separation at the interfaces. This assumption simplifies the computational process by eliminating the need for complex contact definitions, which could increase computational time and potentially cause convergence issues given the high number of elements and nodes [99].

To determine the effect of damping alone, the FEM model simulated the effects of the hybrid structure's damping capacity compared to metal structures under free-free conditions without any preload or boundary constraints. Analyses were conducted without considering the nonlinear effects of loads and boundary conditions. The material properties used in the FEM models are summarized in Table 3.1.

Figure 3.3: *FEM model of hybrid structure*



The selection of polymer materials plays a pivotal role in achieving the desired damping characteristics for the study at hand. Within the context of hybrid structures

featuring TPMS architectures, silicone emerged as the chosen material for the viscoelastic layer of the CLD TPMS structure. This decision is underscored by silicone's superior mechanical damping traits and its notable characteristics in mechanical and acoustic damping criteria, including characteristic acoustic velocity and mechanical loss parameters, making it the most appropriate choice among other polymers for this application [38].

Table 3.1: *Material parameters used in FEM model.*

Material	**Elastic Modulus (GPa)**	**Poisson's Ratio (-)**	**Density (g/cm^3)**
AlSi10Mg	71	0.33	2.77
Silicone	0.03	0.47	1.1

3.3 Damping Characterization Methods

This section provides detailed information on the damping analysis techniques used in this study. The damping characteristics are identified as crucial for demonstrating the benefits achieved using the hybrid structure in this research.

The vibration damping characteristic of an engineering system can be quantified as a time-dependent or frequency space-related measure. Enhancing the damping characteristic in both measurement domains is a key goal of this study, aimed at revealing the damping performance of the hybrid CLD TPMS structure. This dual domain method verification not only strengthens the reliability of the results but also highlights the practical implications of integrating advanced damping technologies in engineering applications. The two distinct damping characterization methods are explained briefly next.

3.3.1 The Logarithmic Decrement Method

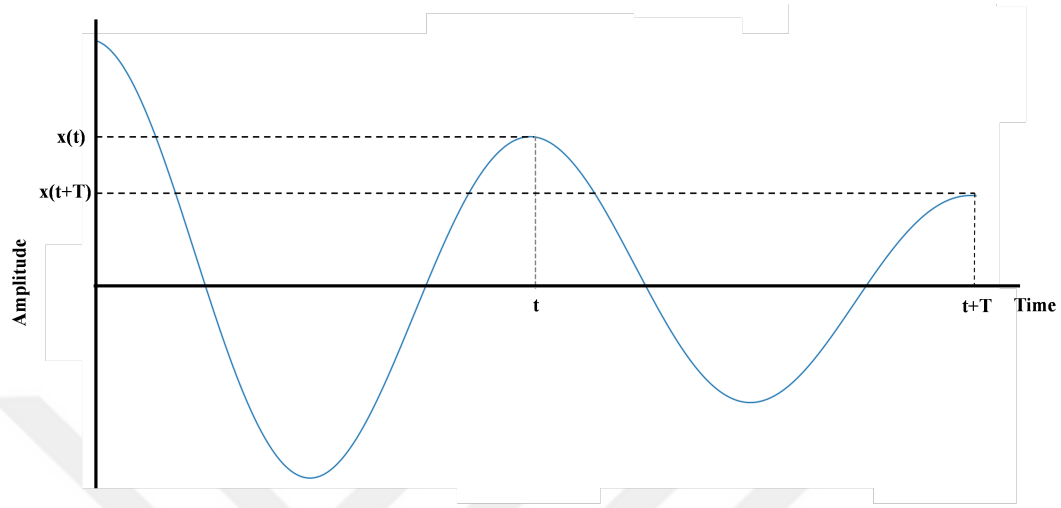
The analysis initially focuses on the time-dependent amplitude reduction of damping structures, utilizing the logarithmic decrement method. This approach provides a precise assessment of how vibrations decay over time, which is vital for understanding the efficiency of the damping provided. By employing this method, the study aims to capture a detailed picture of the dynamic response, further enhancing the understanding of how hybrid structures contribute to improved damping characteristics.

Following the initial focus on damping characteristics, it is essential to delve deeper into the logarithmic decrement method, a crucial analytical tool in this study. The logarithmic decrement is a measure used to quantify the rate of damping in underdamped systems exhibiting oscillatory behavior. It is defined as the natural logarithm of the ratio of two successive peak amplitudes in an underdamped system, represented mathematically as in Eq. (3.3) [104]:

$$\delta = \ln\left(\frac{x(t)}{x(t+T)}\right) \tag{3.3}$$

where $x(t)$ is the amplitude at time t and $x(t+T)$ is the amplitude after one period T, explained in Figure 3.4.

Figure 3.4: *The logarithmic decrement*



3.3.2 Integral of Frequency Response Method

In addition to other damping analysis methods, the Integral of Frequency Response method (IFR) was employed to evaluate the damping characteristics in the frequency domain. This approach utilizes the frequency response data obtained from modal tests, focusing on the transfer functions. By integrating the transfer function, $T_h(\omega)$, over a specified frequency range, the IFR method provides a comprehensive assessment of the system's dynamic behavior. This integration captures the cumulative energy response over the frequency range of interest, offering valuable insights into the damping performance across different frequency bands as given in Eq. (3.4):

$$\text{IFR} = \int_a^b T_h(\omega)\, d\omega \tag{3.4}$$

The function $T_h(\omega)$ represents the amplitude of the frequency response function. The parameters a and b denote the frequency range, specifically the critical frequency band where the analysis is conducted. In this study, this frequency band spans from 250

Hz to 4500 Hz, encompassing the first four natural frequencies observed.

IFR offers crucial insights into the overall dynamic behavior of a system by calculating the total energy or response over a specified frequency range. This analysis is especially valuable for evaluating the energy content of vibrations, enabling comparisons between different systems or the same system under varying conditions. Response fields serve as a foundation for directly comparing the dynamic responses of systems, facilitating the assessment of their performance and stability. High-energy indicates that the system may generate increased vibrations and noise, critical factors in evaluating and optimizing system design and functionality [109].

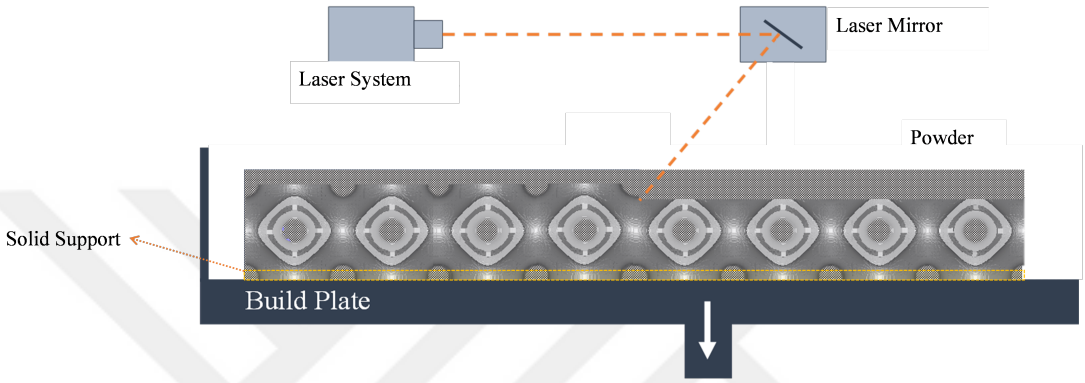
3.4 Manufacturing Process of Test Specimen

In this research, an AlSi10Mg test specimen filled with primitive lattices was printed using LPBF technology. To minimize distortions that could lead to structural defects caused by high thermal gradients, a solid support was employed between the lattice structure and the build plate. The support structure was designed to follow the contours of the main geometry, ensuring that the geometric integrity was maintained after the support was removed from the primary structure.

During the production phase (see Figure 3.5), the design data was input into the system in a machine-readable format. The powder bed was loaded with spherical AlSi10Mg powder characterized by a particle size distribution ranging from 10 to 30 µm. The LPBF process parameters were carefully calibrated, with a layer thickness set at 30 µm, laser power at 370 W, scan speed at 1300 mm/s, and scan spacing at 190 µm, all performed under a controlled Argon atmosphere. Following the LPBF process, residual powder particles adhering to the samples were removed using the SFM-AT800-S system. The samples were then separated from the build plate using WEDM. To minimize void spaces, we optimized the process parameters of the LPBF technique, ensuring consistent

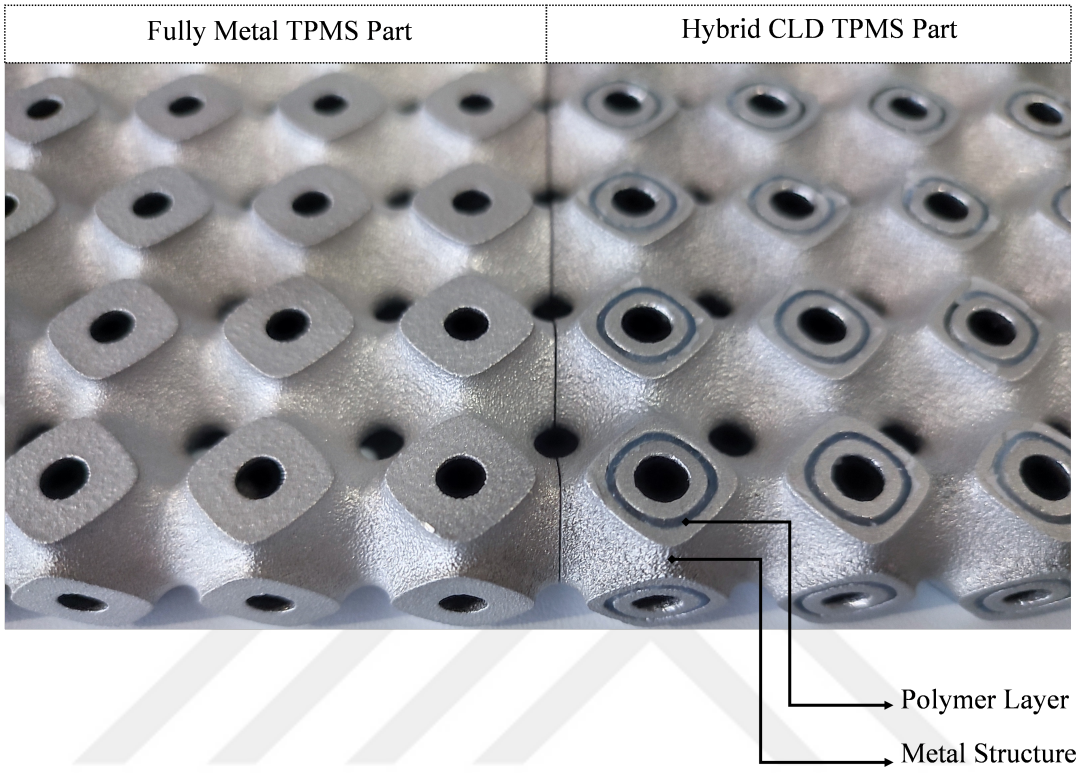
power distribution and layer consolidation. Additionally, custom designed fixtures and support structures were employed to hold the layers in place, preventing any translation or misalignment that could affect the thickness of the silicone layer.

Figure 3.5: *The manufacturing process of the test specimen*



After successfully obtaining test specimens suitable for modeling without any damage, the process moved on to creating the CLD hybrid structure. For the hybrid structure, the damping layer utilized liquid silicone mixed with a curing activator as the polymer. Specifically, a 5-shore translucent silicone, commercially known as RTV 3005, was mixed with a 2% ratio of a commercial catalyst called RTV-3000. The mixture was then vacuum applied in liquid form into the voids of the TPMS metal structure. During the vacuum process, other cavities in the geometry were masked, ensuring the vacuum only affected the polymer layer. After a 24-hour curing period at room temperature, the desired hybrid structure was achieved. The complete filling of the voids was meticulously measured by combining the known density of the polymer with strict control over the void volume. Using this methodology, the total weight of the hybrid structure post-filling was compared to a theoretical weight derived from the known density of the silicone polymer and the calculated fill volume. Photographs of the metal and hybrid structures are shown in Figure 3.6.

Figure 3.6: *Fabricated metal and hybrid CLD structures*

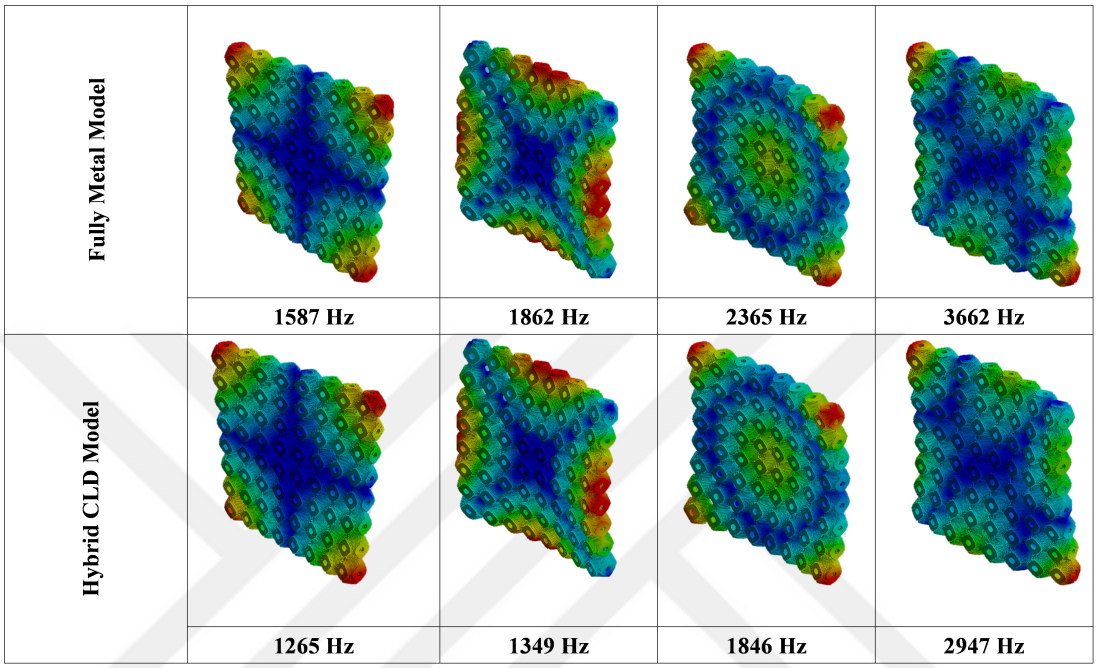


3.5 Results

3.5.1 FEM analysis

The FEM-based modal analysis mesh was meticulously designed to optimally represent both metal and hybrid CLD structures. The model utilized the first four natural frequencies and their corresponding mode shapes as validation parameters for the modal analysis outputs. The natural frequencies and mode shapes for both the metal structure and the hybrid CLD TPMS structure are compared in Figure 3.7.

Figure 3.7: *Modes and mode shapes of the metal and hybrid CLD structure from FEM analysis*



3.5.2 Modal test and validation

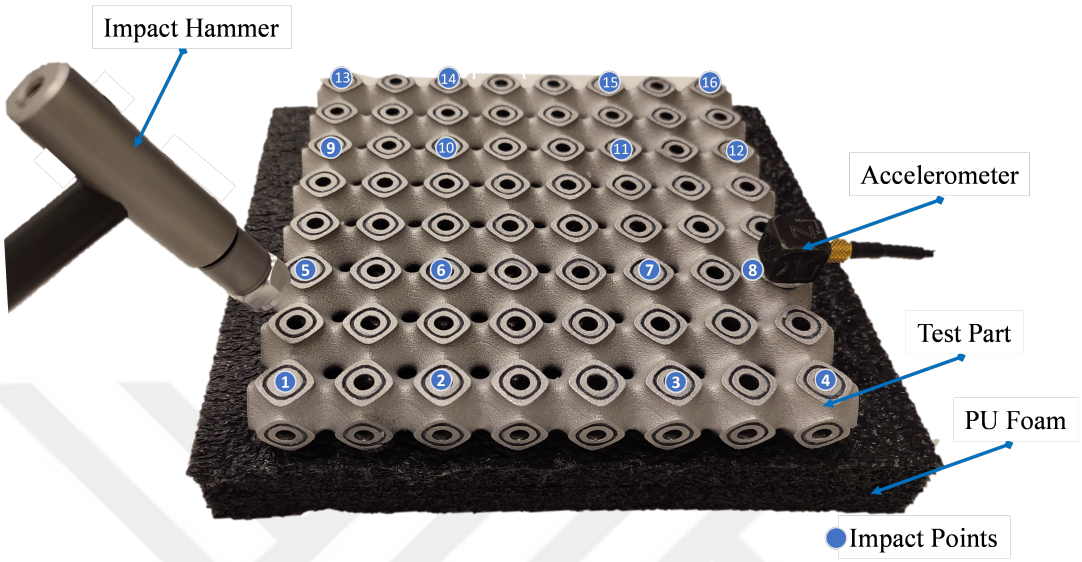
Modal testing is an experimental technique used to identify the natural frequencies and corresponding mode shapes of structural systems. This method generally consists of three main steps: excitation, measurement, and post-processing of the results. Initially, structures are excited using devices such as impact hammers or shakers. The subsequent vibration response of the structural system is then measured with accelerometers. The collected data is finally post-processed to ascertain the natural frequencies and mode shapes of the structural system. In this study, modal testing was conducted using an impact hammer and an accelerometer to determine the natural frequencies and mode shapes of both the full metal and CLD TPMS structural systems.

The modal test setup, shown in Figure 8, replicates the boundary conditions considered in the FEM model. To simulate a free structure without boundary conditions or preloads, the test specimen in the modal test was placed on polyurethane foam. DEWESoft hardware and software were employed for data acquisition and processing of the modal test results. Analog signals were converted to digital signals using DEWESoft Sirius hardware. The test equipment included an MMF accelerometer with a sensitivity of 105 mV/g and a DJB impact hammer with a sensitivity of 2.5 mV/N.

Modal tests can be conducted using various methods depending on the size of the structure. In this study, to better identify the modal shapes, a modal test was performed using the MISO method [101]. The impact hammer excited the structure from 16 different locations, shown in Figure 3.8, while acceleration data were collected from a single point using the accelerometer. This multi-point excitation method allowed for an effective transfer function to be obtained for each region of the system, resulting in smooth transfer functions. The consistency of the impact force and acceleration levels is crucial for accurate FRF calculations. To minimize the influence of variability we continuously monitored the coherence function during testing to assess the quality of the measurements. High coherence values indicated a reliable relationship between the input force and output acceleration signals. Any impact with low coherence or inconsistent force levels was discarded and repeated to ensure data integrity.

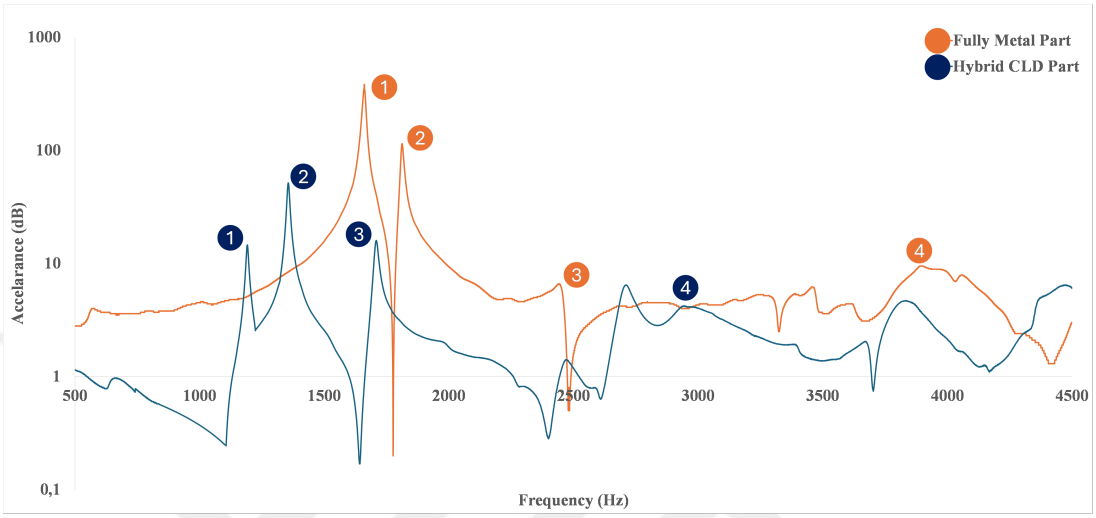
To synthesize these multiple FRFs into a single representative function, we employed the Complex Mode Indicator Function (CMIF) technique. CMIF is a well-established method in modal analysis that utilizes Singular Value Decomposition (SVD) to combine multiple FRFs and extract the modal parameters of the structure. By applying CMIF, we obtained a singular value spectrum that highlights the natural frequencies and mode shapes of the specimen [101].

Figure 3.8: *Modal Test Setup*



The accelerance frequency response results from modal testing are shown for metal structure and hybrid CLD structure in Figure 3.9. The accelerance amplitude is given in dB. The peak points in the transfer function graphs represent the natural frequency points.

Figure 3.9: *Comparison of the test results in terms of accelerance: metal structure vs. hybrid CLD structure*



The natural frequencies of both structures have been identified through peaks, as indicated in the graph. Due to the presence of additional peaks observed in the frequency band where the fourth natural frequency of the hybrid CLD structure is expected, the natural frequency has been determined using the imaginary part of the transfer functions. Since the mode shapes of the systems can be derived from the imaginary part of the transfer function data, we compared the expected mode shape with the peaks in these bands. This allowed us to identify the system's fourth natural frequency value.

3.5.3 Time domain damping results

Logarithmic decay data, which show the damping characteristics of vibration amplitudes under the same load applied to the same region of the systems, demonstrate another excellent damping capability of the CLD TPMS structure in the time domain analysis. In this experiment, the impact was applied at point number 1, as illustrated in Figure 3.8. This point was selected because impact effects are more effectively induced

Table 3.2: *Comparison of FEM and experimental results.*

Mode No	Test Results (Hz)	FEM Results (Hz)	Rel. Error (%)
Metal Structure			
1. Mode	1578	1661	5%
2. Mode	1862	1811	3%
3. Mode	2365	2457	4%
4. Mode	3662	3809	4%
Hybrid CLD Structure			
1. Mode	1265	1190	6%
2. Mode	1349	1357	1%
3. Mode	1846	1708	7%
4. Mode	2947	2944	1%

when applied at the endpoints of the test model.

In this analysis, settling time refers to the duration it takes for the amplitude to reach 0(±0.1). A high number of peaks during this period, along with a longer settling time, indicates a low damping ratio. Figure 3.10 illustrates how the acceleration in the systems dissipates after both the metal and the hybrid CLD structures are excited using an impact hammer. While the metal structure dampened the same high amplitude vibration with over 300 peaks, the CLD structure achieved damping with approximately 140 peaks. Considering the damping times, the hybrid structure overcame the same amplitude of structural vibration in 0.09 seconds, whereas the metal structure took 0.16 seconds. In light of this information, when the damping capability in the time domain is calculated, the CLD structure exhibits approximately 5 times better damping capability compared to the metal structure.

Figure 3.10: *Acceleration vs time history*

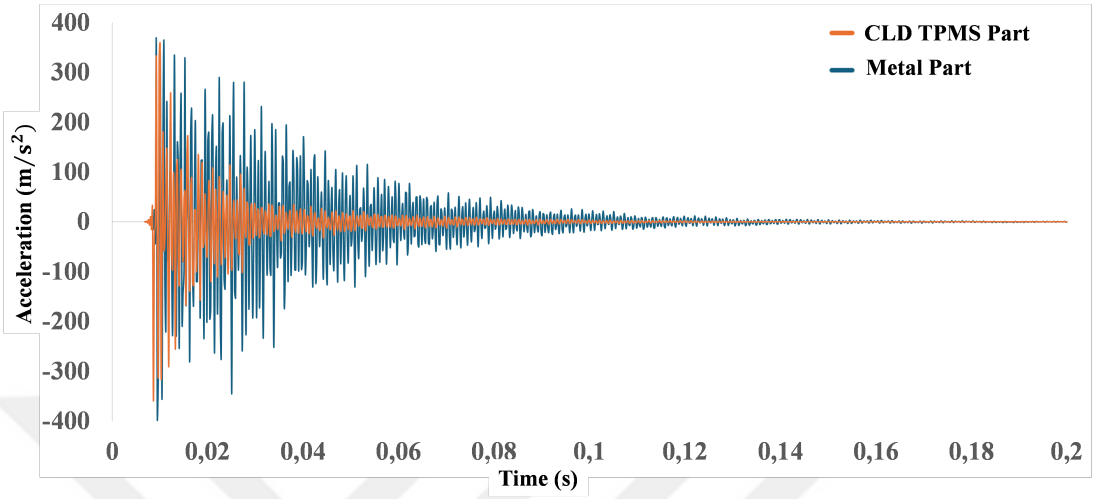


Table 3.3: *Damping ratio (δ) and settling time.*

Test Part	Damping Ratio (δ)	Settling Time (s)	Number of Peaks
Metal	0.16	0.16	326
Hybrid CLD	0.89	0.09	142

3.5.4 IFR results

When the IFR data, another frequency domain analysis, was examined, it was found that the hybrid structure generates 76% less cumulative vibration compared to the metallic structure in the same frequency band. This indicates that the CLD TPMS application will result in 76% less vibration in dynamic applications within the same band, suggesting that the system could be significantly more stable. This finding has been added to the study's results as an important indicator. On the other hand, IFR analysis was performed around each natural frequency band of the structures (± 10 Hz). The purpose of this analysis is to estimate the energy levels in the system during potential resonance conditions. High amplitudes in these values represent high energy levels during resonance,

which is undesirable for structural integrity. The CLD TPMS structure demonstrated a 30-fold reduction in IFR value and cumulative vibration amplitude in the first natural frequency band, considered the most critical for systems.

Table 3.4: *IFR Results ($\frac{ms^{-2}}{NHz}$).*

Test Part	1. Mod	2. Mod	3. Mod	4. Mod	Overall Band
Metal	5812	1984	135	196	39031
Hybrid CLD	222	791	286	87	9027

3.6 Summary

This study investigates the vibration and damping performance of the innovative CLD TPMS structure. In the realm of modern engineering approaches, metamaterials, which demonstrate groundbreaking performance in various fields such as mechanics, acoustics, and magnetics, are integrated with CLD applications into TPMS structures through a novel perspective. This innovative approach examines the vibration and damping performance of the CLD TPMS structure in detail using several different methods.

The FEM model's natural frequencies and mode shapes were the primary focus of the core validation process in this investigation. The validation was accomplished with minimal errors, as evidenced by the comparison of the natural frequency values obtained from FEM analysis and modal test results. From an engineering standpoint, it would be advantageous to extend the scope of CLD TPMS to encompass other forms of TPMS. Furthermore, the importance of the results of this research will be emphasized by future research that validates the use of various polymer types and multiple polymer layer applications.

The damping analysis conducted in the time domain involved examining the systems' abilities to dampen identical excitation under the same conditions. The CLD TPMS application demonstrated impressive performance from this perspective as well. Proving

its vibration damping behavior under long-duration excitations is crucial for ensuring the application acts as a guarantor of durability under dynamic loads.

In the IFR analysis and frequency-based analysis, the vibration characteristics of the system were calculated based on the cumulative vibration amplitude in the relatively high-frequency region. This approach does not provide the opportunity to examine the vibration behavior below 250 Hz, known as the low-frequency range, for the CLD TPMS structure. Proving the high damping capacity of the CLD TPMS structure in the low-frequency behavior, a critical design aspect in engineering systems, would make this application an attractive alternative for unique designs preferred in many engineering applications.

Another notable observation from the IFR outputs is that the third natural frequency values show a lower degree for the metal structure compared to the hybrid structure. This is believed to be related to the chosen modal testing method. When considering the frequency bands, especially above 2000 Hz, the impact hammer excitation results in lower amplitude responses due to decreased excitation energy at higher frequencies. To test the system more efficiently across broader natural frequency bands, non-contact modal testing setups (e.g., laser vibrometers) should be considered. The first natural frequency, deemed critical for resonance in systems, is the primary focus. In this context, the CLD TPMS structure has demonstrated superior performance without any doubt at these natural frequency values.

While this study employs a single-layer TPMS structure, the incorporating multiple layers of TPMS units is essential to fully realize the micro-mechanical properties inherent to these materials. Previous studies have indicated that at least four layers are necessary along the smallest dimension to capture the complete behavior of TPMS structures in plate and beam applications. Future research will focus on extending this work to multi-layer TPMS configurations to investigate how additional layers impact the damping

performance and to further validate the effectiveness of the CLD approach in more complex structures. In this study, we focused on the surface-oriented Schwarz-P TPMS structure due to its continuous surfaces and uniform mechanical properties, which enhance interaction with the silicone layer and promote distributed deformation for improved damping performance. Different TPMS classifications, such as strut-oriented types, may lead to varying mechanical consequences and damping efficiencies. Future research could explore how various TPMS geometries affect the damping mechanisms and overall performance of CLD TPMS structures.

One limitation of the present study is its focus on linear dynamic analysis, which does not account for nonlinear effects arising from large deformations, material nonlinearity, or contact interactions under high load conditions. Recent studies have highlighted the exceptional mechanical performance of TPMS structures, particularly in dynamic scenarios such as impacts, where strain gradients and graphene platelet reinforcements play a critical role in enhancing energy absorption capacity [110]. Further research has explored how the crystalline rotation of TPMS architectures influences stiffness and energy absorption under nonlinear conditions, demonstrating the impact of such orientations on the mechanical performance of these structures [111]. By not considering nonlinear behavior, our study does not capture the full extent of the energy absorption mechanisms inherent in TPMS structures.

Future research will aim to incorporate nonlinear dynamic analyses to explore the performance of the CLD TPMS structures under large deformations and impact loading conditions, providing a more comprehensive understanding of their potential in applications involving shock absorption and crashworthiness.

Among the most significant findings of this study is the exceptional damping performance observed in the time domain for the CLD TPMS structure. The innovative CLD TPMS material was compared against a fully metallic TPMS material as a reference. In

these comparative studies, the CLD TPMS exhibited five times better damping performance. This suggests that the CLD TPMS application will encounter excitations entering the system with a much faster damping performance than its alternative. This implies a much more stable and reliable system. The frequency-based analysis method used is the IFR method, which reduces the vibration performance of the systems within specific frequency bands to a single value. In this method, the CLD TPMS structure exhibited 76% lower cumulative vibration compared to the reference metallic structure. This indicates that the CLD TPMS structure is a much more reliable system in this frequency band due to its superior damping performance. When examining the cumulative vibration amplitudes in each natural frequency band localized to these natural frequencies using this method, it was observed that the systems demonstrated better performance and a more stable system indicator at the first natural frequency value, which is critical for vibration behavior. The precision of the modeling derived from the test and FEM analyses, with a maximum error of only 7%, underscores the reliability and accuracy of the developed models. The evaluation of results in both frequency and time domains distinctly reveals enhanced damping performance, particularly evident in the reduction of vibration amplitude.

The superior damping performance of the CLD TPMS structures can be attributed to the unique combination of the TPMS geometry and the viscoelastic properties of the silicone material. The intricate TPMS topology facilitates distributed deformation throughout the structure under dynamic loading, enabling effective absorption and dissipation of vibrational energy. The high surface area provided by the TPMS lattice enhances the interaction with the silicone layer, promoting efficient shear deformation. The silicone material's viscoelastic behavior plays a crucial role in damping; when subjected to shear deformation within the CLD configuration, it dissipates energy through internal friction mechanisms associated with its high mechanical loss factor. This energy dissipation is further amplified by the structural flexibility of the TPMS lattice, which accommodates

the deformation of the silicone layer. The synergistic effect of combining the TPMS structure with the silicone material results in multiple damping mechanisms, including material damping within the silicone, interfacial damping due to the metal-polymer interfaces, and structural damping from the TPMS lattice deformation, enhancing the overall damping capacity of the CLD TPMS structure compared to the metallic TPMS alone and effectively reducing vibrations across a broader frequency range. In this study, we focused on the pioneering aspect of the vibration damping mechanism using a single type of TPMS (Schwarz-P) and aimed to discuss the outcomes within this scope. The authors acknowledge that future work will involve enhancing and optimizing the performance of the entire TPMS family, building upon the foundation established by the present research.

The outcomes of this study indicate that the CLD TPMS structure has the potential to play a pivotal role in applications involving vibration damping and acoustics. The demonstrated damping capability of the hybrid structure in this research establishes it as a paradigm for future scientific inquiries aiming to exploit its inherent potential, particularly in dynamic and acoustic isolation systems. Consequently, these hybrid structures serve as a fundamental reference for a variety of studies targeting their application in these domains. As the field of materials science continues to advance, the findings from this study pave the way for future efforts to leverage the optimal benefits of hybrid structures in addressing critical damping and acoustic challenges across diverse engineering disciplines.

4. AI-DRIVEN PARTICLE DAMPER OPTIMIZATION: FEM, ANN, AND GENETIC ALGORITHM INTEGRATION

In this section of the study, the test design, the numerical modeling techniques used, the experimental methods, and the details of the optimization algorithm are presented.

4.1 Concept of Design of Experiments (DoEs)

In this study, Inconel 718 was used because it is a well-documented material in the literature with widely validated mechanical properties. To investigate the influence of the damper cavity size, location, and number on the damping performance, sixteen specimens with integrated particle dampers were designed and produced using additive manufacturing. A fully fused specimen was also included as a control specimen. Each specimen has external dimensions of 148 millimeters by 60 millimeters by 10 millimeters. The thickness and width of the particle dampers were kept constant at 6 millimeters and 40 millimeters, respectively, and were centered in both directions, while their length and location were varied as illustrated in Figure 1. The lengths of the particle dampers were set to 20 millimeters, 40 millimeters, and 80 millimeters to establish a suitable DoEs study. Figure 4.1 shows the dimensions and positions of the particle dampers in all specimens, which makes it possible to explore how the mode shapes affect the damping performance within this DoEs framework [112].

The specimens were divided into groups to determine how the cavity length, location, and number of dampers influence damping performance (see Table 4.1). The length-based groups (from one to four) were designed to reveal the effect of particle damper length on damping performance by holding other parameters—such as the number of dampers and their locations—constant. The location-based groups (from one to six) were

created to analyze the impact of damper position when considering different damper sizes and quantities as shown in Table 2. Finally, the number-of-dampers-based groups (from one to four) were prepared to examine how the total count of dampers influences the vibration response. Within these final groups, specimens numbered one and two had damper cavities placed at the center of the beam, whereas specimens numbered three and four featured damper cavities located at the tip of the beam. Figure 1 provides a schematic side view of the specimens [112].

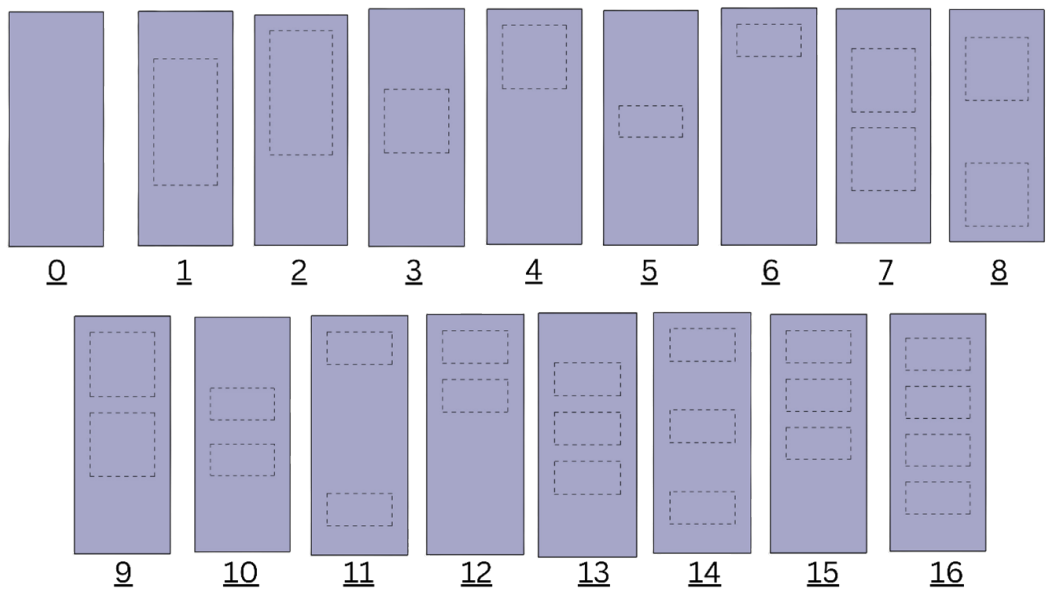
Table 4.1: *Experimental Groups and Parameter Definitions*

Parameter Definition	**Group Name**	**Specimens in Group**
I) Effect of the length of the dampers	Length 1	1, 3, 5
	Length 2	2, 4, 6
	Length 3	8, 11
	Length 4	9, 12
II) Effect of the locations of the dampers	Location 1	1, 2
	Location 2	3, 4
	Location 3	5, 6
	Location 4	7, 8, 9
	Location 5	10, 11, 12
	Location 6	13, 14, 15
III) Effect of the number of cavity	Cavity Number 1	1, 7, 16
	Cavity Number 2	3, 10
	Cavity Number 3	2, 9
	Cavity Number 4	4, 12

Table 4.2: *Specimen design parameters*

Specimen No	Centerline Based Cavity Size (mm)	Number of Cavities	Volume Fraction (%)	Cavity Locations
0	-	-	-	-
1	80x40x6	1	20	Center
2	80x40x6	1	20	Tip
3	40x40x6	1	10	Center
4	40x40x6	1	10	Tip
5	20x40x6	1	5	Center
6	20x40x6	1	5	Tip
7	40x40x6	2	20	Center
8	40x40x6	2	20	2 Tips
9	40x40x6	2	20	Tip
10	40x40x6	2	20	Center
11	20x40x6	2	10	2 Tips
12	20x40x6	2	10	Tip
13	20x40x6	3	15	Center
14	20x40x6	3	15	Center & 2 Tips
15	20x40x6	3	15	Tip
16	20x40x6	4	20	Center

Figure 4.1: *Side view of the test specimens*



4.2 Manufacturing Process of Test Specimen

Concept Laser M2 system was used for production, which was equipped with Inconel 718 powder. The powder had a particle size distribution of d10 = 23 μm, d50 = 35 μm, and d90 = 50 μm, ensuring consistency in the printing process. Once the fabrication was completed, any remaining powder was carefully removed, and the specimens were separated from the build plate using wire electrical discharge machining. No post-processing treatments, such as heat treatment or surface finishing, were applied to maintain the as-printed condition of the specimens [112].

4.3 Damping Characterization Method

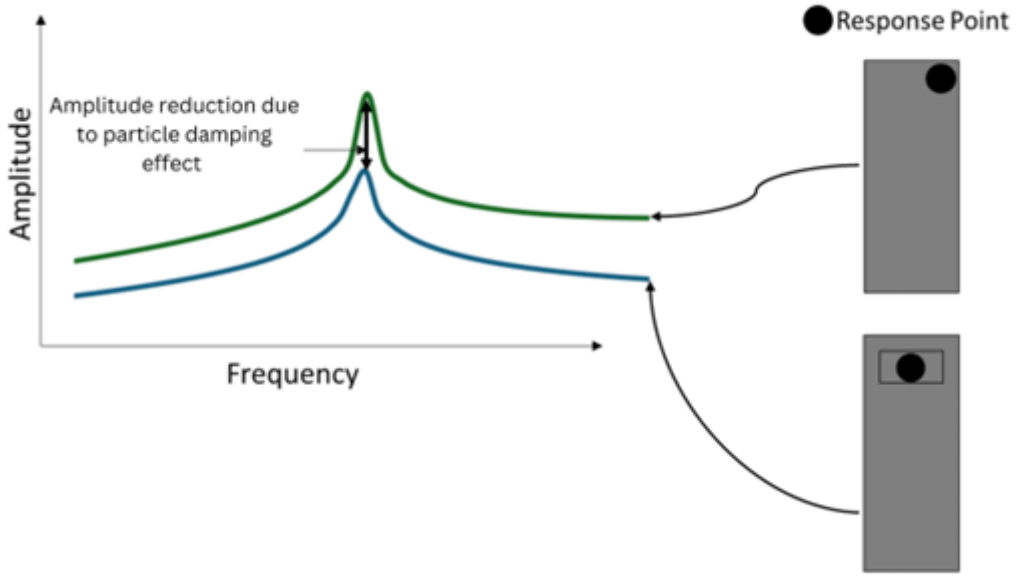
In this study, the primary inputs for the optimization process were derived from experimental tests. Modal testing was chosen as the fundamental experimental method, as it provides crucial insights into key dynamic characteristics of a system, including its natural frequencies and damping behavior at these frequencies. Modal testing, which has a wide range of applications, was conducted using an impact hammer in this study. By exciting the system with a hammer capable of measuring force values and analyzing the acceleration responses collected from the system, transfer functions were constructed. These transfer functions provide critical information about the system's dynamic behavior in the frequency domain, particularly identifying natural frequency candidates and characterizing damping at these frequencies.

To ensure that the modal test results accurately represent the free-free boundary conditions, the specimens were placed on polyurethane foam during testing. This approach was adopted to minimize nonlinear effects caused by boundary conditions and to obtain the system's intrinsic modal response without external constraints. To effectively capture the modal shapes, which simulate the displacement behavior of the system at

its natural frequencies, multiple excitations were applied. Specifically, acceleration responses were recorded from a single measurement point while the system was impacted at twelve different locations.

The resulting transfer functions were generated separately for each excitation point and impact. This approach enabled a clear observation of the system's response at each excitation location. The primary objective of this analysis was to thoroughly examine the system's response in regions containing particle dampers. Transfer functions obtained from the cavities containing the particle dampers were compared to those measured at a reference excitation point located at the free end of each specimen. This comparison provided a clear assessment of the damping efficiency introduced by the particle dampers (see Figure 4.2).

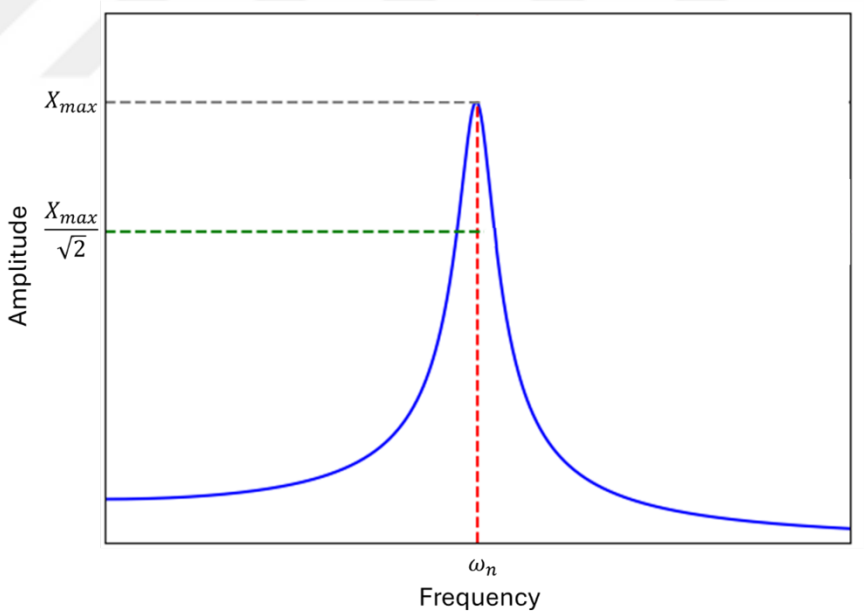
Figure 4.2: *Visualization of the particle damping effect in modal test transfer functions.*



Each transfer function was carefully analyzed to determine the damping characteristics of the particle damper cavities in each specimen. Damping values were extracted

based on the first natural frequency, which is one of the most critical dynamic parameters in structural systems. To ensure consistency with existing literature, the HPBW was employed to determine the damping values. The half-power bandwidth method was utilized to identify the points in the frequency spectrum where the response decreases around a natural frequency [39]. This method determines the bandwidth by measuring the frequency range between two points where the system's power drops to half of its peak value. These half-power points correspond to the lower and upper frequency limits where the mode's amplitude reaches approximately 70.7% of its maximum. By calculating the frequency difference between these two points, the half-power bandwidth provides a quantitative measure of the damping characteristics of the mode (see Figure 4.3).

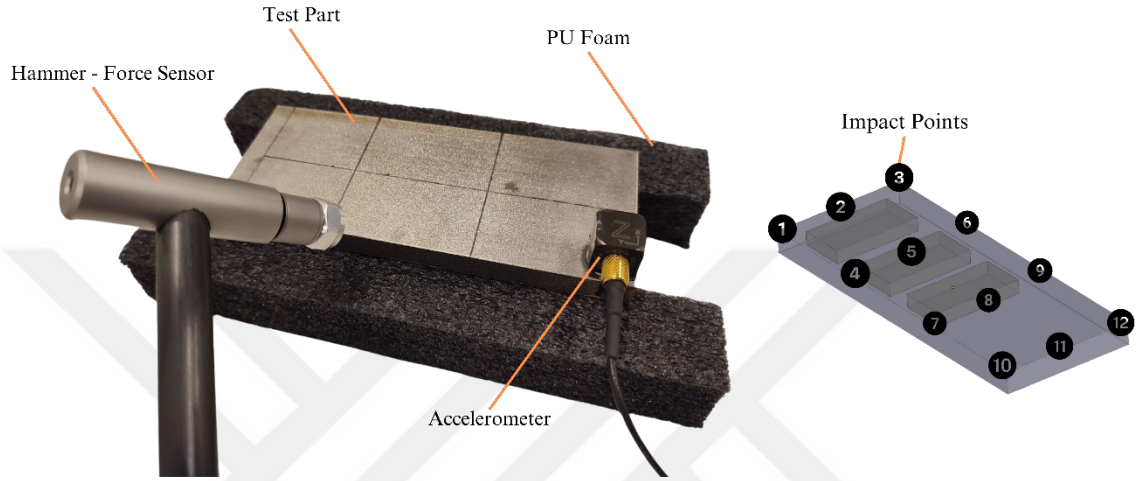
Figure 4.3: *HPBW method for damping.*



In the figure, we show the amplitude–frequency response of a damped single-degree-of- freedom system under forced vibration. The horizontal axis represents the excitation frequency ω, and the vertical axis shows the system's displacement amplitude X. The system reaches its maximum amplitude X_{max} near its natural frequency ω_n, a phenomenon known as resonance. The half-power frequencies, ω_1 and ω_2, are also marked, where the amplitude is $X_{max}/\sqrt{2}$. As the damping ratio ζ increases, the peak becomes lower and broader, indicating that the system is less sensitive to oscillations around the natural frequency [101].

A modal test was performed using the Multiple Input Single Output (MISO) approach. In this setup, the structure was excited at 12 different locations using an impact hammer, while acceleration data was recorded from a single fixed point with an accelerometer. This method allows for a more comprehensive understanding of the system's dynamic behavior by analyzing the responses from multiple excitation points. The exact positions of the excitation locations are indicated as illustrated in Figure 4.4.

Figure 4.4: *Modal test setup.*



4.4 FEM Modeling Approach

In the finite element analysis conducted using Nastran, three key elements were employed to accurately model the system's behavior: CONM2, RBE3, and CDAMP4. The CONM2 element is a concentrated mass element that allows for the specification of mass properties at a specific node, enabling the incorporation of mass effects without the need for detailed geometric modeling. The RBE3 element, a rigid body element, was utilized to distribute the loads from a reference node, where the CONM2 mass is defined, to dependent nodes on the surrounding structure, ensuring that the mass is properly integrated into the model. Additionally, the CDAMP4 element, a discrete damper, was

incorporated to model damping within the system, which is essential for accurately simulating energy dissipation in dynamic analyses such as modal and harmonic responses. Together, these elements enabled a precise and computationally efficient representation of the system's mass, load distribution, and damping characteristics [113].

The primary objective was to obtain FRFs comparable to those acquired from the modal test. To achieve this, the test specimens were meshed in a manner best representing a beam model. The damping values of these elements were assigned for each CDAMP4 element based on data obtained from the modal tests. The CDAMP4 element and CONM2 (particle masses) were integrated into the cavity surfaces using RBE3 rigid connections (see Figure 4.5& 4.6). By doing so, the damping mechanism of the particle dampers was incorporated into the FEM model, thereby accurately replicating the test conditions.

Figure 4.5: *FEM Model*

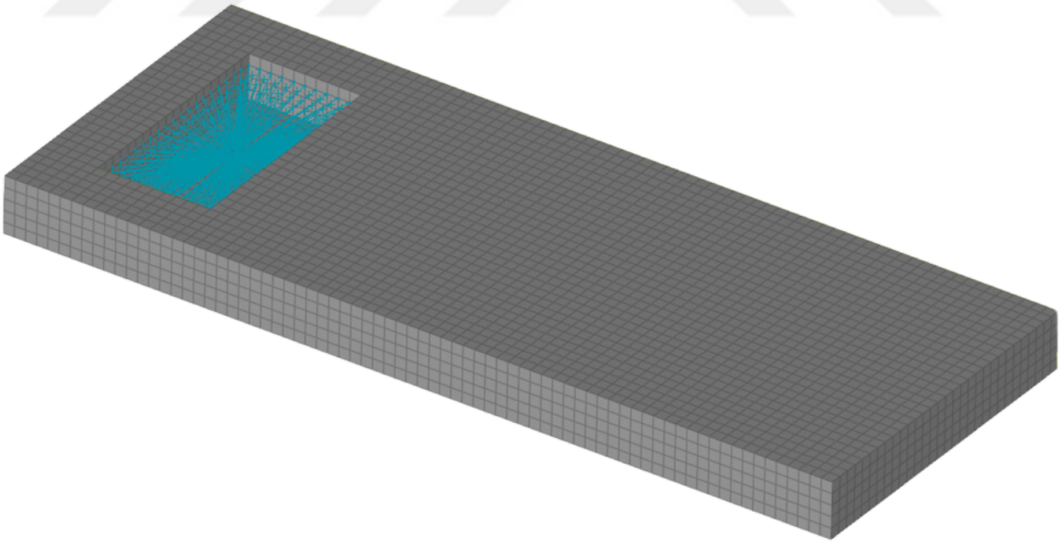
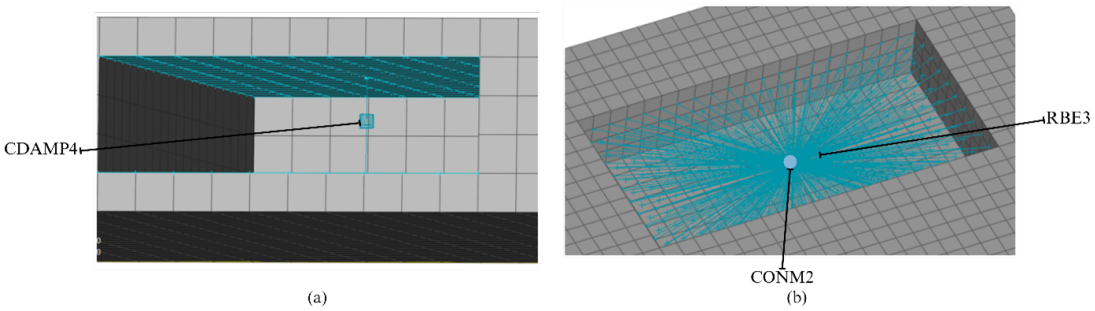
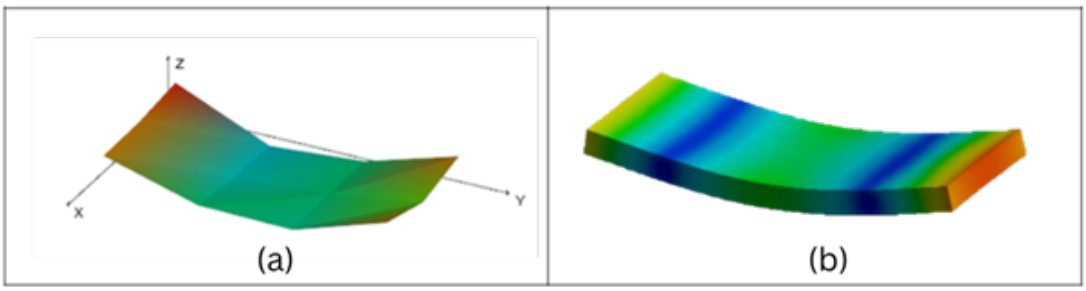


Figure 4.6: *FEM Elements a) CDAMP4 element, and b) CONM2 and RBE3 element*



To confirm the consistency of the finite element model, an initial modal analysis was performed and compared against experimental modal test results. Table 4.3 summarizes the error rates between the numerically predicted modes and those identified experimentally, demonstrating the model's capability to capture the fundamental modal behavior of the test specimens. In addition, Figure 4.7 presents a direct comparison of the first mode shape as obtained from both the modal test and the FEM analysis, illustrating good agreement in deformation patterns and validating the fidelity of the proposed modeling approach.

Figure 4.7: *Mode shapes from (a) modal test, and (b) FEM*



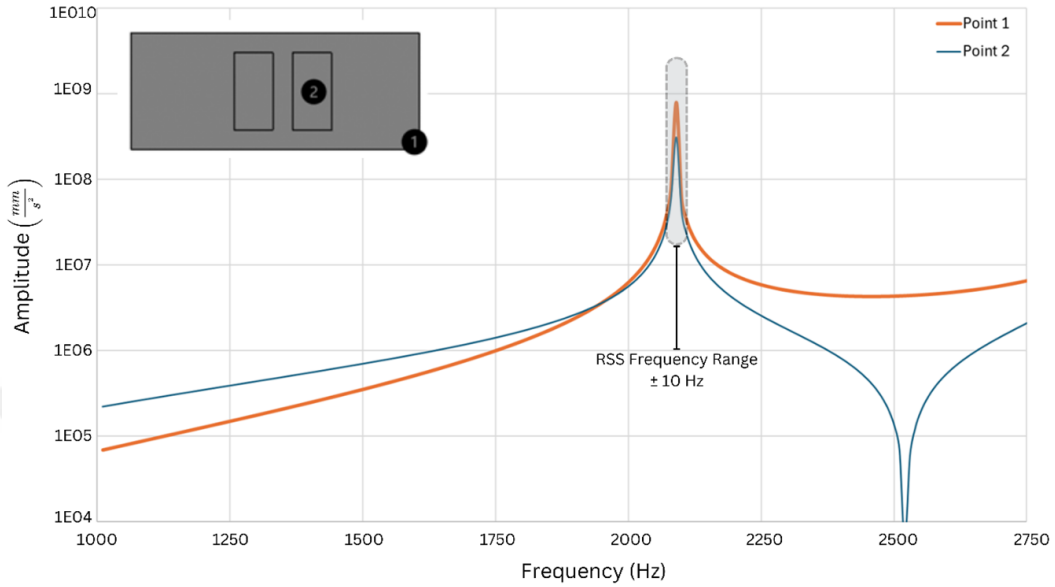
Following the FEM analysis, a two-step process was conducted: first, a modal analysis was performed to identify the modes; subsequently, a harmonic analysis was

Table 4.3: *Comparison of Test and FEM Frequency Results*

Model No	Freq. (Hz) - Test	Freq. (Hz) - FEM	Error (%)
0	2219	2271	2%
1	2222	2284	3%
2	2235	2307	3%
3	2270	2311	2%
4	2181	2290	5%
5	2239	2335	4%
6	2257	2311	2%
7	2152	2234	4%
8	2141	2180	2%
9	2234	2302	3%
10	2215	2252	2%
11	2234	2305	3%
12	2207	2269	3%
13	2166	2239	3%
14	2200	2255	3%
15	2244	2285	2%
16	2158	2254	4%

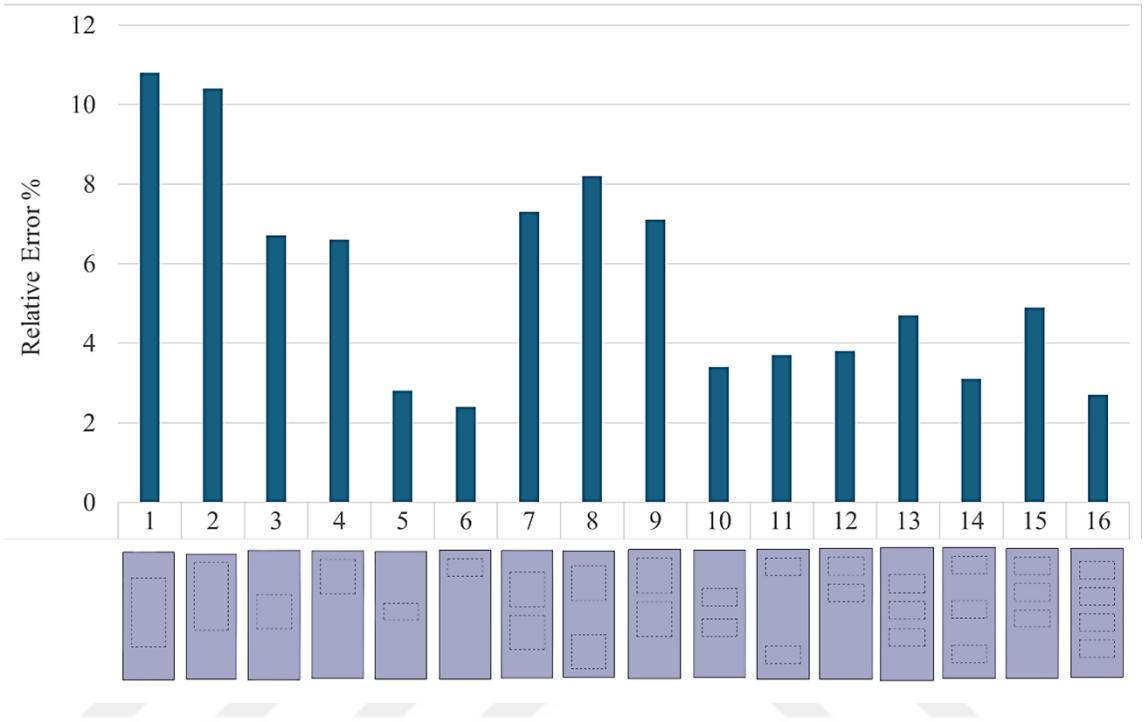
carried out to obtain the FRF response. In this way, cumulative vibration response data were produced and could be compared with the vibration responses from the modal tests. These data were derived by taking the limited integral of the FRFs around the first natural frequency (±10 Hz) for both the modal test reference response point and each particle damper cavity response point from the FEM-based harmonic analysis (see Figure 4.8).

Figure 4.8: *Displacement FRF response between input (point 1) and output (point 2)*



Another factor utilized in validating the FEM models is the cumulative vibration data obtained. The first factor comprises the natural frequency values as well as the cumulative vibration behavior observed around these frequencies. The ratio of the data obtained for the cavity regions to the reference region's RSS data was compared for both the experimental results and the FEM model. In this way, by comparing the cumulative vibration behaviors of the particle damper regions derived from the FEM model's harmonic analysis with those from the tests, the accuracy of the FEM model was evaluated. The comparison of the proportional RSS reduction in the damping regions for both the FEM and the test is presented in Figure 4.9.

Figure 4.9: *Relative error between FEM and modal test*



4.5 Optimization Algorithm

Optimization algorithm focuses on analyzing the effects of multiple design variables to achieve the design objective for the given constraints. In our study, optimization is designed to minimize the first modes of the system cumulative vibration behavior values obtained from validated FEM analyses by determining the optimal placement of cavities on the beam. This is achieved by positioning the minimum number of cavities at the most suitable locations while maintaining the optimal volumetric fraction, ultimately aiming to minimize the RSS value. In this work, the metric is employed to quantify the vibration magnitude:

$$RSS = \sqrt{\sum_{i=1}^{N} (a_i)^2} \tag{4.1}$$

where a_i is the amplitude at the i-th measurement point, and N is the total number of impact points. Achieving the best compromise between weight, damping capacity, and geometric constraints can be a complex, multi-variable optimization task.

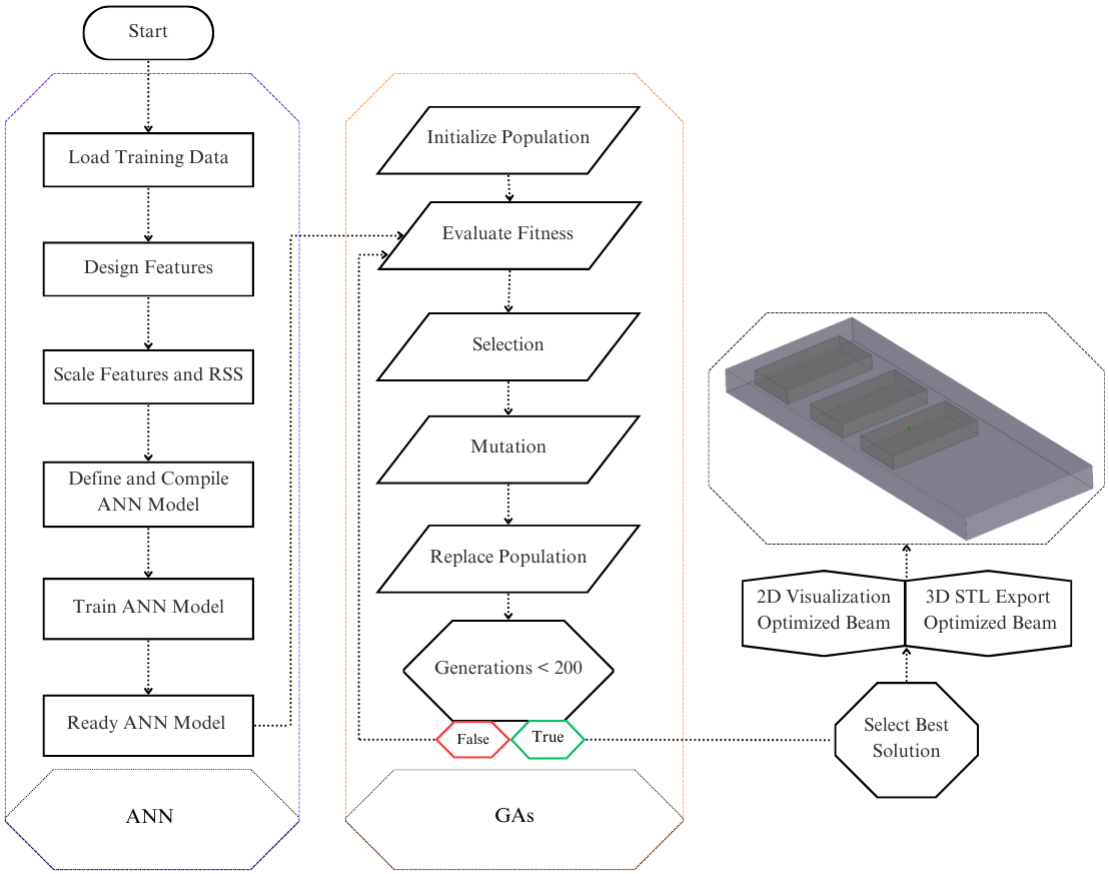
To address this challenge, we propose a hybrid method comprising two main components: ANN, and GA ANN model acts as a quick metamodel that predicts the resulting RSS for any given combination of cavity positions and volumetric fraction, while GA optimization searches for the best arrangement of cavities and volumetric fraction values to minimize the RSS as predicted by the ANN.

The coding of the optimization algorithm was performed using Python with tensorflow, numpy, and the deap library. By training a surrogate model on experimental or FEM-generated data, we reduce the need for time-intensive simulations or repeated prototyping. The GA further refines these designs by mimicking natural evolution (selection, crossover, mutation) to produce high-performing designs in a relatively short number of iterations. The overall progress of the optimization process is given in Figure 10. The formulated optimization approach is presented in Table 4.4.

Table 4.4: *Optimization Problem Formulation*

Design Parameters	**Details**
Design Objectives	Minimize the ANN-predicted RSS value: $f(p_1, p_2, p_3, v_f)$
Design Constraints	Sorted cavity positions must satisfy: $p_{(i+1)} - p_{(i)} \geq 25$ for $i = 1, 2, \ldots$
Design Variables	Cavity positions: p_1, p_2, p_3 Volumetric fraction: v_f
Variable Constraints	$p_i \in \{5, 6, \ldots, 143\}$ for $i = 1, 2, \ldots$ $v_f \in \{0.05, 0.10, 0.15, 0.20\}$

Figure 4.10: *Overall Workflow: GA + ANN Surrogate for Beam Cavity Optimization*



4.5.1 Design Parameters and Feature Set

Before starting the optimization process, fundamental data defining the relationship between cavity positions and the beam's response were obtained. As shown in Figure 4.10, each beam was subjected to FEM-based virtual tests, and its vibration response was measured in terms of RSS values. Additionally, in each beam design, cavity positions and volumetric fractions are among the input parameters for the optimization software.

To transform geometric variables, cavity locations along the beam and the chosen

volumetric fraction, into meaningful inputs for an ANN, we employ a feature design function.

$$x = \Big| n_c \sum_{j=1}^{n_c} p_j, \mu(p_j), \min(p_j), \max(p_j), \\ \sigma(p_j), (\max - \min)(p_j), \text{median}(p_j), v_f \Big| \tag{4.2}$$

where n_c is the number of cavities, p_j denotes the position of the j-th cavity, and v_f is the volumetric fraction. Each of these features captures a different aspect of how the cavities are distributed along the beam, reflecting key mechanical considerations such as centroid location, spread, and boundary constraints.

These features encapsulate both the distribution of cavities and the overall loading scenario. They include:

- Number of cavities: Reflects how many distinct damping zones exist.
- Sum and mean of cavity positions: Provides an overall centroid of the particle damping material placement.
- Minimum and maximum cavity positions: Identifies boundaries of cavity placement to avoid non-ideal damping.
- Standard deviation of cavity positions: Quantifies how spread out the cavities are.
- Range of cavity positions: Offers insight into the span of the damping cavities region along the beam.
- Volumetric fraction: Captures the ratio of particle damping material inserted relative to the total possible volume.

These features can be interpreted to determine how effectively the damping material is distributed along the beam's length.

4.5.2 Network Architecture

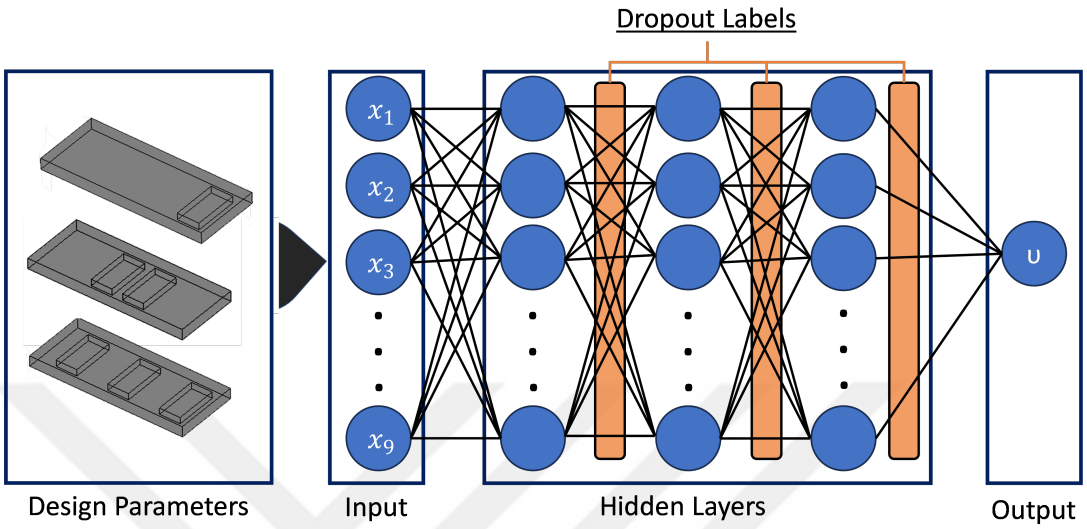
After defining the design parameters and feature set, the ANN is employed to approximate the RSS. The neural network can be viewed mathematically as a function [114].

$$\widehat{RSS} = f(x, \theta) \tag{4.3}$$

where x is the feature vector and θ collectively represents the network parameters (weights and biases).

In this work, the ANN includes an input layer with 9 neurons (one for each feature), and three hidden layers with 16 neurons each, employing the rectified linear unit activation function to introduce non-linearity and capture complex relationships between input parameters and RSS. Dropout layers (rate = 0.2) after each hidden layer are employed, which help prevent overfitting by randomly deactivating 20% of the neurons during training. Finally an output layer with a single neuron is used, producing the predicted $\widehat{RSS}$. The diagram illustrating the ANN flow is presented in Figure 4.11.

Figure 4.11: *ANN Diagram*



4.5.3 Training Procedure

To obtain θ that yields accurate predictions, we minimize the mean squared error (MSE) between the predicted and actual RSS:

$$MSE = \frac{1}{N_{\text{train}}} \sum_{i=1}^{N_{\text{train}}} \left(RSS_i - \widehat{RSS}_i \right)^2 \tag{4.4}$$

where RSS and $\widehat{RSS}$ refer to the true and predicted RSS values for the i-th training sample, respectively, and N_{train} is the total number of training samples.

Standard scaling is applied to both the input features and the target RSS values to ensure consistent training behavior. Given the small dataset in our example, we rely on 200 epochs and a small batch size to refine the network weights. The final model is then used within the GA to predict performance for new cavity configurations.

4.5.4 Genetic Algorithm for Design Optimization

In structural and mechanical engineering problems, certain design tasks, such as finding optimal cavity layouts, can be highly nonlinear, multi-modal, or constrained by manufacturing and operational limits. GA is well-suited for these challenges because they efficiently explore large, complex design spaces and can incorporate constraints relatively easily [115]. Below, we describe each step in the GA process, emphasizing how it applies to beam cavity design and volumetric fraction selection for vibration mitigation. Each candidate design (individual) is represented by a vector containing the cavity positions and the volumetric fraction:

$$\text{Individual Design} = [p_1, p_2, \cdots, p_{n_c}, v_f] \tag{4.5}$$

where p_k is the position of the k-th cavity along the beam, and v_f is a discrete or continuous value for the volumetric fraction.

From a mechanical perspective, this representation ensures that the key geometric variables influencing vibratory response and the amount of particle damping material fraction are both captured in a single parameter set.

The algorithm starts by randomly initializing a population of individuals. This randomization fosters diversity and broad coverage of the design space. However, designs often come with essential constraints, such as a minimum spacing (Δ_{min}) between cavities to avoid overlapping or weak sections. Formally, we require:

$$p_{k+1} - p_k \geq \Delta_{\text{min}} \quad \forall k = 1, 2, \cdots, (n_c - 1) \tag{4.6}$$

If an individual violates these constraints, the algorithm either rejects and re-initializes it or assigns a high penalty to its fitness value, effectively removing it from contention over subsequent generations. This approach mirrors real-world engineering

checks: any design that fails safety or manufacturing constraints is immediately disqualified.

Instead of subjecting each new design to a costly physical or high-fidelity numerical test, we rely on the previously trained ANN surrogate model:

$$\text{Fitness}(x) = \widehat{RSS}(x) \tag{4.7}$$

where x is the feature vector derived from the design's p_k and v_f. A lower fitness value (lower $\widehat{RSS}$) corresponds to better vibration suppression. If a design fails to meet the spacing rule or other geometric constraints (e.g., going outside the beam boundaries), we assign a penalty, ensuring that such infeasible designs do not propagate through the generations [115].

Selection is the mechanism by which the algorithm chooses which individuals pass their genes (design variables) into subsequent generations. We employ tournament selection in this example, though many methods exist. In tournament selection:

- A subset of individuals is randomly picked from the population.
- The individual with the best (lowest) fitness in that subset is selected as a parent.
- This process is repeated until enough parents are chosen to produce the next generation.

The selection mimics iterative refinement toward better designs, beams that exhibit lower vibratory response are more likely to survive and be recombined in subsequent generations.

During crossover, pairs of selected parent designs swap portions of their parameter sets to produce offspring. This mimics the biological process of recombination, where advantageous traits from two distinct lineages can merge to generate improved solutions

[91]. For the beam cavity problem, a simplified approach might swap the cavity positions after a randomly chosen index and exchange the volumetric fraction. By combining successful cavity layouts from different parents, the offspring may discover new or improved configurations that further reduce the beam's RSS.

Mutation, with a specific probability, applies small random alterations to individual parameters [91]. In practice, mutation for our beam design might perturb cavity positions by a small random amount or switch the volumetric fraction to a nearby discrete value. If these changes yield infeasible solutions (e.g., cavities overlap), the individual is penalized or replaced.

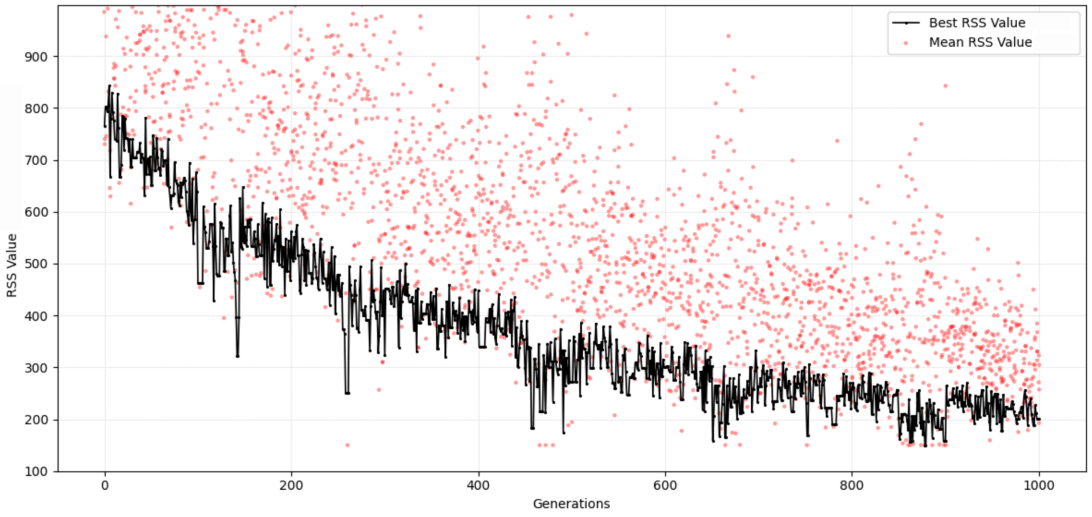
Each generation involves evaluating the population using an ANN-based fitness function, selecting parents based on their fitness, creating offspring through crossover and mutation, and reinserting these offspring, potentially alongside some of the best parents.

This cycle repeats for a predefined number of generations or until a convergence criterion is met—such as when the best fitness stops improving below a threshold for several generations. This iterative process can be seen as trial-and-error refinement underlined by engineering judgment: designs that consistently exhibit desirable vibration characteristics are favored, while those that violate constraints or produce high RSS values are sidelined. Upon convergence, we select the top-performing individual, and a final visualization—such as that produced by the plot function—depicts the positions of each cavity along the beam, the predicted RSS according to the ANN, and the volumetric fraction used.

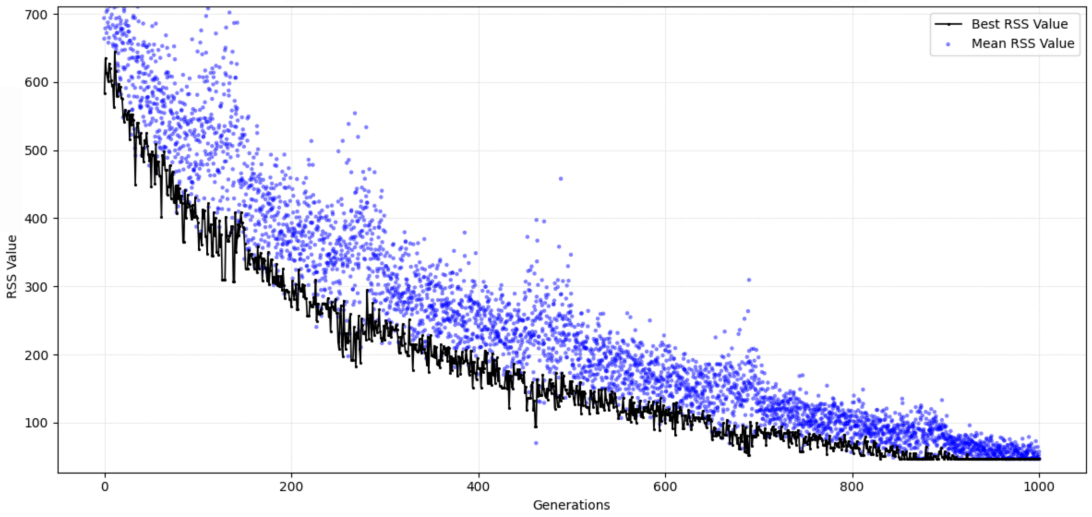
The integration of an ANN as a surrogate model for RSS prediction demonstrably enhances the convergence characteristics of the GA in this beam design optimization task. By learning the complex, potentially non-linear relationships between cavity configurations, volumetric fraction, and the resulting RSS directly from training data, the

ANN furnishes a more accurate and representative fitness landscape for the GA to explore. This higher fidelity evaluation provides superior guidance compared to heuristic or artificially noisy methods, enabling the GA to more efficiently distinguish between genuinely promising and suboptimal design candidates. Consequently, the optimization process exhibits a smoother and more consistent convergence trajectory, as observed in Figure 4.12, the progressive reduction of the best RSS value per generation. Ultimately, this leads to the discovery of significantly better solutions, reflected in the considerably lower final RSS values achieved compared to simulations relying on less accurate evaluation functions.

Figure 4.12: *Convergence History Performace of the Optimization Code a) without ANN integration, b) with ANN Integration*



(a)



(b)

4.6 Results & Summary

A notable characteristic of the proposed GA framework is its inherent stochasticity. Since GAs rely on randomized processes for population initialization, crossover, and mutation, each run can yield a distinct final beam configuration. In this study, repeated executions of the same GA setup produced slightly varied cavity layouts, especially regarding the upper cavities' positions. Nonetheless, these different layouts often resulted in comparable RSS values, implying that multiple near-optimal solutions exist. This is consistent with the broader literature on evolutionary algorithms, where multiple good solutions can lie close together in the design space, each offering desirable performance under similar constraints.

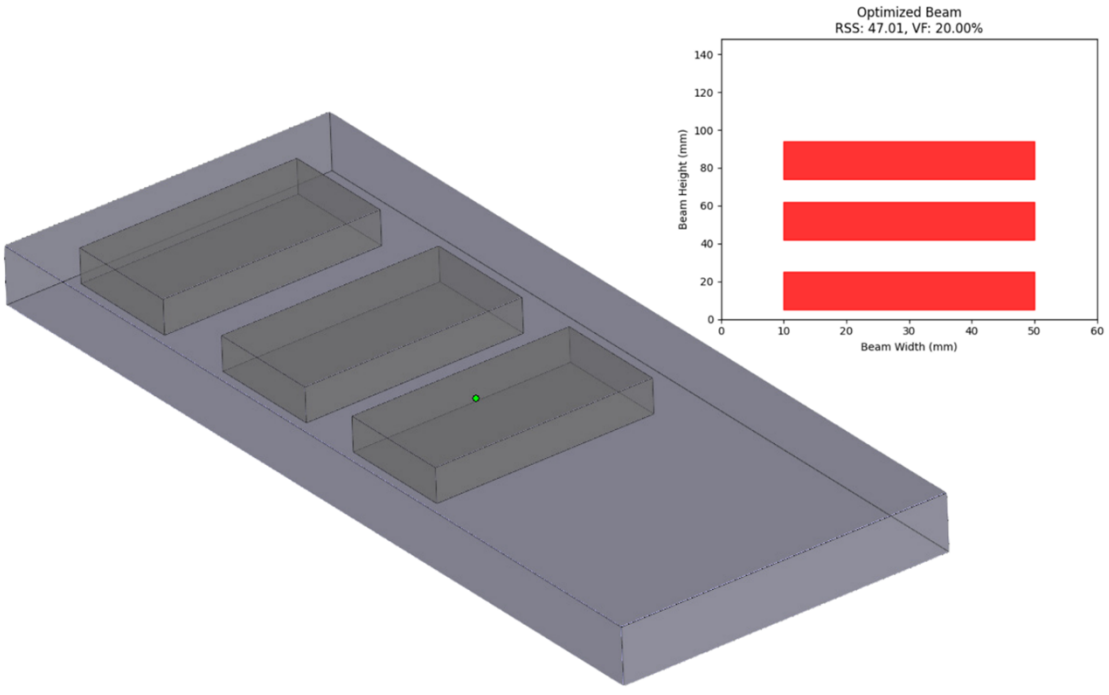
From a practical engineering standpoint, this probabilistic nature offers both advantages and considerations. On one hand, designers gain flexibility: running the GA several times and selecting the best or most manufacturable solution is a straightforward way to accommodate diverse production requirements or material availability. On the other hand, some applications demand a single, definitive design, prompting the need for additional decision criteria, such as cost, weight, or ease of installation, to select among multiple high-performing candidates. For instance, if certain cavity locations require less post-processing or allow simpler mechanical integration, these factors might tip the scales in favor of one arrangement over another, even if its RSS is marginally higher. In addition, comparing or averaging solutions across multiple GA runs can provide deeper insight into the most critical design variables.

Lastly, while the slight variations in solution layouts highlight the GA's stochastic foundation, they also emphasize the robustness of the approach: even if the algorithm takes different evolutionary paths, it reliably produces solutions with strong vibration-damping performance. This makes GA-based optimization particularly attractive for real-world applications that can tolerate minor geometric discrepancies if they yield significant

improvements in vibration suppression. Consequently, the hybrid GA-ANN method not only demonstrates its effectiveness in exploring a complex design space, but also allows engineers to tailor final decisions in a way that balances performance, manufacturability, and cost-effectiveness.

After several runs of the GAs, guided by the ANN surrogate, one of the most practically appealing solutions is shown in Figure 10. In this final configuration, three rectangular cavities are distributed along the beam's height, and the volumetric fraction of particle damping material is set to 20.0%. The predicted RSS of the beam's vibratory response for this layout is 47.01, a marked reduction compared to the baseline reference design with no cavities.

Figure 4.13: *Optimized Beam Design Plot & 3D Model*



This arrangement appears more feasible from a mechanical design perspective as

the cavities are spaced in a way that:

- Avoids overlapping and respects the minimum spacing constraints.
- Distributes the damping material at multiple heights, potentially targeting significant mode shapes.
- Uses a higher volumetric fraction (20.0%), which, while adding some additional mass, may yield more robust vibration attenuation.

The final RSS of 47.01 represents a notable 94% decrease in vibratory response relative to the cavity-free baseline (RSS = 773). This significant improvement underlines the effectiveness of combining targeted cavity placement with a substantial volumetric fraction of damping material. This distribution suggests that the GA identified critical zones where damping would most efficiently suppress the dominant vibration modes. While 20.0% is the maximum volumetric fraction allowed in the discrete set the algorithm settled on this value in several runs, indicating that the additional material consistently contributed to greater damping effectiveness.

A key contribution of this work lies in the accurate modeling and validation of particle damper materials within a FEM framework. While particle dampers are increasingly utilized in vibration control applications, properly capturing their nonlinear damping characteristics in FEM software remains challenging. By incorporating experimental test data, specifically, modal test results, we developed a set of FEM damping elements that reliably represent the energy dissipation introduced by the particle dampers. This validation step was crucial for ensuring that the model would yield physically meaningful predictions across a range of frequencies and damping scenarios. Once the FEM was established and validated against experimental data, we used its output metrics, modal frequencies and damping responses, to train an ANN. This ANN effectively serves as a surrogate model, approximating the vibratory performance of the beam for any given cavity arrangement

and volumetric fraction. By incorporating the ANN into our genetic algorithm process, we created a hybrid optimization approach that drastically reduces the computational expense of brute-force or fully simulation-driven methods. The GA leverages the ANN predictions in each generation's fitness evaluation, accelerating convergence toward high-quality solutions without repeatedly running full, scale FEM analyses. From an engineering design standpoint, this methodology provides two major advantages. First, it ensures fidelity to real-world physics, given that the underlying FEM captures the particle damper's damping behavior, a feature verified through experimental modal tests. Second, it significantly streamlines the optimization process by offloading most of the iterative computation to the ANN. As a result, engineers can explore an expansive design space, varying cavity positions and volumetric fractions, without prohibitive simulation or experimental costs.

In essence, this hybrid GA-ANN strategy opens a new avenue for vibration-damping optimization by combining the robustness of genetic algorithms with the speed and flexibility of a neural network surrogate. Such an approach is particularly valuable for complex damping systems where experimental validation is essential but cannot realistically be performed for every design iteration. By bridging the gap between high-fidelity modeling and practical computational constraints, this method serves as a novel blueprint for efficiently tackling a variety of design optimization challenges involving particle dampers or other advanced damping solutions.

5. CONCLUSIONS

Effective vibration control is a critical challenge in engineering, impacting the performance, safety, and durability of structures across industries such as aerospace, automotive, and civil engineering. This thesis investigates three innovative approaches to enhance damping in structures, leveraging advanced materials and computational techniques. By synthesizing findings from studies on hybrid TPMS structures with silicone polymers, metamaterial-integrated CLD TPMS systems, and optimized particle dampers, this work demonstrates significant advancements in damping technology. These approaches collectively offer versatile solutions to mitigate vibrations, validated through precise FEM and experimental testing.

The first study explored the combination of additively manufactured TPMS metal parts with silicone polymers, revealing substantial improvements in damping performance. Frequency-based analyses showed a 25% increase in damping capacity using the HPBW method and a remarkable 30-fold increase via the Nyquist diagram method compared to a metallic TPMS baseline. In the time domain, a sixfold enhancement in damping effectiveness was observed using the log-decay method, alongside a tenfold reduction in RSS accelerance data under dynamic loads. With FEM models accurate to within a 6% error margin, this hybrid structure excels in vibration suppression and acoustic isolation, making it a strong candidate for engineering applications requiring robust damping.

The second study advanced damping technology by integrating metamaterials with CLD techniques in TPMS structures. Compared to a fully metallic TPMS reference, the CLD TPMS design achieved five times better damping performance in the time domain. Frequency-based analysis using the IFR method indicated a 76% reduction in cumulative vibration, highlighting its stability across critical frequency bands. The FEM simulations, with a maximum error of 7%, confirmed the reliability of these findings. This approach showcases the potential of hybrid material systems to deliver superior vibration

control and acoustic performance, broadening the scope of TPMS applications.

The third study utilized a hybrid computational framework combining FEM, ANN, and GA to optimize particle dampers within a beam structure. The optimized design, featuring three cavities and a 20% volumetric fraction of damping material, achieved a 94% reduction in RSS vibratory response compared to a baseline without cavities. The ANN surrogate model accelerated the GA optimization process, while the GA's flexibility produced multiple high-performing configurations, offering practical design options. Validated by experimental modal data, this method highlights the power of computational optimization in creating efficient, adaptable damping solutions for complex systems.

Together, these studies push the boundaries of structural damping by harnessing additive manufacturing, hybrid materials, and advanced computational tools. The hybrid TPMS-silicone system excels in broadband damping, the CLD TPMS structure targets frequency-specific stability, and the optimized particle dampers provide a customizable, high-efficiency solution. These findings lay a foundation for future research to integrate these approaches, refine material properties, and apply them in real-world scenarios. As engineering demands evolve, this thesis offers a roadmap for developing next-generation damping technologies that enhance structural resilience and performance across diverse applications.The contributions of the study to the literature can be listed with the following points:

- The hybrid combination of metallic TPMS structures with silicone polymers demonstrates a significant increase in damping performance, confirmed through experimental and numerical (FEM) analyses, effectively covering a broad frequency range for vibration and acoustic isolation.

- The integration of metamaterials and CLD in TPMS structures provides high-level stability and damping, especially in critical frequency ranges, validated by FEM models with a 7% margin of error.

- The hybrid use of FEM, ANN, and genetic algorithms for optimizing particle dampers achieves up to a 94% reduction in vibration levels, offering flexible and high-efficiency damping solutions suitable for multi-criteria engineering requirements.
- These approaches, hybrid TPMS-silicone, CLD-TPMS, and optimized particle dampers, offer modular and scalable methods applicable across various industries such as aerospace, automotive, and construction, paving the way for advanced vibration control strategies.
- Combining these three methods, improving material properties, and adapting them to real-world scenarios creates a roadmap for developing next-generation damping technologies, meeting increasing demands for safety, performance, and durability in engineering.

6. FUTURE WORK

Building upon the findings of this research, several avenues for future work are recommended to further expand the applicability and scientific understanding of the proposed damping strategies. One potential direction is to explore the acoustic performance of the hybrid TPMS and CLD structures. Given their demonstrated effectiveness in vibration damping, investigating their behavior in terms of sound transmission loss and acoustic isolation capabilities would provide valuable insights, particularly for applications where both vibration and noise control are critical, such as in automotive or aerospace systems.

Additionally, the particle damper optimization framework presented in this study can be further enhanced by incorporating Discrete Element Method (DEM) simulations. While the current FEM-ANN-GA approach effectively predicts and optimizes damping performance, integrating DEM would allow for a more detailed and realistic representation of particle-to-particle and particle-to-wall interactions within the cavities. This would significantly improve the model's ability to capture the nonlinear and complex behavior of particle dampers, particularly under varying excitation conditions.

Future studies may also focus on developing a fully coupled FEM-DEM framework to bridge the gap between computational efficiency and physical accuracy. Such an approach would facilitate more accurate predictions of energy dissipation mechanisms and enable a deeper understanding of how particle characteristics, such as size, shape, and material properties, affect the overall damping performance. This extension would be particularly valuable for optimizing particle damper designs in practical applications where precise dynamic behavior modeling is essential.

REFERENCES

[1] M. S. Pham, C. Liu, I. Todd, and J. Lertthanasarn, "Metallic gyroid structures: Additive manufacturing, properties and performance," *Procedia CIRP*, vol. 42, pp. 658–663, 2016.

[2] L. Montuori, P. Trovalusci, and G. De Bellis, "On the mechanical properties of cellular structures with triply periodic minimal surfaces," *Materials & Design*, vol. 148, pp. 1–12, 2018.

[3] G. T. M. Bachtiar, N. Ghazali, and M. A. Azam, "Additive manufacturing for the production of lattice structures: Design, parameter optimization and challenges," *International Journal of Advanced Manufacturing Technology*, vol. 102, no. 9–12, pp. 3893–3902, 2019.

[4] T. B. Gittens, M. Olivet, M. Carter, and E. Collings, "Properties and applications of triply periodic minimal surfaces in manufacturing," *Journal of Materials Engineering and Performance*, vol. 29, pp. 2179–2190, 2020.

[5] K. Monkova, M. Vasina, M. Zaludek, P. P. Monka, and J. Tkac, "Mechanical vibration damping and compression properties of a lattice structure," *Materials*, vol. 14, no. 6, p. 1502, 2021.

[6] R. Rajpal, K. P. Lijesh, and K. V. Gangadharan, "Parametric studies on bending stiffness and damping ratio of sandwich structures," *Additive Manufacturing*, vol. 22, pp. 583–591, 2018.

[7] A. Abusabir, M. A. Khan, M. Asif, and K. A. Khan, "Effect of architected structural members on the viscoelastic response of 3d printed simple cubic lattice structures," *Polymers*, vol. 14, no. 3, p. 618, 2022.

[8] Z. Xu *et al.*, "Additive manufacturing of two-phase lightweight, stiff and high damping carbon fiber reinforced polymer microlattices," *Additive Manufacturing*, vol. 32, p. 101106, 2020.

[9] W. Elmadih, W. P. Syam, I. Maskery, D. Chronopoulos, and R. Leach, "Mechanical vibration bandgaps in surface-based lattices," *Additive Manufacturing*, vol. 25, pp. 421–429, 2019.

[10] J. Zhang *et al.*, "Design and mechanical testing of porous lattice structure with independent adjustment of pore size and porosity for bone implant," *Journal of Materials Research and Technology*, vol. 18, pp. 3240–3255, 2022.

[11] M. J. Prajapati, A. Kumar, S. C. Lin, and J. Y. Jeng, "Multi-material additive manufacturing with lightweight closed-cell foam-filled lattice structures for enhanced

mechanical and functional properties," *Additive Manufacturing*, vol. 54, p. 102766, 2022.

[12] T. Ehlers, S. Tatzko, J. Wallaschek, and R. Lachmayer, "Design of particle dampers for additive manufacturing," *Additive Manufacturing*, vol. 38, p. 101752, 2021.

[13] H. Guo *et al.*, "Numerical and experimental analysis of additively manufactured particle dampers at low frequencies," *Powder Technology*, vol. 396, pp. 696–709, 2022.

[14] B. C. Chakraborty and D. Ratna, *Polymers for Vibration Damping Applications*. Amsterdam: Elsevier, 2020.

[15] P. S. Badkar and M. M. Benal, "Estimation of damping ratio of silicone rubber using half power bandwidth method," *Materials Today: Proceedings*, vol. 59, pp. 679–682, 2022.

[16] L. Yu, S. Liu, L. Ye, G. Huang, and Y. Xu, "The dynamic characteristics of silicone rubber isolator," *Journal of Wuhan University of Technology-Mater. Sci. Ed.*, vol. 27, pp. 130–133, 2012.

[17] C. Zhang, K. Pal, J. U. Byeon, S. M. Han, and J. K. Kim, "A study on mechanical and thermal properties of silicone rubber/epdm damping materials," *Journal of Applied Polymer Science*, vol. 119, no. 5, pp. 2737–2741, 2011.

[18] Y. Lin, X. Wu, and Z. Gao, "Graphene-reinforced silicone composites: Enhanced viscoelastic and damping properties," *Composites Science and Technology*, vol. 192, p. 108063, 2023.

[19] H. Chen, R. Zhou, and W. Zhang, "Microstructural optimization of silicone-based damping materials under cyclic loading," *Materials and Design*, vol. 237, p. 111530, 2023.

[20] M. Ahmed, K. El-Sayed, and T. Brown, "Energy absorption and vibration control of 3d-printed silicone structures," *Additive Manufacturing*, vol. 47, p. 102322, 2023.

[21] Y. Liu, Z. Liu, Q. Song, and B. Wang, "Analysis and implementation of chatter frequency dependent constrained layer damping tool holder for stability improvement in turning process," *Journal of Materials Processing Technology*, vol. 266, pp. 687–695, 2019.

[22] Z. Fang, L. Yao, J. Hou, and Y. Xiao, "Concurrent topology optimization for maximizing the modal loss factor of plates with constrained layer damping treatment," *Materials*, vol. 15, no. 10, p. 3512, 2022.

[23] A. S. Dalaq, D. W. Abueidda, R. K. Abu Al-Rub, and I. M. Jasiuk, "Finite element prediction of effective elastic properties of interpenetrating phase composites with architectured 3d sheet reinforcements," *International Journal of Solids and Structures*, vol. 83, pp. 169–182, 2016.

[24] I. Hussain *et al.*, "Design and prototyping soft–rigid tendon-driven modular grippers using interpenetrating phase composites materials," *The International Journal of Robotics Research*, vol. 39, no. 14, pp. 1635–1646, 2020.

[25] A. Singh, O. Al-Ketan, and N. Karathanasopoulos, "Mechanical performance of solid and sheet network-based stochastic interpenetrating phase composite materials," *Composites Part B: Engineering*, vol. 251, p. 110478, 2023.

[26] X. Guo *et al.*, "Interpenetrating phase composites with 3d printed triply periodic minimal surface (tpms) lattice structures," *Composites Part B: Engineering*, vol. 248, p. 110351, 2023.

[27] E. D. Betters *et al.*, "Dynamic stiffness modification by internal features in additive manufacturing," *Precision Engineering*, vol. 66, pp. 125–134, 2020.

[28] J. Fan, L. Zhang, S. Wei, Z. Zhang, S. K. Choi, B. Song, and Y. Shi, "A review of additive manufacturing of metamaterials and developing trends," *Materials Today*, vol. 50, pp. 303–328, 2021.

[29] F. Ren *et al.*, "Transition boundaries and stiffness optimal design for multi-tpms lattices," *Materials & Design*, vol. 210, p. 110062, 2021.

[30] Y. Feng, T. Huang, Y. Gong, and P. Jia, "Stiffness optimization design for tpms architected cellular materials," *Materials & Design*, vol. 222, p. 111078, 2022.

[31] K. Krishnan, D. W. Lee, M. Al Teneji, and R. K. A. Al-Rub, "Effective stiffness, strength, buckling and anisotropy of foams based on nine unique triple periodic minimal surfaces," *International Journal of Solids and Structures*, vol. 238, p. 111418, 2022.

[32] H. Fu, X. Huang, and S. Kaewunruen, "Experimental investigations into nonlinear dynamic behaviours of triply periodical minimal surface structures," *Composite Structures*, vol. 323, p. 117510, 2023.

[33] C. Zhang *et al.*, "Vibration characteristics of additive manufactured iwp-type tpms lattice structures," *Composite Structures*, vol. 327, p. 117642, 2024.

[34] J. Jin *et al.*, "Ni–ti multicell interlacing gyroid lattice structures with ultra-high hyperelastic response fabricated by laser powder bed fusion," *International Journal of Machine Tools and Manufacture*, vol. 95, p. 104099, 2024.

[35] H. Gharehbaghi and A. Farrokhabadi, "Experimental, analytical, and numerical studies of the energy absorption capacity of bi-material lattice structures based on quadrilateral bipyramid unit cell," *Composite Structures*, vol. 337, p. 118042, 2024.

[36] X. Zhang *et al.*, "Multi-dimensional hybridized tpms with high energy absorption capacity," *International Journal of Mechanical Sciences*, vol. 273, p. 109244, 2024.

[37] D. Y. Kim *et al.*, "Tpms-based auxetic structure for high-performance airless tires with variable stiffness depending on deformation," *Scientific Reports*, vol. 14, no. 1, p. 11419, 2024.

[38] M. C. Ozden, U. Simsek, M. Ozdemir, C. E. Gayir, and P. Sendur, "Enhancement of damping characteristics through hybridization: Investigating the synergistic effects of triply periodic minimal surface (tpms) additive metals and silicone polymers," *Advanced Engineering Materials*, vol. 26, no. 11, p. 202302181, 2024.

[39] A. M. Baz, *Active and Passive Vibration Damping*. College Park, MD: John Wiley & Sons, 2019.

[40] A. Jackstadt, W. V. Liebig, and L. Kärger, "Analytical modeling and investigation of constrained layer damping in hybrid laminates based on a unified plate formulation," *International Journal of Mechanical Sciences*, vol. 216, p. 106964, 2022.

[41] Z. Ling, D. Dongdong, Y. Yinong, S. Shuhong, L. Ye, and G. Guiqian, "Topology optimization of a constrained layer damping plate coupled with an acoustical cavity," *International Journal of Acoustics & Vibration*, vol. 21, no. 4, 2016.

[42] J. F. A. Madeira, A. L. Araújo, C. M. Soares, and C. M. Soares, "Multiobjective optimization for vibration reduction in composite plate structures using constrained layer damping," *Computers & Structures*, vol. 232, p. 105810, 2020.

[43] M. Li, W. Sun, Y. Liu, and H. Ma, "Influence analysis of control signal phase on the vibration reduction effect of active constrained layer damping," *Applied Acoustics*, vol. 190, p. 108658, 2022.

[44] W. C. Chi, X. G. Sun, and Y. Q. Wang, "Vibration control of piezoelectric beams with active constrained layer damping treatment using ladrc algorithm," *Structures*, vol. 62, p. 106297, 2024.

[45] Y. Fang, L. Li, D. Zhang, S. Chen, and W. H. Liao, "Vibration suppression of a rotating functionally graded beam with enhanced active constrained layer damping treatment in temperature field," *Thin-Walled Structures*, vol. 161, p. 107522, 2021.

[46] Y. Zhang *et al.*, "Vibration and damping analysis of pipeline system based on partially piezoelectric active constrained layer damping treatment," *Materials*, vol. 14, no. 5, p. 1209, 2021.

[47] H. Min and B. Wang, "Enhancing sound insulation performance with active constrained layer damping plates at low frequencies," *Applied Acoustics*, vol. 222, p. 110062, 2024.

[48] F. Jiang, L. Li, W. H. Liao, and D. Zhang, "Vibration control of a rotating hub-plate with enhanced active constrained layer damping treatment," *Aerospace Science and Technology*, vol. 118, p. 107081, 2021.

[49] A. Jackstadt *et al.*, "On the influence of low-velocity impact damage on constrained-layer damping in hybrid cfrp-elastomer-metal laminates," *Materials & Design*, vol. 241, p. 112882, 2024.

[50] B. Wang and H. Min, "Damping contribution of viscoelastic core on airborne sound insulation performance of finite constrained layer damping panels at low and middle frequencies," *Scientific Reports*, vol. 13, no. 1, p. 15556, 2023.

[51] M. Gröhlich, M. Böswald, and J. Wallaschek, "Viscoelastic damping design–a novel approach for shape optimization of constrained layer damping treatments at different ambient temperatures," *Journal of Sound and Vibration*, vol. 555, p. 117703, 2023.

[52] G. Sharma, A. Kumaraswamy, and S. Rath, "Analyzing five-layer constrained layer damping structures: A comparative study," in *Proceedings of Meetings on Acoustics*, vol. 52, 2023.

[53] D. Zhang, Y. Wu, X. Lu, and L. Zheng, "Topology optimization of constrained layer damping plates with frequency-and temperature-dependent viscoelastic core via parametric level set method," *Mechanics of Advanced Materials and Structures*, vol. 29, no. 1, pp. 154–170, 2022.

[54] R. Zhang, W. Sun, H. Luo, H. Ma, and H. Zhang, "Finite element dynamic modeling and vibration reduction analysis of the double-lap bolted thin plate with partially attached constrained layer damping," *Thin-Walled Structures*, vol. 196, p. 111522, 2024.

[55] A. Gupta, S. Panda, and R. S. Reddy, "Damping capabilities of viscoelastic composites for active/passive constrained layer damping of the plate vibration: a comparative study," *Journal of Vibration Engineering & Technologies*, vol. 12, no. 1, pp. 891–908, 2024.

[56] T. Trzepieciński *et al.*, "Incremental sheet forming of metal-based composites used in aviation and automotive applications," *Journal of Composites Science*, vol. 6, no. 10, p. 295, 2022.

[57] H. Xiao *et al.*, "Recent developments in the mechanical properties of hybrid fiber metal laminates in the automotive industry: A review," *Reviews on Advanced Materials Science*, vol. 62, no. 1, p. 20220328, 2023.

[58] Y. Gur, S. Abhyankar, and D. Wagner, "Radiating panel nvh performance evaluations for vehicle design," in *SAE Technical Paper*, no. 2013-01-1991, 2013.

[59] L. Gagnon, M. Morandini, and G. L. Ghiringhelli, "A review of particle damping modeling and testing," *Journal of Sound and Vibration*, vol. 459, p. 114865, 2019.

[60] A. Schönle, C. Gnanasambandham, and P. Eberhard, "Broadband damping properties of particle dampers mounted to dynamic structures," *Experimental Mechanics*, vol. 62, no. 9, pp. 1569–1578, 2022.

[61] M. C. Ozden, U. Simsek, M. Ozdemir, C. E. Gayir, and P. Sendur, "Innovative vibration control of triply periodic minimum surfaces lattice structures: A hybrid approach with constrained layer damping silicone–viscoelastic layer integration," *Advanced Engineering Materials*, vol. 26, no. 24, p. 2401851, 2024.

[62] Z. Lu, Z. Wang, S. F. Masri, and X. Lü, "Particle impact dampers: past, present, and future," *Structural Control and Health Monitoring*, vol. 25, no. 1, p. e2058, 2017.

[63] T. Ehlers and R. Lachmayer, "Design of particle dampers for laser powder bed fusion," *Applied Sciences*, vol. 12, no. 4, p. 2237, 2022.

[64] S. Tomita, T. Masutani, and H. Sato, "Locally resonant metamaterials damped by particles embedded through additive manufacturing," *Journal of Sound and Vibration*, vol. 596, p. 118715, 2025.

[65] Y. Badri, G. Dodd, J. Cater, A. Hall, G. Schmid, G. Emms, and E. Calius, "Review of granular material damping and sound absorption for possible application in the sound insulation of lightweight floors," *Journal of Building Engineering*, p. 110881, 2024.

[66] Y. Badri, S. Sassi, M. Hussein, and J. Renno, "Experimental and numerical investigation of damping in a hybrid automotive damper combining viscous and multiple-impact mechanisms," *Journal of Vibration and Control*, vol. 28, no. 23–24, pp. 3676–3687, 2021.

[67] N. Meyer and R. Seifried, "Numerical and experimental investigations in the damping behavior of particle dampers attached to a vibrating structure," *Computers & Structures*, vol. 238, p. 106281, 2020.

[68] N. Meyer and R. Seifried, "Toward a design methodology for particle dampers by analyzing their energy dissipation," *Computational Particle Mechanics*, vol. 8, no. 4, pp. 681–699, 2020.

[69] F. Terzioglu, J. Rongong, and C. Lord, "Motional phase maps for estimating the effectiveness of granular dampers," *Mechanical Systems and Signal Processing*, vol. 188, p. 110038, 2023.

[70] X. Li, Y. Yang, and W. Shi, "Study on the damping effect of particle dampers considering different surface properties," *Shock and Vibration*, vol. 2019, no. 1, 2019.

[71] N. Meyer and R. Seifried, "Toward a design methodology for particle dampers by analyzing their energy dissipation," *Computational Particle Mechanics*, vol. 8, no. 4, pp. 681–699, 2020.

[72] T. Kuriyama and M. Saeki, "Investigation of dynamic characteristics of rolling particle dampers," *Journal of Vibration and Control*, vol. 27, no. 19–20, pp. 2243–2252, 2020.

[73] R. Ma, S. Fu-qiang, M. Juan, J. Wang, J. Jin, and T. Yu, "Numerical and experimental investigations of particle dampers attached to a pipeline system," *Applied Sciences*, vol. 13, no. 24, p. 13217, 2023.

[74] S. Kumar and A. Kumar, "Vibration attenuation of a pcb enclosure in a radar system employing internal particle dampers," *International Journal of Mechanics and Materials in Design*, 2024.

[75] Y. Luo, W. Xiao, and H. Zhu, "Vibration mitigation of l-shaped pipes in different intensity of vibration with particle dampers," *Preprint*, 2024.

[76] K. Zhang, Y. Xi, T. Chen, and Z. Ma, "Experimental studies of tuned particle damper: design and characterization," *Mechanical Systems and Signal Processing*, vol. 99, pp. 219–228, 2018.

[77] M. Żurawski and R. Zalewski, "Damping of beam vibrations using tuned particles impact damper," *Applied Sciences*, vol. 10, no. 18, p. 6334, 2020.

[78] N. Meyer and R. Seifried, "Systematic design of particle dampers for transient vertical vibrations," *Granular Matter*, vol. 25, no. 1, 2022.

[79] G. Jin, Z. Zhao, B. Liu, W. Cun, Z. Zhao, M. Hou, and G. Chen, "Design of a particle damper and experimental study on vibration damping of the pipeline," *Advances in Mechanical Engineering*, vol. 13, no. 9, 2021.

[80] C. Song, Y. Han, B. Jia, X. Xiong, Y. Jiang, P. Wang, Y. Liang, and H. Fang, "Analysis of vibration reduction performance of vibration isolation system based on particle damping," *Journal of Low Frequency Noise, Vibration and Active Control*, vol. 43, no. 3, pp. 1244–1260, 2024.

[81] B. Wang, H. Wang, Z. He, D. Liu, and P. Pan, "Test and analysis of multi-cavity particle damper for horizontal vibration control of pipeline structures," *Journal of Vibration and Control*, vol. 30, no. 7–8, pp. 1487–1501, 2023.

[82] X. Huang, X. Li, and J. Wang, "Optimal design of inerter-based nonpacked particle damper considering particle rolling," *Earthquake Engineering & Structural Dynamics*, vol. 50, no. 7, pp. 1908–1930, 2021.

[83] H. He, B. Wang, and W. Yan, "Mechanical model and optimization analysis of multiple unidirectional single-particle damper," *Journal of Engineering Mechanics*, vol. 147, no. 7, p. 04021040, 2021.

[84] X. Lei and C. Wu, "Investigating the optimal damping performance of a composite dynamic vibration absorber with particle damping," *Journal of Vibration Engineering & Technologies*, vol. 6, pp. 503–511, 2018.

[85] C. Snoun and M. Trigui, "Design parameters optimization of a particles impact damper," *International Journal on Interactive Design and Manufacturing*, vol. 12, pp. 1283–1297, 2018.

[86] T. Qu, S. Guan, Y. T. Feng, G. Ma, W. Zhou, and J. Zhao, "Deep active learning for constitutive modelling of granular materials: From representative volume elements to implicit finite element modelling," *International Journal of Plasticity*, vol. 164, p. 103576, 2023.

[87] X. Ye, Y. Q. Ni, M. Sajjadi, Y. W. Wang, and C. S. Lin, "Physics-guided, data-refined modeling of granular material-filled particle dampers by deep transfer learning," *Mechanical Systems and Signal Processing*, vol. 180, p. 109437, 2022.

[88] B. Vaissier, J. Pernot, L. Chougrani, and P. Véron, "Genetic-algorithm based framework for lattice support structure optimization in additive manufacturing," *Computer-Aided Design*, vol. 110, pp. 11–23, 2019.

[89] C. Zhu, X. Chen, H. Wu, J. Zhu, T. Peng, J. Lv, and Y. Wu, "Multi-objective optimization of selective laser melting processes for minimizing energy consumption and maximizing product tensile strength," *Metals*, vol. 12, no. 11, p. 1782, 2022.

[90] M. S. Saad, M. Z. Zakaria, M. E. Baharudin, A. M. Nor, and M. F. M. Ju, "Multi-objective optimization of tensile strength and material consumption of fdm parts using multi-objective symbiotic organisms search (mosos)," *Preprint*, 2023.

[91] M. Özdemir, U. Şimşek, G. Kızıltaş, C. E. Gayir, A. Çelik, and P. Şendur, "A novel design framework for generating functionally graded multi-morphology lattices via hybrid optimization and blending methods," *Additive Manufacturing*, vol. 70, p. 103560, 2023.

[92] S. Grozav, A. D. Sterca, M. Kočiško, M. Pollák, and V. Ceclan, "Artificial neural network-based predictive model for finite element analysis of additive-manufactured components," *Machines*, vol. 11, no. 5, p. 547, 2023.

[93] X. Qi, G. Chen, Y. Li, X. Cheng, and C. Li, "Applying neural-network-based machine learning to additive manufacturing: current applications, challenges, and future perspectives," *Engineering*, vol. 5, no. 4, pp. 721–729, 2019.

[94] S. Subramonian, K. Kadirgama, A. S. M. Al-Obaidi, M. S. Mohd Salleh, U. K. Vatesh, S. Pujari, D. Rao, and D. Ramasamy, "Artificial neural network performance modeling and evaluation of additive manufacturing 3d printed parts," *Engineering, Technology & Applied Science Research*, vol. 13, no. 5, pp. 11677–11684, 2023.

[95] R. Wang, Y. Chen, X. Peng, N. Cong, D. Fang, X. Liang, and J. Shang, "Topological design of the hybrid structure with high damping and strength efficiency for additive manufacturing," *Rapid Prototyping Journal*, vol. 28, no. 10, pp. 1995–2003, 2022.

[96] M. Ozdemir, U. Simsek, E. Kuser, C. E. Gayir, A. Celik, and P. Sendur, "Experimental and numerical modal characterization for additively manufactured triply periodic minimal surface lattice structures: Comparison between free-size and homogenization-based optimization methods," *Advanced Engineering Materials*, p. 2201811, 2023.

[97] M. Gröhlich, M. Böswald, and J. Wallaschek, "Viscoelastic damping design–a novel approach for shape optimization of constrained layer damping treatments at different ambient temperatures," *Journal of Sound and Vibration*, vol. 555, p. 117703, 2023.

[98] R. Zhang, W. Sun, H. Luo, H. Ma, and H. Zhang, "Finite element dynamic modeling and vibration reduction analysis of the double-lap bolted thin plate with partially attached constrained layer damping," *Thin-Walled Structures*, vol. 196, p. 111522, 2024.

[99] U. Simsek, A. Akbulut, C. E. Gayir, C. Basaran, and P. Sendur, "Modal characterization of additively manufactured tpms structures: comparison between different modeling methods," *International Journal of Advanced Manufacturing Technology*, vol. 115, no. 3, pp. 657–674, 2021.

[100] Ansys® GRANTA Research Selector, "Release 2023 r2, ansys, inc., usa." Software, 2023. Material database and selection tool.

[101] D. J. Ewins, *Modal Testing: Theory, Practice and Application*. London: John Wiley & Sons, 2009.

[102] J. S. Bendat and A. G. Piersol, *Random Data: Analysis and Measurement Procedures*. California: John Wiley & Sons, 2011.

[103] B. Singh and B. K. Nanda, "Estimation of damping in layered welded structures with unequal thickness," *Shock and Vibration*, vol. 19, no. 6, pp. 1463–1475, 2012.

[104] C. Beards, *Structural Vibration: Analysis and Damping*. MA: Elsevier, 1996.

[105] W. J. Bottega, *Engineering Vibrations*. Boca Raton, FL: CRC Press, 2014.

[106] O. Al-Ketan and R. K. Abu Al-Rub, "Multifunctional mechanical metamaterials based on triply periodic minimal surface lattices," *Advanced Engineering Materials*, vol. 21, no. 10, p. 1900524, 2019.

[107] H. Jia *et al.*, "An experimental and numerical investigation of compressive response of designed schwarz primitive triply periodic minimal surface with non-uniform shell thickness," *Extreme Mechanics Letters*, vol. 37, p. 100671, 2020.

[108] W. Ren, L. Yang, and L. Wang, "Viscoelastic damping behaviors of laminated composites with polymer interlayers," *Composite Structures*, vol. 237, p. 111885, 2020.

[109] S. V. Modak, *Analytical and Experimental Modal Analysis*. Boca Raton, FL: CRC Press, 2023.

[110] N. V. Nguyen, K. Q. Tran, J. Lee, and H. Nguyen-Xuan, "Nonlocal strain gradient-based isogeometric analysis of graphene platelets-reinforced functionally graded triply periodic minimal surface nanoplates," *Applied Mathematics and Computation*, vol. 466, p. 128461, 2024.

[111] K. Q. Tran, T. D. Le, N. V. Nguyen, and H. Nguyen-Xuan, "Design of 3d rotating triply periodic minimal surface (rottpms) lattice plates: Meanings of crystalline rotations and porosity," *International Journal of Mechanical Sciences*, vol. 270, p. 109090, 2024.

[112] B. Ozcevik, E. Söylemez, B. Bediz, and U. Şimşek, "Effects of particle damper design parameters on the damping performance of laser powder bed fused structures," *The International Journal of Advanced Manufacturing Technology*, vol. 130, no. 7–8, pp. 3917–3928, 2024.

[113] MSC Software Corporation, *MSC Nastran Quick Reference Guide*. MSC Software Corporation, 2018.

[114] H. Cartwright and Marton, *Artificial Neural Networks*, vol. 1260. Humana Press, 2015.

[115] E. Wirsansky, *Hands-on Genetic Algorithms with Python: Applying Genetic Algorithms to Solve Real-World Deep Learning and Artificial Intelligence Problems*. Birmingham, UK: Packt Publishing Ltd., 2020.

VITA

Murat Can Özden

Education:

Ph.D.: Özyegin University, Mechanical Engineering

Master of Science: Cukurova University, Automotive Engineering

Bachelor of Science: Cukurova University, Automotive Engineering

Work Experience:

Mercedes Benz Turk – Senior Durability CAE Engineer

Baykar Technologies – Senior NVH Engineer

Standard Profil Automotive GmbH – R&D Acoustics Specialist

SANKO Construction Machinery – R&D Product Design & NVH Engineer

Scientific Publications:

Özden, M. C., Şimşek, U., Özdemir, M., Gayır, C. E., & Sendur, P. (2024). Enhancement of damping characteristics through hybridization: Investigating the synergistic effects of triply periodic minimal surface additive metals and silicone polymers. *Advanced Engineering Materials, 26*(11), 2302181. https://doi.org/10.1002/adem.202302181

Özden, M. C., Şimşek, U., Özdemir, M., Gayır, C. E., & Sendur, P. (2024). Innovative vibration control of triply periodic minimum surfaces lattice structures: A hybrid approach with constrained layer damping silicone-viscoelastic layer integration. *Advanced Engineering Materials, 26*(4), 2401851. https://doi.org/10.1002/adem.202401851